January 2011

Molecular Mechanism Of The Allosteric Coupling For Ca(2+) Activation Of The Voltage- And Ca(2+)-Activated K(+) (Bk) Channels

Junqiu Yang
Washington University in St. Louis

Follow this and additional works at: https://openscholarship.wustl.edu/etd

WASHINGTON UNIVERSITY IN ST. LOUIS

School of Engineering and Applied Science

Department of Energy, Environmental and Chemical Engineering

Dissertation Examination Committee:
Jianmin Cui, Chair
Milorad Dudukovic
Christopher Lingle
Cynthia Lo
Lawrence B. Salkoff
Yinjie Tang

MOLECULAR MECHANISM OF THE ALLOSTERIC COUPLING FOR

Ca^{2+} ACTIVATION OF THE

VOLTAGE- AND Ca^{2+}-ACTIVATED K^+ (BK) CHANNELS

by

Junqiu Yang

A dissertation presented to the
Graduate School of Arts and Sciences
of Washington University in
partial fulfillment of the
requirements for the degree
of Doctor of Philosophy

August 2011

Saint Louis, Missouri

Acknowledgments

I am truly grateful to my advisor, Dr. Jianmin Cui, for his enthusiastic and expert guidance. I am also grateful to every member of the Cui laboratory for their friendship and professional collaboration. I am particularly indebted to the support from our molecular biology team: Dr. Jingyi Shi, Kelli Delaloye, Allen X. Yang, and Alyssa Moller.

I would like to thank my committee for their time and attention and for their comments and suggestions: Dr. Milorad Dudukovic, Dr. Christopher Lingle, Dr. Cynthia Lo, Dr. Lawrence B. Salkoff, and Dr. Yinjie Tang.

Not least, I should thank my dearest friend, Jena, for her loveable companionship!

Dedicated to my parents

Mr. Baogen Yang and Mrs. Furong Chen

Table of Contents

We are all in the gutter,
but some of us are looking at the stars.

— Oscar Wilde

Chapter 1: Introduction

Background

Bioelectricity is the electrical field or current produced by living cells, tissues, or organisms. Examples of bioelectricity include the cell membrane potential and the electric currents that flow in nerves and muscles.

The cell membrane potential is the voltage difference across the cell membrane – conventionally, a positive membrane potential denotes a higher voltage inside the membrane than on the outside. The membrane potential is generated due to uneven net charges between the inside and outside solutions. Since the membrane separates the inside solution from the outside, the compositions of the inside and outside solutions are usually different. For example, in mammalian neurons, $[K^+]$ inside the membrane is 140 mM, but it is 5 mM outside the membrane [1]. Because K^+ is usually permeable for cell membranes, K^+ tends to flow along the concentration gradient from the inside to the outside solution. As a result, the flow of K^+ makes the outside solution more positively charged than the inside solution so that a voltage gradient is generated across the cell membrane. This voltage gradient tends to drive K^+ inward, which quickly balances the

outward K^+ flow so that an electrochemical equilibrium is established. The voltage

gradient at the electrochemical equilibrium is called the equilibrium potential of K^+ ion,

which is calculated using the Nernst equation $E_X = \dfrac{RT}{z_X F} \ln \dfrac{[X]_o}{[X]_i}$, where E_X is the

equilibrium potential for ion X, R is the gas constant, T is the absolute temperature, z_X is

the valence of ion X, and F is the Faraday constant. Based on the Nernst equation, any

ions other than K^+ may also contribute to the voltage gradient across the membrane if the

inside and outside concentrations are different (Table 1) and the membrane is permeable

to those ions. The combined effect of all permeable ions, i.e. the summed contribution of

each ion weighed by its membrane permeability, is the actual voltage difference across

the membrane and thereby termed as the membrane potential. When the cell is at rest, the

membrane potential of a typical mammalian cell is about -70 mV.

Table 1. Intracellular and extracellular concentrations of permeable ions in mammalian neurons[1].

Ion	Concentration (mM)		Equilibrium potential (mV)
	Intracellular	Extracellular	
K^+	140	5	- 102
Na^+	5 – 15	145	56
Cl^-	4 – 30	110	-76
Ca^{2+}	0.0001	1 – 2	125

The concentration gradient across the membrane is created and maintained by membrane proteins called active transporters or pumps. For example, the Na^+ pump, which is one of the most important active transporters, hydrolyzes ATP and transports Na^+ to the extracellular side and K^+ to the intracellular side against their concentration gradients. Other transporters also produce and maintain concentration gradients for all other physiologically important ions, such as Cl^-, Ca^{2+}, and H^+. Additionally, other membrane proteins, such as exchangers and co-transporters, also play important roles in maintaining the ionic concentration gradients.

The permeability of the cell membrane for different ions is governed by membrane proteins called ion channels. Each ion channel forms a pore across the membrane. In most cases, each ion channel selectively permits only one ion species to flow through the pore. Thus, ion channels are generally categorized by the permeable ion species. For example, there are K^+ channels, Na^+ channels, Cl^- channels, and so on. Most ion channels change their conformation in response to external stimuli. The most important conformational change is gating, i.e. the opening and closing of the gate, which controls the accessibility of the conducting pore. Ions are permitted to flow through the pore when the gate is at the open state, but not at the closed state. Therefore, in addition to conductance, gating also determines the permeability of ion channels.

Gating of most ion channels is regulated by a variety of external stimuli, including the membrane potential, extracellular chemical signals such as neurotransmitters,

intracellular signals such as second messengers, temperature, and mechanical stimuli.

Among these external stimuli, the membrane potential affects the gating of the largest

population of ion channels; these channels are hence called voltage-gated ion channels.

Since gating itself changes the permeability and thereby the membrane potential, these

channels provide a feedback mechanism for the membrane potential to change

continuously [2]. Furthermore, because the local membrane potential has its influence on

the adjacent ion channels and thereby changes the potential of the adjacent cell

membrane, the change in the local membrane potential can propagate along the cell

membrane.

One important form of the propagated change in membrane potential is the action

potential. Action potentials conduct electrical signals along cell membranes so that

information is conveyed from one place to another. Two types of ion channels play major

roles in action potentials: Na^+ channels and K^+ channels[1]. Under certain stimuli, the

membrane potential increases (depolarization), leading to the rapid opening of voltage-

gated Na^+ channels. Since the extracellular concentration of Na^+ is higher than

intracellular, Na^+ ions flux from the extracellular side to the intracellular side upon

channel opening, which raises the membrane potential even more positively and

stimulates more Na^+ channel openings. However, after the rapid increase of the

membrane potential, Na^+ channels spontaneously close, which is called inactivation, and

cease conducting Na^+ ions. Meanwhile, the opening of K^+ channels is slowly prompted

by depolarization and K^+ ions start fluxing from the intracellular side to the extracellular

side since intracellular K^+ concentration is higher. The flux of K^+ ions brings down the membrane potential to end the action potential. Action potentials are able to propagate along the cell membrane because depolarization on the local cell membrane exerts influence on the nearby cell membrane and increases the nearby membrane potential to open Na^+ channels there.

K^+ Channels: Structure and Activation

K^+ channels are one of the key players in action potentials, and they play important roles in many other functions, including setting the resting membrane potential in neurons, regulating the action potential duration in cardiac muscle, and regulating the secretion of hormones [3]. K^+ channels are the most distributed ion channels among all the ion channels and are found in almost all cell types. The 71 cloned mammalian K^+ channels in different families are shown in Figure 1.1.
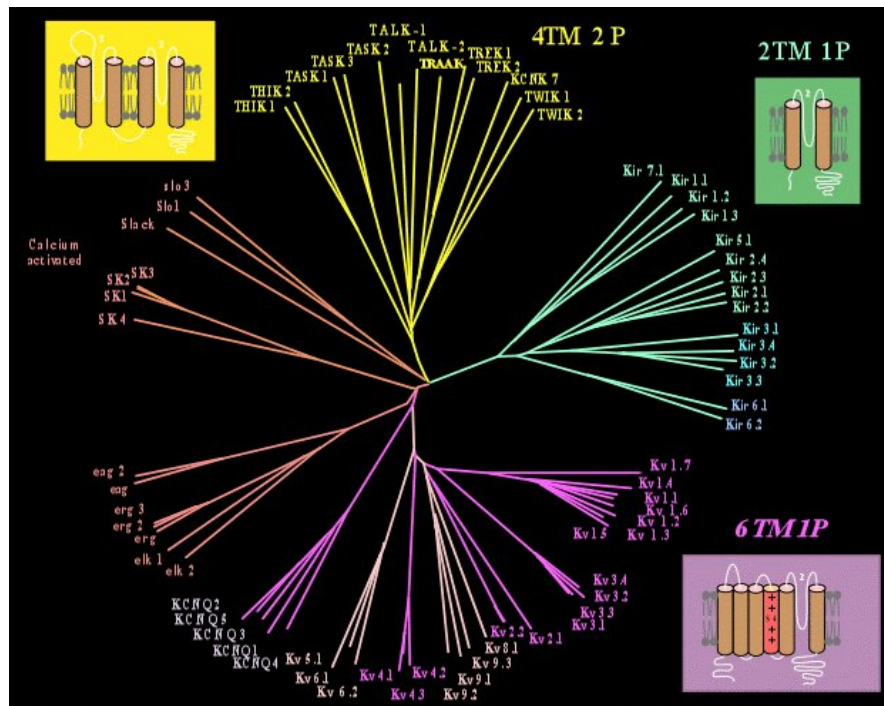
Figure 1.1. Dendrogram of the 71 cloned mammalian K$^+$ channels. TM represents transmembrane segment and P represents pore domain. BK channels are one of the branches labeled as Slo1. Figure adapted from: http://www.ipmc.cnrs.fr/~duprat/ipmc/nomenclature.htm.

Despite the diversity of K$^+$ channels, their sequences share a highly conserved segment called the K$^+$ channel signature sequence [4], which makes K$^+$ channels easy to identify. The K$^+$ signature sequence forms the selectivity filter, a structure that permits K$^+$ ions to flow across the membrane but not Na$^+$ ions. The selectivity filter, together with the conducting pore, is formed by four usually identical subunits that surround the filter and the pore with four-fold symmetry [5, 6]. As shown in the KcsA K$^+$ channel structure

(Figure 1.2), the conducting pore is formed by two α-helices from each subunit: the one

lining the pore is the inner helix and the other is the outer helix [5].
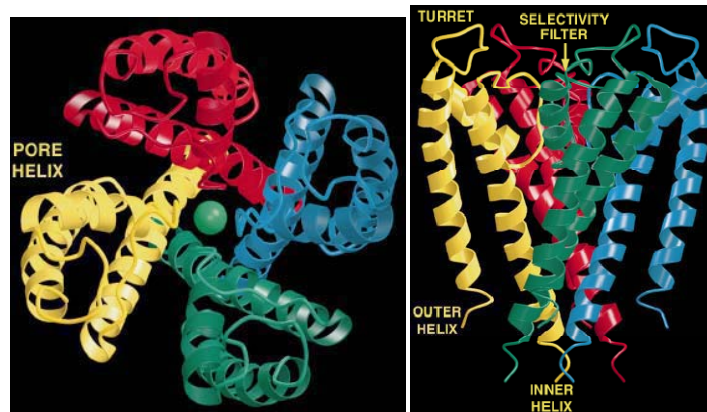
Figure 1.2. Crystallographic structure of the KcsA channel. The tetramer structure

is viewed from top (left) or side (right). Subunits are distinguished from each other

by different colors. Figures adapted from ref. [5].

The intracellular part of the inner helix is widely accepted as the gate, whose

conformational change opens or closes the pore, thereby controlling the accessibility of

the pore [7]. As suggested by the crystal structures of the KcsA and MthK channels

(Figure 1.3), the gate is closed when the four inner helices are straight and form a bundle

with a narrow gap on the intracellular side, and it is open when the inner helices are bent

at a point and spread open [8]. The process of gate opening is called activation and the

closing process is called deactivation. Sometimes, part of channel structure may block the

ionic flow even though the gate is at its open state. This process is known as inactivation.
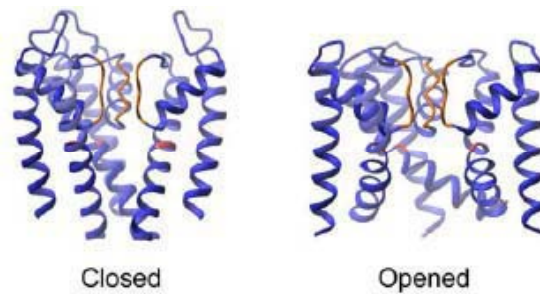
Figure 1.3. Closed and open conformations of the gate. Side view of the three subunits of the closed gate in KcsA (left) and the open gate in MthK (right) channels. The selectivity filter and the bending points are colored. Figure adapted from ref. [8].

The diversity of different K^+ channels mainly arises from the various stimuli by which the gate of K^+ channel is prompted to open. Some K^+ channels are voltage gated (Kv channels in Figure 1.1), meaning that the gate opening is regulated by the movement of a charged voltage-sensing module – the voltage sensor [9, 10]. The voltage sensors usually consist of four transmembrane segments (called S1-S4) with the forth one (S4) containing positively charged residues at every third position on the amino acid sequence [11-16]. In the crystal structure of voltage-gated Kv1.2 channel, the voltage sensors are located on the periphery of the channel, surrounding the central conducting pore (Figure 1.4) [17]. It is known that upon changes in membrane potential, the voltage sensor moves along the electric field [9-11]. In some channels, the movement of the voltage sensor may open the gate through direct interactions between the S4-S5 linker and the cytoplasmic side of the

gate-forming inner helix so that the voltage sensor movement and the gate opening are tightly coupled [18]. But the coupling mechanisms may vary channel by channel.
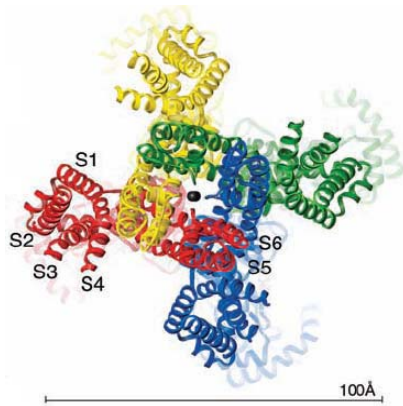
Figure 1.4. Top view of the crystallographic structure of the Kv1.2 channel. The four subunits are distinguished from each other by different colors. The position of each transmembrane segment is indicated. Figure adapted from ref. [17].

Some K^+ channels are ligand gated, which means that the gate opening is regulated by the binding of ligand molecules, including ions [19], small organic molecules, and sometimes other proteins [20]. Ligand-gated K^+ channels usually have cytosolic or extracellular domains as the binding structure. As an example of ligand-gated K^+ channels, the MthK channel (Figure 1.5) is gated by intracellular Ca^{2+} ions [21]. Ca^{2+} binds between the RCK domains (regulatory domains of K^+ conductance) in the cytosolic structure. The cytosolic structure is formed by eight identical RCK domains and is in an octameric ring-like shape (called the gating ring) [21]. Ca^{2+} binding at the interfaces of RCK domains causes the RCK domains to alter their relative position, which enlarges the diameter of the gating ring and pulls the gate to open through the peptide linkers between the gate and the gating ring [21]. The RCK domain is suggested as the ligand sensing module in many other ligand-gated K^+ channels [21-26]. A noteworthy implication is that the Ca^{2+} binding sites

10

in the MthK channel are distal away from the gate; the Ca^{2+} binding energy is transported

to the gate through the conformational change of RCK domains, which enlarges the

gating ring and thereafter exerts a pulling force to the peptide linkers between the S6

activation gate and the RCK domain (Figure 1.5).
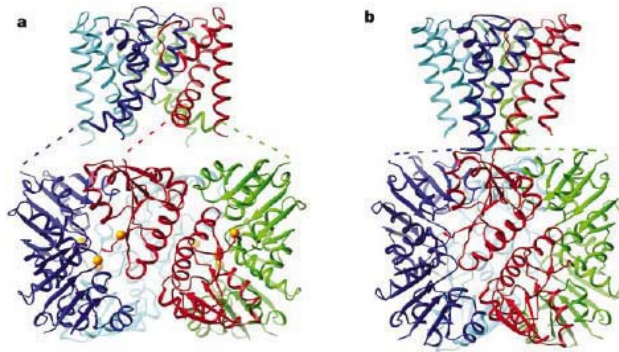
Figure 1.5. Proposed Ca^{2+}-dependent activation of the MthK channel. **a**. Side view of the crystallographic structure of the open channel. The pore- gate domain (top half) is connected with the cytosolic domain (bottom half) by peptide linkers (dashed lines). The cytosolic domain is formed by eight identical RCK domains. Yellow spheres denote bound Ca^{2+} ions. **b**. Hypothetical structure of the closed channel. Figures adapted from ref. [21].

BK Channels

BK channels are voltage- and Ca^{2+}-gated K^+ channels with extraordinarily large single-

channel conductance (~ 100 – 300 pS); thereby they are also known as Big K^+ (or MaxiK)

channels [19, 27, 28]. BK channels are expressed in a wide range of cell types, including skeletal [29-31] and smooth muscles [32-39], inner hair cells of cochlea [40-44], chromaffin cells [45-49], and neurons [50-54]. BK channels function as negative feedback regulators for neuronal signals in many physiological activities, including modulating endocrine secretion [43, 55-59] and neurotransmitter release [60-62], controlling the interspike interval and spike frequency adaptation [51, 52, 55, 63-66], tuning hair cell firing frequencies in the auditory system [41, 42, 67-72], and so on. Consistently, malfunction of BK channels leads to different diseases, including epilepsy [73, 74], hypertension [75-82], asthma [83], and motor impairment [84].

Each BK channel is formed by four identical α subunits [85, 86], which is encoded by the *slo1* gene [14-16]. Similarly to most K^+ channels, the four α subunits form a symmetrical tetramer surrounding the conducting pore [85, 86]. Based on electrophysiology and immunocytochemistry studies, each α subunit is composed of a transmembrane domain which contains seven transmembrane segments (S0-S6) and a large cytosolic domain (Figure 1.6) [87, 88]. There are three major structural domains in BK channels: the voltage-sensing domain (VSD) including S1-S4, the pore-gate domain (PGD) including S5-S6, and the cytosolic domain which senses various intracellular signaling ligands.
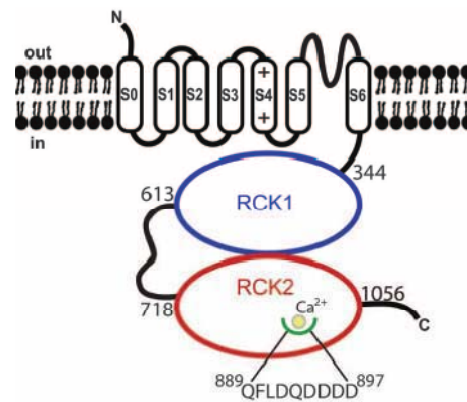
Figure 1.6. Structure scheme of the α subunit of BK channels. The transmembrane domain contains seven transmembrane segments (S0-S6), among which S1-S4 form the voltage-sensing domain (VSD) and S5-S6 form the pore-gate domain (PGD). The large cytosolic domain contains two RCK domains (regulators of K^+ conductance). Domain boundaries and the Ca^{2+} bowl are indicated. Each BK channel is formed by four identical subunits. Figure adapted from ref. [89].

Physiological functions

The BK channel is ubiquitously expressed in the body and plays important roles in many physiological functions. The BK channel is unique among K^+ channels because of its extraordinarily large conductance to K^+ ions (>200 pS in 100 mM symmetrical K^+). Therefore, the BK channel is particularly effective in conducting K^+ current and regulating membrane potential.

The BK channel is unique among K^+ channels also because it can be activated by multiple physiological stimuli, including membrane voltage and intracellular Ca^{2+}. As a result, the BK channel can integrate these two different signals, which makes it an important regulator of intracellular Ca^{2+}, a critical second messenger for a variety of cell activities. For example, the integration of membrane voltage and intracellular Ca^{2+} by the BK channel is critical in smooth muscle cells [90]. In arterial smooth muscle, membrane depolarization triggers opening of the L-type Ca^{2+} channel, which leads to Ca^{2+} influx into the cell. This Ca^{2+} influx results in sarcoplasmic reticulum Ca^{2+} release and thereby increases global cytoplasmic Ca^{2+} level, which promotes muscle cell contraction. At this moment, the BK channel is activated by both elevated Ca^{2+} level and membrane voltage, which leads to outward K^+ flux and lowers membrane voltage. As a result, the Ca^{2+} channel closes and Ca^{2+} level drops, leading to cell relaxation [91, 92]. Loss of function of BK channel in smooth muscle cells results in impaired relaxation in smooth muscle cells, leading to increased constriction in cerebral arteries [75] and tibial arteries [93].

The BK channel can play important roles in varied tissues because its function is tuned to serve different purposes. The major tuning sources include alternative splicing, phosphorylation, and association with modulatory proteins.

Alternative splicing is a process by which the exons of the same pre-mRNA are reconnected in multiple ways during RNA splicing, resulting in different mRNAs which may be translated into different protein isoforms. The BK channel gene (*mslo1*) can be

translated into different variants due to extensive alternative splicing, tuning the function

of the channel [94-98]. For example, the STREX (stress axis-regulated exon) variant is

formed by including an exon that encodes a 59-amino-acid addition in the cytosolic

domain of the channel. The STREX variant is more active than the variant lacking the

exon (the ZERO variant). The inclusion of the STREX exon during translation is

stimulated by exposing adrenal chromaffin cells to androgens or myometrial cells to

progesterone or estrogen receptor antagonists [99, 100]. On the other hand, the exclusion

of the STREX exon is induced by exposing adrenal chromaffin cells to glucocorticoids

[99].

Phosphorylation is the addition of a phosphate group to a protein. Due to its dense

negative charge, the phosphate group may trigger dramatic conformational changes and

alter protein functions. Phosphorylation is catalyzed by an enzyme group named protein

kinases. The BK channel is known to be a phosphorylation target for multiple protein

kinases [101, 102]. Phosphorylation by protein kinase A (PKA) inhibits the STREX

variant of the BK channel but stimulates the ZERO variant [103]. Protein kinase G (PKG)

activates the BK channel through the nitric oxide/cyclic guanosine monophosphate

(cGMP) pathway [104-106]. However, the effect of protein kinase C (PKC) on the BK

channel is unclear. It shows both stimulatory and inhibitory effects on the channel in

different cell types [107-113].

Moreover, association with auxiliary β-subunits tunes the function of the BK channel.

There are four β-subunits (β1- β4), each of which is expressed in specific cell types.

These four β-subunits have distinctive effects on the function of the BK channel [114].

Table 1 summarizes the tissue specificity, effects on BK channel, and physiological

functions of the four β-subunits. Nevertheless, the four β-subunits share structural

homology. They are comprised of two transmembrane segments with intracellular N and

C-termini and a long extracellular loop.

Table 1. β–subunit waveforms and characteristics. Table adapted from ref. [114].

	α	α+β1	α+β2	α+β3a	α+β4
Most abundant expression		Smooth muscle	Brain Pancreas Ovary	Brain Pancreas Spleen Liver	Brain Testes Adrenal gland
Effects on BK channel		↑ Apparent Ca sensitivity ↑ Surface trafficking	Activating Rapid inactivation	Perhaps activating Rapid inactivation Outward rectification	Inhibits channel at low calcium Promotes channel opening at high calcium
Physiologic function		Blood pressure Glomerular filtration Potassium metabolism Bladder function	Unknown	Brain function	Brain function Alcohol tolerance

Shown above are BK channel waveforms and characteristics.

Besides the β-subunits, leucine-rich repeat (LRR)-containing protein 26 (LRRC26) is

recently found to associate with the BK channel in LNCaP prostate cancer cells [115].

The BK channel co-expressed with LRRC26 can be activated at much less membrane

voltage (~ - 140 mV) than BK channel alone, enabling the channel to be activated under

normal physiological conditions for non-excitable cells.

Structure

The detailed structure for the entire BK channel is not available. However, the x-ray

structure of the cytosolic domain has been resolved in two recent papers (Figure 1.7) [89,

116]. In both papers, the cytosolic domain forms a ring-like structure comprising eight

RCK domains (regulators of K^+ conductance) – each of the four subunits contains two

RCK domains: the N-terminal one is called RCK1 and the C-terminal one RCK2 (Figure

1.6). Each RCK1 domain contacts with the RCK2 domain of the same subunit through a

"flexible interface" and contacts with the RCK2 domain of the neighboring subunit

through an "assembly interface". The interfaces are formed by multiple hydrophobic

residues. It is suggested that Ca^{2+} binding to the cytosolic domain may induce

conformational changes of the gating ring that lead to the opening of the gate. Moreover,

in the structure which was crystallized in the presence of high $[Ca^{2+}]$, Ca^{2+} ion is shown

bound to the binding site in the RCK2 domain (Figure 1.7) [89].
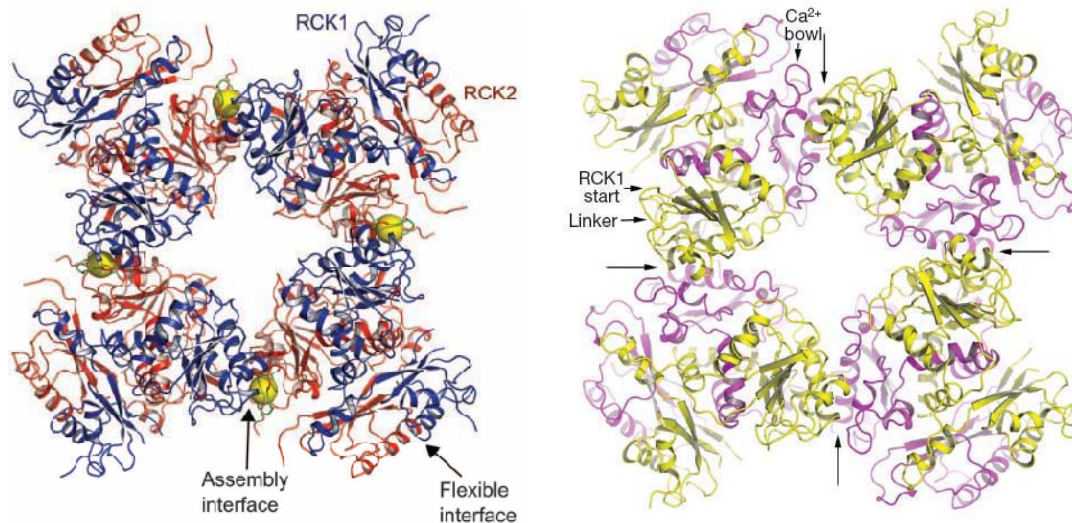
Figure 1.7. Crystallographic structure of the BK channel cytosolic domain viewed down the fourfold symmetry axis. (**left**) The re-constructed cytosolic domain crystallized in the presence of 50 mM Ca^{2+}, with the RCK1 domains colored in blue and RCK2 in red. Golden spheres indicate the Ca^{2+} ions bound to the Ca^{2+} bowl binding site. Arrows indicate the flexible and assembly interfaces. Figure adapted from ref. [89]. (**right**) The cytosolic domain crystallized in the absence of Ca^{2+}, with the RCK1 domains colored in yellow and RCK2 in magenta. Long arrows indicate the assembly interfaces. The linker between the transmembrane and cytosolic domains, the starting point of RCK1, and the Ca^{2+} bowl in RCK2 are labeled for the upper left subunit. Figure adapted from ref. [116].

On the other hand, as of the transmembrane domain that does not have x-ray structure, its similarity in amino acid sequences suggests that the structure is homologous to other K^+ channels. First of all, most parts of the transmembrane domain, including the voltage sensing domain (VSD) and the pore-gate domain (PGD), are homologous to the Kv1.2 channel [117-120]. The Kv1.2 channel is a voltage-gated K^+ channel which comprises a

transmembrane domain and a small cytosolic domain [17]. The transmembrane domain

of the Kv1.2 channel has six transmembrane segments on each subunit (S1-S6). Among

the six segments, S1-S4 form the voltage sensors which are on the periphery of the

channel and surround the pore and gate formed by S5-S6 (Figure 1.4). Nevertheless, in

BK channels, the additional S0 transmembrane segment, which is absent in the Kv1.2

channel, may result in a different arrangement of the other segments.

Secondly, the structural similarity in the transmembrane domain is also suggested by a

BK channel structure with low resolution (17 – 20 Å) [121]. This BK channel structure is

based on a single-particle cryo-EM study. The extracellular side of this BK structure is

very similar to the Kv1.2 channel with only a little variation which may be attributed to

the additional S0 segment (Figure 1.8).
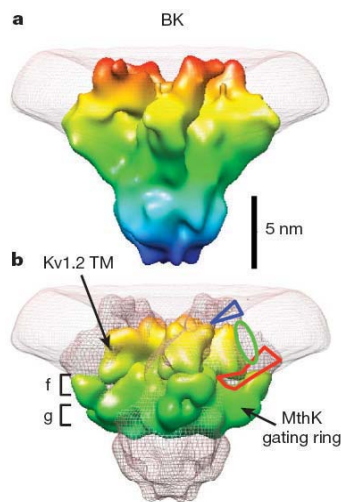
Figure 1.8. Comparison of the BK channel structure with the Kv1.2 and MthK channels. **a**. Side view of the BK channel (colored according to the *z*-coordinate) and the surrounding membrane (white mesh). The structure is based on single-particle cryo-EM study. **b**. Side view of the BK channel (gray mesh) docked with the Kv1.2 transmembrane domain and the MthK gating ring. The peripheral domains of the MthK gating ring are tilted by 36°. The colored voids indicate the possible positions for S0 segment (green), N-

Nevertheless, lack of the entire channel structure leaves the alignment between the

transmembrane and cytosolic domains undetermined. The inter-domain alignment in BK

channels are suggested to be different from other K^+ channels in a functional study by

Yang et al. [119] According to their study, the VSD of one BK channel subunit resides on

top of the cytosolic domain of a neighboring subunit (Figure 1.9), which is different from

the homology model combining the structures of Kv1.2 and MthK which suggests that

the VSD should reside on the cytosolic domain of the same subunit [119, 122]. The

variation may arise from possible interactions between the transmembrane and cytosolic

domains, or from the linker structure between the pore-gate domain and the cytosolic
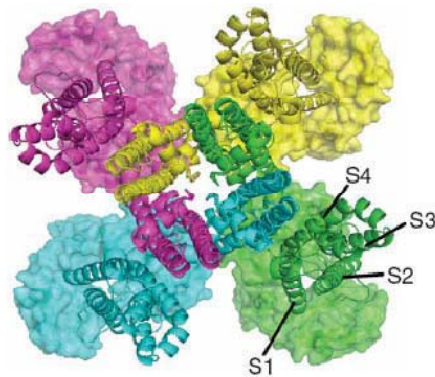
domain.

Figure 1.9. Top view of the BK channel homology structure combining the Kv1.2 and

MthK structures. The Kv1.2 and MthK structures are aligned at their selectivity filters.

Only the transmembrane domain of Kv1.2 and the top four RCK domains of MthK are shown. The four subunits are distinguished from each other by different colors. S1-S4 segments of the transmembrane domain are indicated. Figure adapted from ref. [119].

Activation

The gate opening of BK channels is promoted in response to different stimuli, including depolarization of the membrane potential and elevation of intracellular Ca^{2+} or Mg^{2+} concentration [27, 28, 123, 124]. One important characteristic of the gate activation in BK channels is that the activation gate has a finite open probability even when the voltage sensors are at the resting state and the Ca^{2+} and Mg^{2+} binding sites are empty [125-127]. The transition of the voltage sensors from their resting state to the active state or the binding of Ca^{2+} or Mg^{2+} energetically favors the activation gate at the open state, which leads to a higher open probability. In other words, the opening of the activation gate is modulated, but not completely determined, by the sensors.

Nevertheless, the molecular mechanisms of this modulation remain unclear, although the voltage, Ca^{2+}, and Mg^{2+} sensing sites (the sensors) have been studied extensively and their locations and amino-acid compositions identified (see below). The sensors in BK channels are probably located away from the gate based on the x-ray structures of the cytosolic domain [89, 116] and its sequence homology to the Kv1.2 and MthK channels

[119]. Therefore, the key to this modulation is the allosteric coupling between the sensors and the gate. However, firstly, little is known about the protein structure connecting the sensors with the gate, i.e. the structural pathway conveying local conformational changes at the sensors to the gate is unclear. Furthermore, how the energy of sensor movements propagates to the activation gate is unknown. The studies in my thesis aim to address these questions.

In the following part of the introduction, the key residues for the voltage-, Mg^{2+}-, and Ca^{2+}-dependent activations in BK channels will be presented, and their individual coupling mechanisms with the gate will be discussed.

Voltage-Dependent Activation

BK channels are activated by membrane potential depolarization. In BK channels, the voltage sensor is formed by S1-S4 segments. The voltage sensor moves in response to voltage change and the movement of the voltage sensor is propagated to the activation gate during channel activation. The movement of the voltage sensor is driven by four charged residues: D153 and R167 in S2, D186 in S3, and R213 in S4 [117, 128]. Neutralizing any of these charges by mutagenesis reduces the slope of the G-V relation, thereby partially impairs the voltage sensitivity of the channels.

The voltage sensor moves from a resting state to an active state in response to depolarizing membrane potentials. The movement of the voltage sensors generates

transient gating currents due to the translocation of the above four voltage-sensing charged residues along the electric field [128, 129]. Although the activation of the voltage sensor increases the open probability of the activation gate, it is not obligatory for gate opening, meaning that the movement of the voltage sensor and the opening of the activation gate are allosterically coupled [125]. This conclusion is based on two facts: 1) The movement of the voltage sensor, which is observed as gating currents, is almost completed before the start of the gate opening [125]. 2) At negative voltages (< 20 mV), where the voltage sensor is mostly at the resting state, the open probability of the channels is less voltage dependent. Moreover, at extremely negative voltages (< - 120 mV), where the voltage sensor is completely at the resting state, the open probability remains more than zero [125]. These two facts prove that although the activation of voltage sensor and the gate opening affect each other, neither is obligatory for the other to occur, which satisfies the criteria as an allosteric coupling.

Based on the fact that the transition between the closed and open states of the activation gate occurs despite the state of the voltage sensors, Horrigan et al. proposed the HCA model to illustrate this allosteric coupling [125]. In the HCA model, any number $(0 - 4)$ of voltage sensors can be at the active state no matter whether the activation gate is open or closed, resulting in five closed states $(C_0 - C_4)$ and five open states $(O_0 - O_4)$ of the channel (Figure 1.10). The open probability is calculated as $P_o = 1/(1 + \dfrac{(1+J)^4}{L(1+DJ)^4})$, where

$J = \exp[\dfrac{z_J e}{kT}(V - V_{hC})]$ and $L = L_0 \exp[\dfrac{z_L e}{kT}V]$. P_o is the open probability, J is equilibrium

constant for voltage-sensor activation for each subunit, L is the intrinsic open probability when all voltage sensors are at the resting state, D is the allosteric factor coupling voltage-sensor activation to channel opening, z_J is the amount of net charge movement during voltage-sensor activation, z_L is the amount of net charge movement during gate opening, e is the elementary charge, k is Boltzmann's constant, T is absolute temperature, V_{hC} is the voltage for half of the voltage sensors to be at their activation state when the gate is closed, and V is voltage.
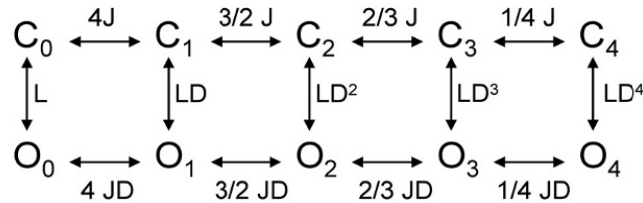
Figure 1.10. HCA model for the allosteric coupling in the voltage activation of BK channels. $C_0 - C_4$ represent closed states of the activation gate with different numbers (0 − 4) of voltage sensor at the active state. $O_0 - O_4$ represent different open states. Figure adapted from ref. [122].

The HCA model has been shown to account for the allosteric coupling in the voltage activation. However, the key structures and residues that convert the voltage sensor movement to the gate opening, i.e. the structure basis for the allosteric coupling, is unclear [122].

Mg^{2+}-Dependent Activation

BK channels are activated by elevation of intracellular Mg^{2+} concentration [123, 124]. The Mg^{2+} binding site is composed of D99 and N172 from the transmembrane domain and E374 and E399 from the cytosolic domain (Figure 1.11) [119, 130, 131]. These four binding coordinates are identified based on the impact of their mutations on the Mg^{2+} activation: neutralizing any of the three negatively charged residues abolishes the Mg^{2+} activation and the Mg^{2+} activation is rescued by mutating N172 to negative residues. Besides these four Mg^{2+} binding coordinates, another residue, Q397, is noteworthy with respect to Mg^{2+} activation. Q397 is not part of the Mg^{2+} binding site, but it is located very close to the binding site and the charges at this residue alters Mg^{2+} activation through electrostatic interaction with the bound Mg^{2+} (Figure 1.11) [130, 132]. More interestingly, when both D99 and Q397 are mutated to cysteines, the two cysteines form a disulfide bond which alters the channel activation. This again proves that Q397 is located in the vicinity of the Mg^{2+} binding site [119].
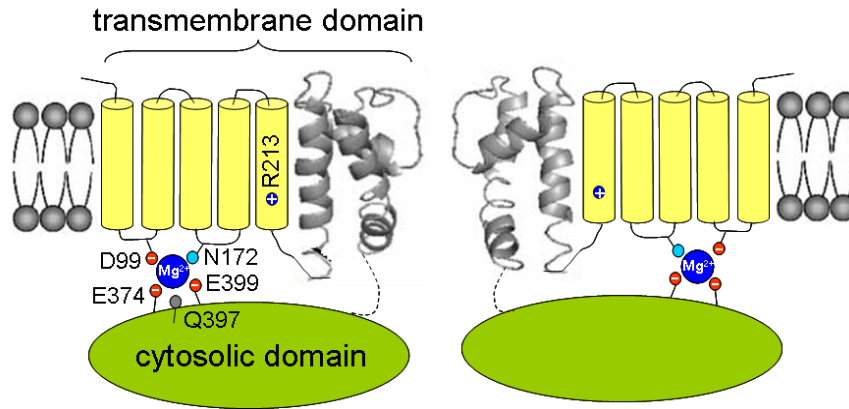
Figure 1.11. Geometry of key residues for the Mg^{2+}-dependent activation in BK channels. The side view of two subunits is shown. The Mg^{2+} binding site is formed by D99 and N172 from the transmembrane domain (yellow) and E374 and E399 from the cytosolic domain (green). The bound Mg^{2+} interacts with R213 to promote channel activation. Q397 is located in the vicinity of the Mg^{2+} binding site.

The bound Mg^{2+} mediates the opening of the activation gate through its electrostatic repulsion with R213, the positive residue that contributes the most gating charge in the voltage sensor [133, 134]. Moreover, its electrostatic interaction with R213 is strongly state-dependent because 10 mM intracellular $[Mg^{2+}]$ reduces the amplitude of the off gating currents (Ig_{OFF}) and slows its relaxation rate, while its effect on the on gating currents (Ig_{ON}) is much smaller [133]. Since Ig_{ON} indicates the movement of the voltage sensor from the resting state to the active state when the channels are closed and Ig_{OFF} indicates the opposite movement when the channels are open, the difference in the effect of Mg^{2+} on Ig_{ON} and Ig_{OFF} suggests that the interaction between the bound Mg^{2+} and R213 is much stronger when the channels are open than closed [133]. Therefore, the

bound Mg^{2+} activates the channels through its influence on the allosteric coupling between the voltage sensor and the activation gate by stabilizing the voltage sensor at its active state when the channels are open.

In addition, when Q397 carries a positive charge by mutagenesis or chemical modification, it mimics the Mg^{2+} effect such that it interacts with R213 through electrostatic interaction and the interaction is much stronger when the channels are open than closed [133].

Ca^{2+}-Dependent Activation

Ca^{2+} binds to the cytosolic domain of BK channels to promote channel activation [135]. Each subunit contains two putative Ca^{2+} binding sites of high-affinity (K_d: 0.8 – 11 μM) [22, 131, 136-139]. One site is known as the calcium bowl which is located at the RCK2 domain where a series of Asp residues reside (Figures 6 and 7) [137]. The other site is located in the RCK1 domain at D367 [131].

There are several residues in the calcium bowl site that are important for the Ca^{2+} activation [138]. The mutation of five sequential Asp (D897–D901) to Asn (the 5D5N mutation) reduces the most Ca^{2+} activation [137, 138]. Similarly, the site in the RCK1 domain also has multiple, but discrete, important residues regarding Ca^{2+} activation. First of all, the mutation of two Asp residues (D362A/D367A) was found to abolish the rest of the Ca^{2+} activation after the calcium bowl is mutated by the 5D5N mutation [131].

Secondly, the mutation of a Met residue (M513I) partially disrupts, though not entirely, the Ca^{2+} activation that is derived from the RCK1 domain [139]. Either of the putative binding sites is studied by mutating the other site, using the mutations mentioned above. The effects of the two binding sites are additive, meaning that the summed Ca^{2+} activation of either site when the other site is mutated approximately equals to the Ca^{2+} activation in the intact wild-type channels. Therefore, the two Ca^{2+} binding sites activate the activation gate through independent molecular mechanisms [131, 139]. However, a study based on single-channel recordings found that the Ca^{2+} binding sites on the same subunits cooperate positively in activating the gate [140]. But the impact of this positive cooperativity on macroscopic currents is unclear [122].

The Ca^{2+} activation that is derived from the RCK1 Ca^{2+} binding site has been suggested to be the target for other modulation mechanisms. For example, carbon monoxide (CO) and H^+ may associate in the vicinity of the D367 residue, altering the Ca^{2+} binding at D367 so that the channel activation is modulated [141, 142]. Moreover, D367 is located only two residues in front of an Asp residue (D369), whose Gly mutation is associated with the human disease of coexistent generalized epilepsy and paroxysmal dyskinesia (GEPD) [73]. The D369G mutation enhances the Ca^{2+} activation of the BK channels probably also through its influence on the Ca^{2+} activation derived from the RCK1 binding site.

The Ca^{2+} binding activates the activation gate through a mechanism that is independent from the mechanisms for the voltage or Mg^{2+} activation. It is independent from the voltage activation because at extremely negative voltages, where the voltage sensor is at the resting state, 100 μM Ca^{2+} increases the open probability by more than 2000 times [126, 127]. Meanwhile, 100 μM Ca^{2+} increases the channel activation to the same extent despite the Mg^{2+} concentration [143, 144]. Therefore, neither the voltage nor Mg^{2+} activation is necessary for the Ca^{2+} activation. The coupling between the Ca^{2+} binding sites and the activation gate is through an independent mechanism.

Since neither the opening of the activation gate nor the Ca^{2+} binding to the binding site is obligatory for the other to occur, the coupling between the two processes is allosteric. Similar to the HCA model, the MWC model is used to describe allosteric couplings but more specialized in ligand binding processes [145]. The central idea of the MWC model is that the ligand binding at one of the multiple binding sites would alter the overall conformation of the protein such that the binding affinity of all the binding sites is altered consequentially. In the case of BK channel activation, the overall conformational change includes the opening of the activation gate, as well as the local conformational change at the Ca^{2+} binding sites that results in higher Ca^{2+} binding affinity. Therefore, the binding site bound with Ca^{2+} energetically prefers the high-affinity conformation so as to induce the overall conformational change and favor the opening of the activation gate.

The structure scheme of the MWC model (Figure 1.12) is the same as the HCA model, in which the activation of voltage sensors is replaced by the activation of Ca^{2+} sites upon Ca^{2+} binding [146] [147].

$$C \xleftrightarrow{4K_C} CCa \xleftrightarrow{3/2K_C} CCa_2 \xleftrightarrow{2/3K_C} CCa_3 \xleftrightarrow{1/4K_C} CCa_4$$

$$\updownarrow L \quad \updownarrow Lc \quad \updownarrow Lc^2 \quad \updownarrow Lc^3 \quad \updownarrow Lc^4$$

$$O \xleftrightarrow{4K_O} OCa \xleftrightarrow{3/2K_O} OCa_2 \xleftrightarrow{2/3K_O} OCa_3 \xleftrightarrow{1/4K_O} OCa_4$$
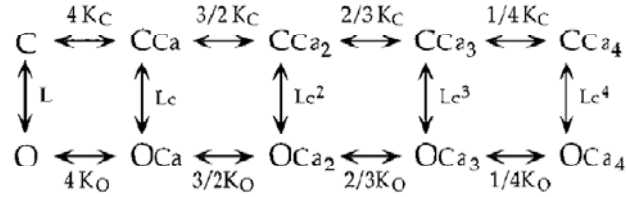
Figure 1.12. MWC model for the allosteric coupling in the Ca^{2+} activation of BK channels. $C - C_{Ca4}$ represent the closed states of the activation gate with different numbers $(0 - 4)$ of Ca^{2+} binding sites occupied by Ca^{2+}. $O - O_{Ca4}$ represent different open states. The binding of every Ca^{2+} alters the balance between the closed and open states of the gate by the factor $c = K_O/K_C$. Figure adapted from ref. [126].

Following is the open probability versus Ca^{2+} concentration and membrane potential:

$$P_{open} = \cfrac{1}{1 + L(0) \cdot e^{\frac{-zeV}{kT}} \cdot \left[\cfrac{1 + \cfrac{[Ca^{2+}]}{K_C}}{1 + \cfrac{[Ca^{2+}]}{K_O}} \right]^4}$$

30

Where P_{open} is channel's open probability; $L(0)$ is the equilibrium-state ratio of closed to open channels ([C]/[O]) in the absence of bound Ca^{2+} at 0 mV; z is the number of equivalent charges; e, V, k, and T are the same as above in the HCA model; K_c and K_o are the dissociation constants of Ca^{2+} in the closed and open states, respectively. Note that this form of MWC model assumes only one Ca^{2+} binding site on each subunit. However, in the MWC model, the dependence on membrane potential is simplified in that all the voltage sensors are assumed to move simultaneously. A more complicated model may be derived as in Figure 1.13 if the movement of the voltage sensor is independent from other voltage sensors [127]:
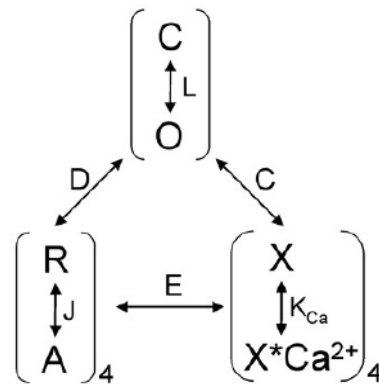
Figure 1.13. Allosteric coupling between the gate opening (C − O), voltage-sensor activation (R − A), and Ca^{2+} binding (X − X*Ca^{2+}). The allosteric factors coupling these processes are C, D, and E. Here each subunit is assumed to have only one Ca^{2+} binding site. Figure adapted from ref. [122].

In the studies on the molecular mechanisms of the allosteric coupling between Ca^{2+} binding and gate opening, progress has been made in identifying important structural components regarding the Ca^{2+} activation. Firstly, a peptide linker of 16 amino acids connects the S6 transmembrane segment (S6 functions as the activation gate in many K^+ channels) with the cytosolic domain. Altering the length of the linker by inserting or deleting a different number of amino acids not only changes the open probability of the activation gate in the absence of Ca^{2+}, but also changes the Ca^{2+} activation [148]. A longer linker decreases the open probability and reduces the Ca^{2+} activation, while a shorter linker increases the open probability and enhances the Ca^{2+} activation. This result is consistent with the hypothesis that the cytosolic domain pulls the S6 segment via the linker to promote gate activation, same as in the Ca^{2+}-activated MthK channel [21].

Secondly, chimera studies suggest that the N-terminal part of the RCK1 domain (the AC region) is responsible for the *Drosophila* BK channels (dSlo1) to have higher Ca^{2+} activation than the mouse BK channels (mSlo1) [149]. The molecular dynamics simulation based on the MthK AC region structure indicates that the AC region of the dSlo1 channel is more tightly packed and less flexible than that of the mSlo1 channel, which suggests that the dynamics of the AC region may play an important role in the allosteric coupling of Ca^{2+} activation. Moreover, the AC region is found to be close to the transmembrane domain, even making physical contact at multiple locations [119, 133]; thereby, the AC region may directly interact with the activation gate to realize the allosteric coupling for Ca^{2+} activation.

Additionally, the chimera studies on the β subunits suggest that both the linker and the AC region are critical for β2 to enhance the Ca^{2+} activation [150].

The next two chapters of this dissertation both focus on the molecular mechanism of the allosteric coupling for Ca^{2+} activation. In the first chapter, the pathway for the RCK1 Ca^{2+} binding site is dissected and the importance of its dynamics for Ca^{2+} activation is proven. In the second chapter, the inter-domain alignment between the transmembrane and cytosolic domains is proven to be important for many channel properties, including Ca^{2+} activation.

References

1.   Augustine, G.J., et al., *Neuroscience*. Fourth ed, ed. D. Purves, et al. 2008, Sunderland, MA, USA: Sinauer Associates, Inc.

2.   Hodgkin, A.L. and A.F. Huxley, *A quantitative description of membrane current and its application to conduction and excitation in nerve.* J Physiol, 1952. 117(4): p. 500-44.

3.   Hille, B., *Ion Channels of Excitable Membranes*. 3rd ed. 2001, Sunderland, MA: Sinauer Associates, Inc.

4.   Heginbotham, L., et al., *Mutations in the K+ channel signature sequence.* Biophys J, 1994. 66(4): p. 1061-7.

5.   Doyle, D.A., et al., *The structure of the potassium channel: molecular basis of K+ conduction and selectivity.* Science, 1998. 280(5360): p. 69-77.

6.   Zhou, Y., et al., *Chemistry of ion coordination and hydration revealed by a K+ channel-Fab complex at 2.0 A resolution.* Nature, 2001. 414(6859): p. 43-8.

7.   Jiang, Y., et al., *The open pore conformation of potassium channels.* Nature, 2002. 417(6888): p. 523-6.

8.   MacKinnon, R., *Potassium channels.* FEBS Letters, 2003. 555(1): p. 62-65.

9.   Sigworth, F.J., *Voltage gating of ion channels.* Q Rev Biophys, 1994. 27(1): p. 1-40.

10.   Bezanilla, F., *The voltage sensor in voltage-dependent ion channels.* Physiol Rev, 2000. 80(2): p. 555-92.

11.   Bezanilla, F. and C.M. Armstrong, *Gating currents of the sodium channels: three ways to block them.* Science, 1974. 183(126): p. 753-4.

12.   Schoppa, N.E., et al., *The size of gating charge in wild-type and mutant Shaker potassium channels.* Science, 1992. 255(5052): p. 1712-5.

13.   Seoh, S.A., et al., *Voltage-sensing residues in the S2 and S4 segments of the Shaker K+ channel.* Neuron, 1996. 16(6): p. 1159-67.

14.   Atkinson, N.S., G.A. Robertson, and B. Ganetzky, *A component of calcium-activated potassium channels encoded by the Drosophila slo locus.* Science, 1991. 253(5019): p. 551-555.

15.   Butler, A., et al., *mSlo, a complex mouse gene encoding "maxi" calcium-activated potassium channels.* Science, 1993. 261(5118): p. 221-224.

16.   Adelman, J.P., et al., *Calcium-activated potassium channels expressed from cloned complementary DNAs.* Neuron, 1992. 9(2): p. 209-216.

17.   Long, S.B., E.B. Campbell, and R. MacKinnon, *Crystal structure of a mammalian voltage-dependent shaker family K$^+$ channel.* Science, 2005. 309(5736): p. 897-903.

18.   Long, S.B., E.B. Campbell, and R. MacKinnon, *Voltage sensor of Kv1.2: structural basis of electromechanical coupling.* Science, 2005. 309(5736): p. 903-908.

19.   Marty, A., *Ca-dependent K channels with large unitary conductance in chromaffin cell membranes.* Nature, 1981. 291(5815): p. 497-500.

20.   Wickman, K. and D.E. Clapham, *Ion channel regulation by G proteins.* Physiol Rev, 1995. 75(4): p. 865-85.

21.   Jiang, Y., et al., *Crystal structure and mechanism of a calcium-gated potassium channel.* Nature, 2002. 417(6888): p. 515-522.

22.   Lingle, C.J., *Gating rings formed by RCK domains: keys to gate opening.* J Gen Physiol, 2007. 129(2): p. 101-7.

23.   Jiang, Y., et al., *Structure of the RCK domain from the E. coli K$^+$ channel and demonstration of its presence in the human BK channel.* Neuron, 2001. 29(3): p. 593-601.

24.   Fodor, A.A. and R.W. Aldrich, *Statistical limits to the identification of ion channel domains by sequence similarity.* J Gen Physiol, 2006. 127(6): p. 755-66.

25.   Fodor, A.A. and R.W. Aldrich, *Convergent evolution of alternative splices at domain boundaries of the BK channel.* Annu Rev Physiol, 2009. 71: p. 19-36.

26.   Albright, R.A., et al., *The RCK domain of the KtrAB K+ transporter: multiple conformations of an octameric ring.* Cell, 2006. 126(6): p. 1147-59.

27.   Latorre, R. and C. Miller, *Conduction and selectivity in potassium channels.* J. Membr. Biol., 1983. 71(1-2): p. 11-30.

28.   Latorre, R., et al., *Varieties of calcium-activated potassium channels.* Annu. Rev. Physiol., 1989. 51: p. 385-99.

29.   Latorre, R., C. Vergara, and C. Hidalgo, *Reconstitution in planar lipid bilayers of a Ca2+-dependent K+ channel from transverse tubule membranes isolated from rabbit skeletal muscle.* Proc Natl Acad Sci U S A, 1982. 79(3): p. 805-9.

30.   Barrett, J.N., K.L. Magleby, and B.S. Pallotta, *Properties of single calcium-activated potassium channels in cultured rat muscle.* J Physiol, 1982. 331: p. 211-30.

31.   Pallotta, B.S., K.L. Magleby, and J.N. Barrett, *Single channel recordings of Ca2+-activated K+ currents in rat muscle cell culture.* Nature, 1981. 293(5832): p. 471-4.

32.   Inoue, R., K. Kitamura, and H. Kuriyama, *Two Ca-dependent K-channels classified by the application of tetraethylammonium distribute to smooth muscle membranes of the rabbit portal vein.* Pflugers Arch, 1985. 405(3): p. 173-9.

33.   Toro, L., L. Vaca, and E. Stefani, *Calcium-activated potassium channels from coronary smooth muscle reconstituted in lipid bilayers.* Am J Physiol, 1991. 260(6 Pt 2): p. H1779-89.

34.   McCobb, D.P., et al., *A human calcium-activated potassium channel gene expressed in vascular smooth muscle.* Am J Physiol, 1995. 269(3 Pt 2): p. H767-77.

35.   Meredith, A.L., et al., *Overactive bladder and incontinence in the absence of the BK large conductance Ca2+-activated K+ channel.* J Biol Chem, 2004. 279(35): p. 36746-52.

36.   Kume, H., et al., *Regulation of Ca2+-dependent K+-channel activity in tracheal myocytes by phosphorylation.* Nature, 1989. 341(6238): p. 152-4.

37.   Kume, H., M.P. Graziano, and M.I. Kotlikoff, *Stimulatory and inhibitory regulation of calcium-activated potassium channels by guanine nucleotide-binding proteins.* Proc Natl Acad Sci U S A, 1992. 89(22): p. 11051-5.

38.   Savaria, D., et al., *Large conducting potassium channel reconstituted from airway smooth muscle.* Am J Physiol, 1992. 262(3 Pt 1): p. L327-36.

39.   Markwardt, F. and G. Isenberg, *Gating of maxi K+ channels studied by Ca2+ concentration jumps in excised inside-out multi-channel patches (myocytes from guinea pig urinary bladder).* J Gen Physiol, 1992. 99(6): p. 841-62.

40.   Ohmori, H., *Studies of ionic currents in the isolated vestibular hair cell of the chick.* J Physiol, 1984. 350: p. 561-81.

41.   Hudspeth, A.J. and R.S. Lewis, *Kinetic analysis of voltage- and ion-dependent conductances in saccular hair cells of the bull-frog, Rana catesbeiana.* J Physiol, 1988. 400: p. 237-74.

42.   Fuchs, P.A., T. Nagai, and M.G. Evans, *Electrical tuning in hair cells isolated from the chick cochlea.* J Neurosci, 1988. 8(7): p. 2460-7.

43.   Roberts, W.M., R.A. Jacobs, and A.J. Hudspeth, *Colocalization of ion channels involved in frequency selectivity and synaptic transmission at presynaptic active zones of hair cells.* J Neurosci, 1990. 10(11): p. 3664-84.

44.   Issa, N.P. and A.J. Hudspeth, *Clustering of Ca2+ channels and Ca(2+)-activated K+ channels at fluorescently labeled presynaptic active zones of hair cells.* Proc Natl Acad Sci U S A, 1994. 91(16): p. 7578-82.

45.   Neely, A. and C.J. Lingle, *Two components of calcium-activated potassium current in rat adrenal chromaffin cells.* J Physiol, 1992. 453: p. 97-131.

46.   Neely, A. and C.J. Lingle, *Effects of muscarine on single rat adrenal chromaffin cells.* J Physiol, 1992. 453: p. 133-66.

47.   Solaro, C.R., et al., *Inactivating and noninactivating Ca(2+)- and voltage-dependent K+ current in rat adrenal chromaffin cells.* J Neurosci, 1995. 15(9): p. 6110-23.

48.   Marty, A. and E. Neher, *Potassium channels in cultured bovine adrenal chromaffin cells.* J Physiol, 1985. 367: p. 117-41.

49.   Lingle, C.J., et al., *Calcium-activated potassium channels in adrenal chromaffin cells.* Ion Channels, 1996. 4: p. 261-301.

50.   Adams, P.R., et al., *Intracellular Ca2+ activates a fast voltage-sensitive K+ current in vertebrate sympathetic neurones.* Nature, 1982. 296(5859): p. 746-9.

51.   Faber, E.S. and P. Sah, *Ca2+-activated K+ (BK) channel inactivation contributes to spike broadening during repetitive firing in the rat lateral amygdala.* J Physiol, 2003. 552(Pt 2): p. 483-97.

52.   Lancaster, B. and R.A. Nicoll, *Properties of two calcium-activated hyperpolarizations in rat hippocampal neurones.* J Physiol, 1987. 389: p. 187-203.

53.   Knaus, H.G., et al., *Distribution of high-conductance Ca(2+)-activated K+ channels in rat brain: targeting to axons and nerve terminals.* J Neurosci, 1996. 16(3): p. 955-63.

54.   Maue, R.A. and V.E. Dionne, *Patch-clamp studies of isolated mouse olfactory receptor neurons.* J Gen Physiol, 1987. 90(1): p. 95-125.

55.   Hu, H., et al., *Presynaptic Ca2+-activated K+ channels in glutamatergic hippocampal terminals and their role in spike repolarization and regulation of transmitter release.* J Neurosci, 2001. 21(24): p. 9585-97.

56.   Robitaille, R. and M.P. Charlton, *Presynaptic calcium signals and transmitter release are modulated by calcium-activated potassium channels.* J Neurosci, 1992. 12(1): p. 297-305.

57.   Robitaille, R., et al., *Functional colocalization of calcium and calcium-gated potassium channels in control of transmitter release.* Neuron, 1993. 11(4): p. 645-55.

58.   Ling, S., et al., *Syntaxin 1A co-associates with native rat brain and cloned large conductance, calcium-activated potassium channels in situ.* J Physiol, 2003. 553(Pt 1): p. 65-81.

59.   Cibulsky, S.M., H. Fei, and I.B. Levitan, *Syntaxin-1A binds to and modulates the Slo calcium-activated potassium channel via an interaction that excludes syntaxin binding to calcium channels.* J Neurophysiol, 2005. 93(3): p. 1393-405.

60.   Orio, P., et al., *New Disguises for an Old Channel: MaxiK Channel {beta}-Subunits.* News Physiol Sci, 2002. 17(4): p. 156-161.

61.   Wong, B.S., H. Lecar, and M. Adler, *Single calcium-dependent potassium channels in clonal anterior pituitary cells.* Biophys J, 1982. 39(3): p. 313-7.

62.   Findlay, I., M.J. Dunne, and O.H. Petersen, *High-conductance K+ channel in pancreatic islet cells can be activated and inactivated by internal calcium.* J Membr Biol, 1985. 83(1-2): p. 169-75.

63.   Storm, J.F., *Action potential repolarization and a fast after-hyperpolarization in rat hippocampal pyramidal cells.* J Physiol, 1987. 385: p. 733-59.

64.   Shao, L.R., et al., *The role of BK-type Ca2+-dependent K+ channels in spike broadening during repetitive firing in rat hippocampal pyramidal cells.* J Physiol, 1999. 521 Pt 1: p. 135-46.

65.   Faber, E.S. and P. Sah, *Calcium-activated potassium channels: multiple contributions to neuronal function.* Neuroscientist, 2003. 9(3): p. 181-94.

66.   Gu, N., K. Vervaeke, and J.F. Storm, *BK potassium channels facilitate high-frequency firing and cause early spike frequency adaptation in rat CA1 hippocampal pyramidal cells.* J. Physiol., 2007. 580(3): p. 859-882.

67.   Hudspeth, A.J. and R.S. Lewis, *A model for electrical resonance and frequency tuning in saccular hair cells of the bull-frog, Rana catesbeiana.* J Physiol, 1988. 400: p. 275-97.

68.   Art, J.J., Y.C. Wu, and R. Fettiplace, *The calcium-activated potassium channels of turtle hair cells.* J Gen Physiol, 1995. 105(1): p. 49-72.

69.   Wu, Y.C., et al., *A kinetic description of the calcium-activated potassium channel and its application to electrical tuning of hair cells.* Prog Biophys Mol Biol, 1995. 63(2): p. 131-58.

70.   Art, J.J. and R. Fettiplace, *Variation of membrane properties in hair cells isolated from the turtle cochlea.* J Physiol, 1987. 385: p. 207-42.

71.   Fuchs, P.A. and M.G. Evans, *Potassium currents in hair cells isolated from the cochlea of the chick.* J Physiol, 1990. 429: p. 529-51.

72.   Mammano, F., et al., *Ca2+ signaling in the inner ear.* Physiology (Bethesda), 2007. 22: p. 131-44.

73.   Du, W., et al., *Calcium-sensitive potassium channelopathy in human epilepsy and paroxysmal movement disorder.* Nat. Genet., 2005. 37(7): p. 733-738.

74.   Brenner, R., et al., *BK channel [beta]4 subunit reduces dentate gyrus excitability and protects against temporal lobe seizures.* Nat. Neurosci., 2005. 8(12): p. 1752-1759.

75.   Brenner, R., et al., *Vasoregulation by the beta1 subunit of the calcium-activated potassium channel.* Nature, 2000. 407(6806): p. 870-6.

76.   Patterson, A.J., J. Henrie-Olson, and R. Brenner, *Vasoregulation at the molecular level: a role for the beta1 subunit of the calcium-activated potassium (BK) channel.* Trends Cardiovasc Med, 2002. 12(2): p. 78-82.

77.   Amberg, G.C., et al., *Modulation of the molecular composition of large conductance, Ca(2+) activated K(+) channels in vascular smooth muscle during hypertension.* J Clin Invest, 2003. 112(5): p. 717-24.

78.   Amberg, G.C. and L.F. Santana, *Downregulation of the BK channel beta1 subunit in genetic hypertension.* Circ Res, 2003. 93(10): p. 965-71.

79.   Fernandez-Fernandez, J.M., et al., *Gain-of-function mutation in the KCNMB1 potassium channel subunit is associated with low prevalence of diastolic hypertension.* J Clin Invest, 2004. 113(7): p. 1032-9.

80.   Senti, M., et al., *Protective effect of the KCNMB1 E65K genetic polymorphism against diastolic hypertension in aging women and its relevance to cardiovascular risk.* Circ Res, 2005. 97(12): p. 1360-5.

81.   Chang, T., L. Wu, and R. Wang, *Altered expression of BK channel beta1 subunit in vascular tissues from spontaneously hypertensive rats.* Am J Hypertens, 2006. 19(7): p. 678-85.

82.   Pluger, S., et al., *Mice with disrupted BK channel beta1 subunit gene feature abnormal Ca(2+) spark/STOC coupling and elevated blood pressure.* Circ Res, 2000. 87(11): p. E53-60.

83.   Seibold, M.A., et al., *An african-specific functional polymorphism in KCNMB1 shows sex-specific association with asthma severity.* Hum Mol Genet, 2008. 17(17): p. 2681-90.

84.   Sausbier, M., et al., *Cerebellar ataxia and Purkinje cell dysfunction caused by Ca2+-activated K+ channel deficiency.* Proc Natl Acad Sci U S A, 2004. 101(25): p. 9474-8.

85.   Quirk, J.C. and P.H. Reinhart, *Identification of a novel tetramerization domain in large conductance K(ca) channels.* Neuron, 2001. 32(1): p. 13-23.

86.   Shen, K.Z., et al., *Tetraethylammonium block of Slowpoke calcium-activated potassium channels expressed in Xenopus oocytes: Evidence for tetrameric channel formation.* Pflügers Arch., 1994. 426(5): p. 440-445.

87.   Meera, P., et al., *Large conductance voltage- and calcium-dependent K+ channel, a distinct member of voltage-dependent ion channels with seven N-terminal transmembrane segments (S0-S6), an extracellular N terminus, and an intracellular (S9-S10) C terminus.* Proc Natl Acad Sci U S A, 1997. 94(25): p. 14066-71.

88.   Wallner, M., P. Meera, and L. Toro, *Determinant for beta-subunit regulation in high-conductance voltage-activated and Ca(2+)-sensitive K+ channels: an additional transmembrane region at the N terminus.* Proc Natl Acad Sci U S A, 1996. 93(25): p. 14922-7.

89.   Yuan, P., et al., *Structure of the human BK channel Ca2+-activation apparatus at 3.0 A resolution.* Science, 2010. 329(5988): p. 182-6.

90.   Wray, S. and T. Burdyga, *Sarcoplasmic reticulum function in smooth muscle.* Physiol Rev. 90(1): p. 113-78.

91.   Nelson, M.T., et al., *Relaxation of arterial smooth muscle by calcium sparks.* Science, 1995. 270(5236): p. 633-7.

92.   Ohi, Y., et al., *Local Ca(2+) transients and distribution of BK channels and ryanodine receptors in smooth muscle cells of guinea-pig vas deferens and urinary bladder.* J Physiol, 2001. 534(Pt. 2): p. 313-26.

93.   Sausbier, M., et al., *Elevated blood pressure linked to primary hyperaldosteronism and impaired vasodilation in BK channel-deficient mice.* Circulation, 2005. 112(1): p. 60-8.

94.   Ferrer, J., et al., *Cloning of human pancreatic islet large conductance Ca(2+)-activated K+ channel (hSlo) cDNAs: evidence for high levels of expression in pancreatic islets and identification of a flanking genetic marker.* Diabetologia, 1996. 39(8): p. 891-8.

95.   Xie, J. and D.P. McCobb, *Control of alternative splicing of potassium channels by stress hormones.* Science, 1998. 280(5362): p. 443-6.

96.   Zhang, Y., et al., *The appearance of a protein kinase A-regulated splice isoform of slo is associated with the maturation of neurons that control reproductive behavior.* J Biol Chem, 2004. 279(50): p. 52324-30.

97.   Chen, L., et al., *Functionally diverse complement of large conductance calcium- and voltage-activated potassium channel (BK) alpha-subunits generated from a single site of splicing.* J Biol Chem, 2005. 280(39): p. 33599-609.

98.   Ma, D., et al., *Differential trafficking of carboxyl isoforms of Ca2+-gated (Slo1) potassium channels.* FEBS Lett, 2007. 581(5): p. 1000-8.

99.   Lai, G.J. and D.P. McCobb, *Opposing actions of adrenal androgens and glucocorticoids on alternative splicing of Slo potassium channels in bovine chromaffin cells.* Proc Natl Acad Sci U S A, 2002. 99(11): p. 7722-7.

100.   Zhu, N., et al., *Alternative splicing of Slo channel gene programmed by estrogen, progesterone and pregnancy.* FEBS Lett, 2005. 579(21): p. 4856-60.

101. Schubert, R. and M.T. Nelson, *Protein kinases: tuners of the BKCa channel in smooth muscle.* Trends Pharmacol Sci, 2001. 22(10): p. 505-12.

102. Widmer, H.A., I.C. Rowe, and M.J. Shipston, *Conditional protein phosphorylation regulates BK channel activity in rat cerebellar Purkinje neurons.* J Physiol, 2003. 552(Pt 2): p. 379-91.

103. Tian, L., et al., *Distinct stoichiometry of BKCa channel tetramer phosphorylation specifies channel activation and inhibition by cAMP-dependent protein kinase.* Proc Natl Acad Sci U S A, 2004. 101(32): p. 11897-902.

104. White, R.E., et al., *Potassium channel stimulation by natriuretic peptides through cGMP-dependent dephosphorylation.* Nature, 1993. 361(6409): p. 263-6.

105. Stockand, J.D. and S.C. Sansom, *Mechanism of activation by cGMP-dependent protein kinase of large Ca(2+)-activated K+ channels in mesangial cells.* Am J Physiol, 1996. 271(5 Pt 1): p. C1669-77.

106. White, R.E., D.J. Darkow, and J.L. Lang, *Estrogen relaxes coronary arteries by opening BKCa channels through a cGMP-dependent mechanism.* Circ Res, 1995. 77(5): p. 936-42.

107. Barman, S.A., S. Zhu, and R.E. White, *PKC activates BKCa channels in rat pulmonary arterial smooth muscle via cGMP-dependent protein kinase.* Am J Physiol Lung Cell Mol Physiol, 2004. 286(6): p. L1275-81.

108. Barman, S.A., S. Zhu, and R.E. White, *Protein kinase C inhibits BKCa channel activity in pulmonary arterial smooth muscle.* Am J Physiol Lung Cell Mol Physiol, 2004. 286(1): p. L149-55.

109.   Bayguinov, O., et al., *Coupling strength between localized Ca(2+) transients and K(+) channels is regulated by protein kinase C.* Am J Physiol Cell Physiol, 2001. 281(5): p. C1512-23.

110.   Kim, J.Y. and C.S. Park, *Potentiation of large-conductance calcium-activated potassium (BK(Ca)) channels by a specific isoform of protein kinase C.* Biochem Biophys Res Commun, 2008. 365(3): p. 459-65.

111.   Shipston, M.J. and D.L. Armstrong, *Activation of protein kinase C inhibits calcium-activated potassium channels in rat pituitary tumour cells.* J Physiol, 1996. 493 (Pt 3): p. 665-72.

112.   Zhu, S., et al., *Mutation of protein kinase C phosphorylation site S1076 on alpha-subunits affects BK(Ca) channel activity in HEK-293 cells.* Am J Physiol Lung Cell Mol Physiol, 2009. 297(4): p. L758-66.

113.   Zhu, S., R.E. White, and S.A. Barman, *Effect of PKC isozyme inhibition on forskolin-induced activation of BKCa channels in rat pulmonary arterial smooth muscle.* Lung, 2006. 184(2): p. 89-97.

114.   Wu, R.S. and S.O. Marx, *The BK potassium channel in the vascular smooth muscle and kidney: alpha- and beta-subunits.* Kidney Int, 2010. 78(10): p. 963-74.

115.   Yan, J. and R.W. Aldrich, *LRRC26 auxiliary protein allows BK channel activation at resting voltage without calcium.* Nature, 2010. 466(7305): p. 513-6.

116.   Wu, Y., et al., *Structure of the gating ring from the human large-conductance Ca(2+)-gated K(+) channel.* Nature, 2010. doi: 10.1038/nature09252.

117.   Ma, Z., X.J. Lou, and F.T. Horrigan, *Role of charged residues in the S1-S4 voltage sensor of BK channels.* J Gen Physiol, 2006. 127(3): p. 309-28.

118.   Liu, G., et al., *Position and role of the BK channel alpha subunit S0 helix inferred from disulfide crosslinking.* J Gen Physiol, 2008. 131(6): p. 537-48.

119.   Yang, H., et al., *Activation of Slo1 BK channels by Mg^{2+} coordinated between the voltage sensor and RCK1 domains.* Nat. Struct. Mol. Biol., 2008. 15(11): p. 1152-1159.

120.   Liu, G., et al., *Locations of the beta1 transmembrane helices in the BK potassium channel.* Proc Natl Acad Sci U S A, 2008. 105(31): p. 10727-32.

121.   Wang, L. and F.J. Sigworth, *Structure of the BK potassium channel in a lipid membrane from electron cryomicroscopy.* Nature, 2009. 461(7261): p. 292-295.

122.   Cui, J., H. Yang, and U. Lee, *Molecular mechanisms of BK channel activation.* Cell. Mol. Life Sci., 2008. 66(5): p. 852-875.

123.   Golowasch, J., A. Kirkwood, and C. Miller, *Allosteric effects of Mg2+ on the gating of Ca2+-activated K+ channels from mammalian skeletal muscle.* J Exp Biol, 1986. 124: p. 5-13.

124.   Oberhauser, A., O. Alvarez, and R. Latorre, *Activation by divalent cations of a Ca2+-activated K+ channel from skeletal muscle membrane.* J Gen Physiol, 1988. 92(1): p. 67-86.

125.   Horrigan, F.T., J. Cui, and R.W. Aldrich, *Allosteric voltage gating of potassium channels I. Mslo ionic currents in the absence of Ca^{2+}.* J. Gen. Physiol., 1999. 114(2): p. 277-304.

126.   Cui, J. and R.W. Aldrich, *Allosteric linkage between voltage and Ca^{2+}-dependent activation of BK-type mslo1 K$^+$ channels.* Biochemistry, 2000. 39(50): p. 15612-15619.

127.   Horrigan, F.T. and R.W. Aldrich, *Coupling between voltage sensor activation, Ca^{2+} binding and channel opening in large conductance (BK) potassium channels.* J. Gen. Physiol., 2002. 120(3): p. 267-305.

128.   Horrigan, F.T. and R.W. Aldrich, *Allosteric voltage gating of potassium channels II. Mslo channel gating charge movement in the absence of Ca^{2+}.* J Gen Physiol, 1999. 114(2): p. 305-36.

129.   Stefani, E., et al., *Voltage-controlled gating in a large conductance Ca2+-sensitive K+channel (hslo).* Proc Natl Acad Sci U S A, 1997. 94(10): p. 5427-31.

130.   Shi, J., et al., *Mechanism of magnesium activation of calcium-activated potassium channels.* Nature, 2002. 418(6900): p. 876-880.

131.   Xia, X.-M., X. Zeng, and C.J. Lingle, *Multiple regulatory sites in large-conductance calcium-activated potassium channels.* Nature, 2002. 418(6900): p. 880-884.

132.   Yang, H., et al., *Tuning magnesium sensitivity of BK channels by mutations.* Biophys. J., 2006. 91(8): p. 2892-900.

133.   Yang, H., et al., *Mg^{2+} mediates interaction between the voltage sensor and cytosolic domain to activate BK channels.* Proc. Natl. Acad. Sci. U S A, 2007. 104(46): p. 18270-5.

134.   Horrigan, F.T. and Z. Ma, *Mg2+ enhances voltage sensor/gate coupling in BK channels.* J Gen Physiol, 2008. 131(1): p. 13-32.

135.   Wei, A., et al., *Calcium sensitivity of BK-type KCa channels determined by a separable domain.* Neuron, 1994. 13(3): p. 671-81.

136.   Salkoff, L., et al., *High-conductance potassium channels of the SLO family.* Nat. Rev. Neurosci., 2006. 7(12): p. 921-31.

137.   Schreiber, M. and L. Salkoff, *A novel calcium-sensing domain in the BK channel.* Biophys. J., 1997. 73(3): p. 1355-1363.

138.   Bao, L., et al., *Mapping the BKCa channel's "Ca2+ bowl": side-chains essential for Ca2+ sensing.* J Gen Physiol, 2004. 123(5): p. 475-89.

139.   Bao, L., et al., *Elimination of the BK_{Ca} channel's high-affinity Ca^{2+} sensitivity.* J. Gen. Physiol., 2002. 120(2): p. 173-189.

140.   Qian, X., X. Niu, and K.L. Magleby, *Intra- and intersubunit cooperativity in activation of BK channels by Ca^{2+}.* J. Gen. Physiol., 2006. 128(4): p. 389-404.

141.   Hou, S., et al., *Reciprocal regulation of the Ca2+ and H+ sensitivity in the SLO1 BK channel conferred by the RCK1 domain.* Nat Struct Mol Biol, 2008. 15(4): p. 403-10.

142.   Hou, S., et al., *The RCK1 high-affinity Ca2+ sensor confers carbon monoxide sensitivity to Slo1 BK channels.* Proc Natl Acad Sci U S A, 2008. 105(10): p. 4039-43.

143.   Zhang, X., C.R. Solaro, and C.J. Lingle, *Allosteric regulation of BK channel gating by Ca(2+) and Mg(2+) through a nonselective, low affinity divalent cation site.* J Gen Physiol, 2001. 118(5): p. 607-36.

144.   Shi, J. and J. Cui, *Intracellular Mg^{2+} enhances the function of BK-type Ca^{2+}-activated K^+ channels.* J. Gen. Physiol., 2001. 118(5): p. 589-606.

145.   Monod, J., J. Wyman, and J.P. Changeux, *On the Nature of Allosteric Transitions: A Plausible Model.* J Mol Biol, 1965. 12: p. 88-118.

146.   Cox, D.H., J. Cui, and R.W. Aldrich, *Allosteric gating of a large conductance Ca-activated K^+ channel.* J. Gen. Physiol., 1997. 110(3): p. 257-281.

147.   McManus, O.B. and K.L. Magleby, *Accounting for the Ca(2+)-dependent kinetics of single large-conductance Ca(2+)-activated K+ channels in rat skeletal muscle.* J Physiol, 1991. 443: p. 739-77.

148.   Niu, X., X. Qian, and K.L. Magleby, *Linker-gating ring complex as passive spring and Ca^{2+}-dependent machine for a voltage- and Ca^{2+}-activated potassium channel.* Neuron, 2004. 42(5): p. 745-756.

149.   Krishnamoorthy, G., et al., *The NH_2 terminus of RCK1 domain regulates Ca^{2+}-dependent BK_{Ca} channel gating.* J. Gen. Physiol., 2005. 126(3): p. 227-241.

150.   Lee, U.S., J. Shi, and J. Cui, *Modulation of BK channel gating by the {beta}2 subunit involves both membrane-spanning and cytoplasmic domains of Slo1.* Manuscript submitted, 2010.

Chapter 2: Coupling Mechanism of the AC Region

In the following paper which is published in *Neuron*, we identified the AC region as the coupling structure for the RCK1 Ca^{2+} binding site. We further discovered that the dynamics of the AC region regulates the coupling efficiency.

An epilepsy/dyskinesia-associated mutation enhances BK channel activation by potentiating Ca^{2+} sensing [1]

Junqiu Yang[*,1,2], Gayathri Krishnamoorthy[*,1,3], Akansha Saxena[*,4,5], Guohui Zhang[1,5], Jingyi Shi[1,5], Huanghe Yang[1,5], Kelli Delaloye[1,5], David Sept[4,5] & Jianmin Cui[1,5]

[1] *Cardiac Bioelectricity and Arrhythmia Center, Washington University, Saint Louis, Missouri 63130, USA*

[2] *Department of Energy, Environment & Chemical Engineering, Washington University, Saint Louis, Missouri 63130, USA*

[3] *Department of Biomedical Engineering, Case Western Reserve University, Cleveland, Ohio 44106, USA*

[4] *Center for Computational Biology, Washington University, Saint Louis, Missouri 63130, USA*

[5] *Department of Biomedical Engineering, Washington University, Saint Louis, Missouri 63130, USA*

[*] *These authors contributed equally to this work.*

Summary

Ca^{2+}-activated BK channels modulate neuronal activities including spike frequency adaptation and synaptic transmission. Previous studies found that Ca^{2+} binding sites and the activation gate are spatially separated in the channel protein, but the mechanism by which Ca^{2+} binding opens the gate over this distance remains unknown. By studying an Asp to Gly mutation (D434G) associated with human syndrome of generalized epilepsy and paroxysmal dyskinesia (GEPD), we show that a cytosolic motif immediately following the activation gate S6 helix, known as the AC region, mediates the allosteric coupling between Ca^{2+} binding and channel opening. The GEPD mutation inside the AC region increases BK channel activity by enhancing this allosteric coupling. We found that Ca^{2+} sensitivity is enhanced by increases in solution viscosity that reduce protein dynamics. The GEPD mutation alters such a response, suggesting that a less flexible AC region may be more effective in coupling Ca^{2+} binding to channel opening.

Highlights

1) The two Ca^{2+}-activation pathways in BK channels are dissected.

2) The AC region is identified as a structural component of one of the pathways.

3) Protein dynamics plays an important role in the AC region pathway.

4) The disease-associated mutation alters channel dynamics to enhance Ca^{2+} sensing.

53

Introduction

Ion channels are proteins that conduct ions across cell membranes. Channel proteins regulate membrane excitation and ionic homeostasis in response to cellular signals, and mutations of ion channels often induce serious, sometimes life-threatening diseases[1]. Structural studies in recent years have greatly advanced our understanding of the basic working modules of ion channels including the activation gate [2] and sensors to various stimuli such as voltage [3, 4] and chemical ligands [5-8]. However, the structural basis for the energetic coupling between sensors and the activation gate still remains elusive. Considering the fact that many disease-causing mutations are outside of the gate and sensors, it is particularly important to understand the molecular mechanism of the energetic coupling, i.e. the structural components of the allosteric activation pathways, and how they are modified by channel mutations. Activated by both membrane depolarization and increases in intracellular Ca^{2+} concentration ($[Ca^{2+}]_i$), large-conductance, voltage and calcium-activated K^+ (BK) channels become one of the best systems to address this question [9]. Recently, we characterized a mutation D434G in human BK channels (hSlo1, GenBank accession number, GI: 26638649) which was identified from patients with nervous disorders of coexistent generalized epilepsy and paroxysmal dyskinesia [10]. This epilepsy/dyskinesia mutation (hD434G) significantly increases Ca^{2+} sensitivity of BK channels under physiological conditions. More interestingly, the hD434G mutation resides in a cytosolic motif which is important for the allosteric coupling between Ca^{2+} binding and channel activation [7, 11] , but outside of

the putative Ca^{2+} binding sites (Figure 2.1A), implying its role in the allosteric Ca^{2+}-

dependent activation. Thus, this mutation provides us a unique opportunity to uncover the

structural basis and dynamic nature of the coupling between Ca^{2+} binding and BK

channel opening.

A

├ Membrane-spanning domain ┤├──── Cytoplasmic domain ────┤

├── VSD ──┤├ PGD ┤├── RCK1 ──┤

S0 S1 S2 S3 S4 S5 P S6 AC region Ca^{2+} bowl

NH₂ [** ■   ]COOH

| └──── D369G

Ca^{2+} binding site I Ca^{2+} binding site II

B

WT $[Ca^{2+}]_i$ = 1.8 µM   D369G

200 mV
160 mV   200 mV
                                                                160 mV
120 mV   120 mV

                                                                80 mV
80 mV   40 mV

2 nA
5 ms

C

WT $[Ca^{2+}]_i$ (µM)

○ 0.0005
● 1.0
□ 1.8
■ 4.6
△ 9.3
▲ 32.3
◇ 111.5

G/G_{max}

1.0, 0.8, 0.6, 0.4, 0.2, 0.0

-100   0   100   200
Test potential (mV)

D

D369G $[Ca^{2+}]_i$ (µM)

○ 0.0005
● 1.0
□ 1.8
■ 4.6
△ 9.3
▲ 32.3
◇ 111.5

G/G_{max}

1.0, 0.8, 0.6, 0.4, 0.2, 0.0

-100   0   100   200
Test potential (mV)

E

$V_{1/2}$ (mV)

150, 100, 50, 0

○ WT
● D369G

0.001   0.1   10
$[Ca^{2+}]_i$ (µM)

F

Channel	L(0)	z	K_c (µM)	K_o (µM)
WT	5405 ± 613	1.28 ± 0.02	6.66 ± 0.16	0.67 ± 0.02
D369G	3849 ± 360	1.29 ± 0.01	3.44 ± 0.07	0.35 ± 0.01

Figure 2.1. The epilepsy/dyskinesia mutation mD369G enhances Ca^{2+} sensitivity of mSlo1 BK channel activation. (**A**) The Slo1 polypeptide. The membrane-spanning domain contains helices S0-S6 and pore loop (P), of which S1-S4 form the voltage sensor domain (VSD) and S5-S6 form the pore/gate domain (PGD). The cytoplasmic domain contains two putative Ca^{2+} binding sites: the D367 site (Site I) and the Ca^{2+} bowl (Site II). mD369G is located in the AC region, close to the D367 Ca^{2+} binding site. (**B**) Macroscopic current traces from inside-out patches expressing WT and mD369G channels. Currents were elicited in 1.8 µM $[Ca^{2+}]_i$ by voltages as indicated. The voltages before and after the pulses were -50 mV. (**C** and **D**) G-V curves for WT and mD369G channels in $[Ca^{2+}]_i$ from nominal 0 (~0.5 nM) to 111.5 µM. Solid lines are fits with the MWC model (see Methods). (**E**) $V_{1/2}$ of G-V curves versus $[Ca^{2+}]_i$ for WT and mD369G channels. (**F**) Parameters of MWC model fits for WT and mD369G channels (value ± standard deviation).

BK channels are composed of four identical alpha subunits encoded by the *Slo1* gene [12, 13]. Each Slo1 subunit contains a membrane-spanning domain, which includes the voltage sensor and the ionic pore with the activation gate, and a large cytoplasmic C-terminal domain where two putative Ca^{2+} binding sites, D367 and the Ca^{2+} bowl, have been identified [14, 15] (Figure 2.1A). In addition, the channel contains a third site that binds both Ca^{2+} and Mg^{2+} at high (mM) concentrations [15-17], which is not shown in Figure 2.1A because under the experimental conditions used in this paper this site will not be occupied. The atomic structure of the BK channel has not been solved. However, the X-ray crystallographic structure of $K_V1.2$ channel [18] has been used as a model for the membrane-spanning domain of BK channels, while the RCK (regulator of K^+

conductance) domains of the MthK channel [7] are suggested as a model for the cytoplasmic domain [9]. A recent three-dimensional structure of BK channels from electron cryomicroscopy is consistent with these homology models [19]. Structural and functional studies suggested that Ca^{2+} binding activates the channel through an allosteric mechanism [20]. At the molecular level, the allosteric mechanism is suggested to be similar as that for the MthK channel such that Ca^{2+} binding first alters the conformation of the cytosolic domain, which then opens the activation gate by pulling the S6 transmembrane segment [7, 21]. To date, no structural component in the cytosolic domain that changes conformation during Ca^{2+} dependent activation has been identified in BK channels, and the nature of such conformational changes is not known. The hD434G mutation in BK channels causes an increase in the activity of BK channels at the same membrane potentials and $[Ca^{2+}]_i$'s as compared to the wild type (WT) hSlo1 channels. This change may be the basis for the association of the mutation with the neurological disorders [10, 22]. To investigate how this mutation uniquely enhances channel function, we studied the hD434G-equivalent D369G in mouse Slo1 (mSlo1) BK channels (Figure 2.1). These studies identified the N-terminus of the RCK1 domain containing 76 amino acids, a region including the secondary structures βA-αC [7] and thus named the AC region, as part of a structural basis connecting Ca^{2+} binding to channel opening. The results suggested a conformational and dynamical change of the AC region during BK channel activation that is altered by the mD369G mutation. These results also provide a novel allosteric mechanism for how ligand binding opens activation gates in ion channels.

Results

mD369G enhances Ca^{2+} dependent activity

Experiments were carried out on mSlo1 rather than hSlo1. The mSlo1 channel is homologous to hSlo1; aside from the different lengths at the N- and C- termini, 99% amino acids are identical between the two channels [10, 23]. The D369G mSlo1 channels exhibit the same phenotype as D434G hSlo1 such that at the same voltage and physiological [Ca^{2+}]$_i$ the mutant channels activated more than the WT channels (Figure 2.1B). We studied the mSlo1 channels over a more complete range of [Ca^{2+}]$_i$'s from nominal 0 (~0.5 nM) to the near saturating 111.5 μM, and the results revealed that the mutation enhances Ca^{2+} sensitivity of channel activation (Figures 1C-F). The increase of [Ca^{2+}]$_i$ shifted the voltage range of the conductance-voltage (G-V) relations of the mutant channels to more negative voltages as compared to those of the WT channels (Figures 1C and 1D). The G-V relation of BK channel activation can be approximated by fitting the data to the Boltzmann function with two independent parameters: V$_{1/2}$ (voltage at half-maximum conductance) and z (proportional to the steepness of the curve). A plot of V$_{1/2}$ vs. [Ca^{2+}]$_i$ clearly shows that Ca^{2+} binding shifts the G-V relation to more negative voltage ranges, and that the shifts for the mD369G mutant channels are larger than that for the WT channels (Figure 2.1E). To further quantitatively estimate the change of Ca^{2+} sensitivity caused by the mutation, we fit the G-V relations of both mutant and WT channels at various [Ca^{2+}]$_i$ to the MWC model of BK channel activation [20, 24] (Figures

1C and D) and list the parameters (Figure 2.1F), where K_o and K_c are dissociation

constants for Ca^{2+} binding at the open and closed conformations, respectively. The

mD369G mutation decreased both K_o and K_c, consistent with an enhancement of Ca^{2+}

sensitivity. Such a change in Ca^{2+} sensitivity would increase open probability of the

channel by 1.4 - 5 times during a neuronal action potential with an estimated amplitude of

~30 mV and local $[Ca^{2+}]_i$ between 2-10 µM (Figures 1C and 1D). Previous studies

suggested that the increased BK channel activity may be prominent at the peak of

neuronal action potentials, where $[Ca^{2+}]_i$ increases due to Ca^{2+} influx via voltage

dependent Ca^{2+} channels, to reduce the duration and increase the frequency of action

potentials and result in seizures [22].

The shift of G-V relations in response to changes in $[Ca^2]_i$ is an effective measurement of

Ca^{2+} sensitivity of BK channels [25], which has been the primary method for

investigating the gating mechanism of BK channels including the identification of Ca^{2+}

binding sites [15, 26]. However, since BK channels are activated by both voltage and

Ca^{2+} [9], this method does not directly reveal the mechanistic properties of Ca^{2+}

dependent activation. To eliminate the influence of voltage dependent activation, we

further examined Ca^{2+} sensitivities of the WT and D367G mSlo1 using limiting slope

measurements at extremely negative voltages where BK channels open spontaneously

and independently of voltage sensor movements [27]. A patch containing hundreds of BK

channels is held at negative voltages, where the open probability of the channels is so

small that only rare openings of single channels are observed (Figure 2.2A). The open

probability of the channels increases in the presence of Ca^{2+}, resulting in marked increase of single channel openings. Figure 2.2 shows that mutation mD369G enhances Ca^{2+} sensitivity of the channel. At -140 mV, the number of single channel opening events of both WT and mD369G increases with increasing $[Ca^2]_i$, but more prominently for mD369G (Figure 2.2A). The P_o-V relations at various $[Ca^2]_i$ become flat at negative voltages (Figure 2.2B and C), indicating that channel opening at these voltages no longer depends on voltage sensor movements. The Ca^{2+} dependences of P_o at -140 mV for WT and mD369G channels (Figure 2.2D) clearly show that mutation mD369G enhances Ca^{2+} sensitivity. The fit of the data by the Hill equation (solid lines) results in a microscopic dissociation contant of 15 and 8 µM and a Hill coefficient of 2.8 and 3.5 for WT and mD369G, respectively. The larger Hill coefficient for mD369G indicates a higher cooperativity among Ca^{2+} binding sites in the mD369G channels, thus mutation mD369G enhances the allosteric coupling among Ca^{2+} binding sites, possibly via an enhanced allosteric coupling between Ca^{2+} binding sites and the activation gate.
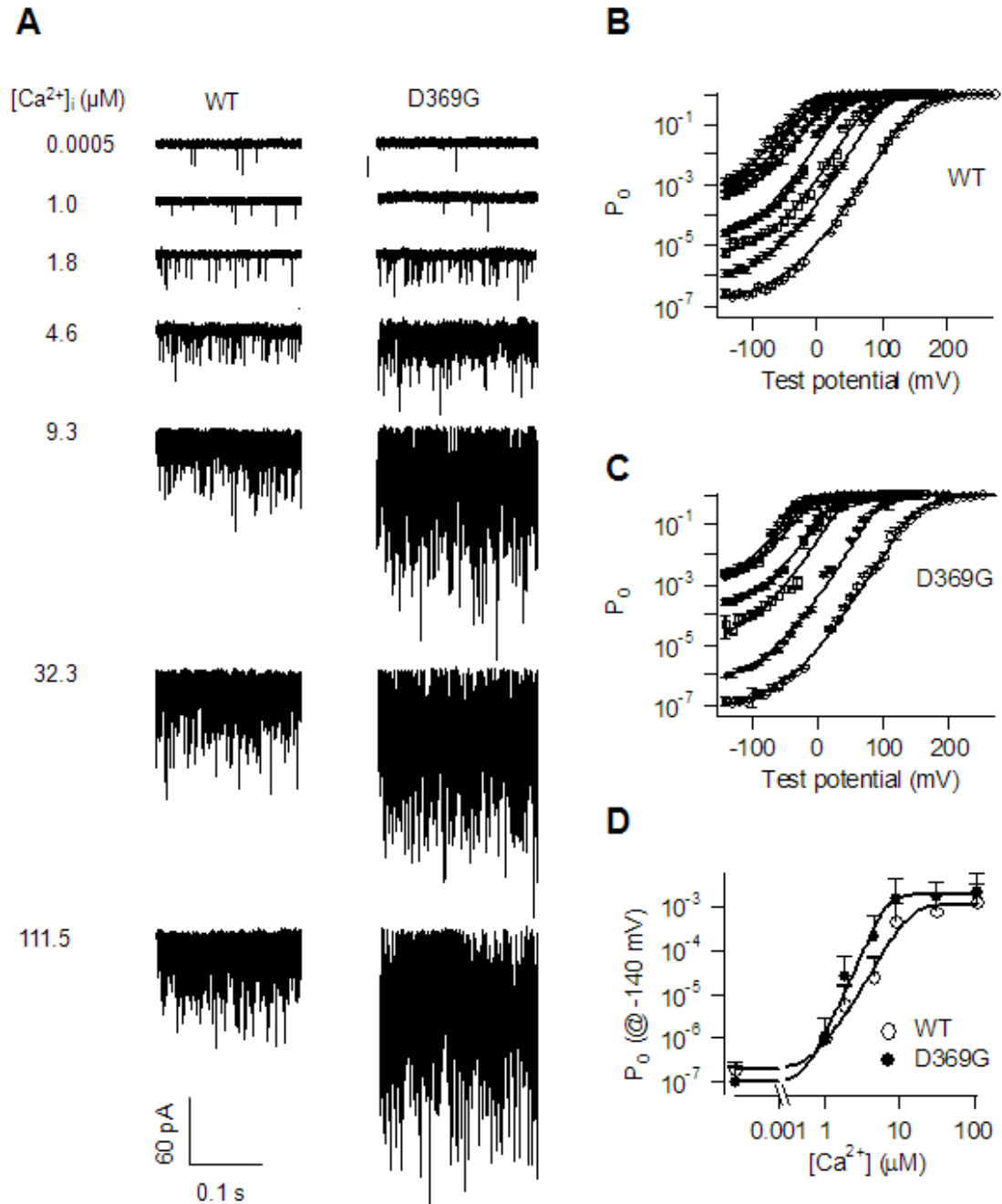
Figure 2.2. mD369G enhances Ca^{2+} sensitivity as shown by limiting slope measurement. (**A**) Current traces at -140 mV under different $[Ca^{2+}]_i$ for WT and mD369G. The patch for

WT has ~ 730 channels, and the one for mD369G has ~ 550 channels. $[Ca^{2+}]_i$ is labelled next to the corresponding traces.(**B** and **C**) P_o-V relations for WT (B) and mD369G (C) under different $[Ca^{2+}]_i$. The symbols for each $[Ca^{2+}]_i$ are identical to Figure 2.1C and D. Solid lines are fittings to the HCA model.(**D**) P_o at -140 mV under different $[Ca^{2+}]_i$ for WT and mD369G. Solid lines are fittings to the Hill equation: $P_o = 1/(1 + (K_A/[Ca^{2+}])^n)$. The microscopic dissociation constant K_A = 15 and 8 µM and the Hill coefficient n = 2.8 and 3.5 for WT and mD369G, respectively.

mD369G alters the D367 activation pathway

How does the mD369G mutation perturb the molecular mechanism of Ca^{2+} dependent activation to result in a gain-of-function? Previous studies showed that the mutation of each of the two putative Ca^{2+} binding sites, D367A and 5D5N (five consecutive Asp residues at 897-901 mutated to Asn), eliminates part of Ca^{2+} dependent activation and the sum of the effects is close to the total high-affinity Ca^{2+} sensitivity of the channel. These results suggest that the channel is activated by two separate Ca^{2+} dependent pathways involving either D367 or the Ca^{2+} bowl, with only a weak cooperativity between the two pathways [15, 28, 29] (Figure 2.3A). Therefore, to answer the above question, we first investigated whether the mD369G mutation affects each of the activation pathways, and then addressed how a particular pathway is affected. We found that eliminating the function of one pathway by D367A also abolishes the difference in Ca^{2+}-induced G-V shift between the mD369G mutant and the WT channels, since $V_{1/2}$ changes with $[Ca^{2+}]_i$ nearly in parallel for the two channels (Figures 3B and 3C). This result indicates that the

62

mD369G mutation no longer enhances Ca^{2+} sensitivity when the pathway associated with D367 is disabled. On the contrary, when the function of the Ca^{2+} bowl pathway is eliminated by the 5D5N mutation, the mD369G mutation continues to enhance Ca^{2+} sensitivity in a similar way as in the WT channel (Figures 3D and 3E). Taken together, these results suggest that the epilepsy/dyskinesia mutation specifically affects the Ca^{2+} dependent activation pathway associated with D367.
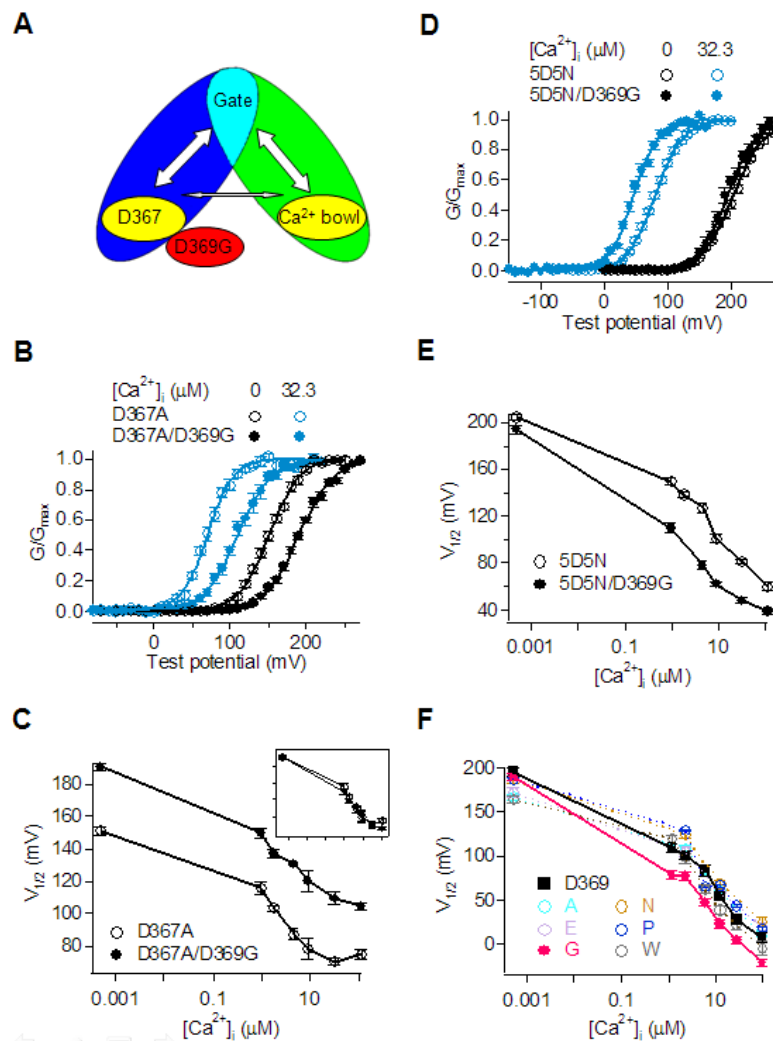
Figure 2.3. mD369G mutation specifically affects the D367-associated Ca^{2+} activation pathway. (**A**) Diagram illustrating the relationship between Ca^{2+} binding sites and the gate. Ca^{2+} binding to the two sites, which are located distant from the activation gate, activates the channel through independent pathways with little cooperativity. mD369G is located close to the D367 site. (**B** and **D**) G-V curves for D367A and D367A/D369G mutants (B), and for 5D5N and 5D5N/D369G mutants (D) with 0 and 32.3 μM $[Ca^{2+}]_i$. Solid lines are fits with the Boltzmann function. (**C** and **E**) $V_{1/2}$ versus $[Ca^{2+}]_i$ for D367A and D367A/D369G mutants (C), and for 5D5N and 5D5N/D369G mutants (E). The curves for D367A and D367A/D369G are shifted vertically to align at 0 $[Ca^{2+}]_i$ in the inset of (C). (**F**) $V_{1/2}$ versus $[Ca^{2+}]_i$ for WT and D369A, E, G, N, P, and W mutants. Note that the data in this panel were obtained in a different batch of experiments with a different set of Ca^{2+} solutions, hence the final Ca^{2+} concentrations are slightly different from those in other figures.

Then, what are the targets in the D367-specific pathway that are subject to modification by mD369G to result in an increase in Ca^{2+} sensitivity? Based on the structural model of the RCK1 domain [7], D367 appears to be located some distance from the activation gate. Thus the D367-specific activation pathway may involve a large structure that includes many residues (Figure 2.3A). Since mutation mD369G is located close to D367, it is possible that the mutation may alter local interactions of the D369 side chain with the putative Ca^{2+} binding site to enhance Ca^{2+} sensitivity [30]. On the other hand, it is also possible that mD369G may alter the conformation of the activation pathway and allosterically enhance Ca^{2+} sensitivity (Figure 2.2D). To distinguish between these two possibilities, we mutated D369 to conservative (D369E) and neutral (D369A, N, W, and

P) amino acids with various side chain sizes and examined the effects of these mutations

on Ca^{2+} sensitivity. Among all these mutations, only mD369G increased Ca^{2+} sensitivity,

with $V_{1/2}$ of the G-V relations shifted to more negative voltage ranges (Figure 2.3F). The

effects of other mutations were not as pronounced and varied at different $[Ca^{2+}]_i$'s,

increasing channel activation at some concentrations, but decreasing activation at other

concentrations. These results suggest that the side chain of D369 is not part of the Ca^{2+}

binding site (also see [15, 16]), and it may not contribute to Ca^{2+} sensitivity by the short

range electrostatic or van der Waals interactions with the putative Ca^{2+} binding site.

Rather, the specific effect of mD369G in increasing Ca^{2+} sensitivity may derive from the

ability of glycine to adopt a wide range of main-chain dihedral angles and make protein

structure flexible at its site, which may alter the conformational changes of the D367-

specific pathway during channel gating. Consistent with this suggestion, the G-V relation

of the mD369G mutant channels shifted a small but significant amount to more negative

voltages ($\Delta V_{1/2} = 8.8 \pm 3.8$ mV (mean of difference $\pm$ standard error of difference, n = 6

for WT and 20 for mD369G), p = 0.029 in unpaired Student's t-test) at 0 $[Ca^{2+}]_i$ (Figure

2.1E), indicating that mD369G can alter channel function by a change in the structure

that links to the activation gate, instead of by merely changing Ca^{2+} binding. Furthermore,

although mD369G no longer enhances Ca^{2+} sensitivity of the channel with the D367A

mutation, it alters channel activation independently of $[Ca^{2+}]_i$, shifting the G-V relation at

all $[Ca^{2+}]_i$'s (Figures 3B and 3C). It is possible that D367A eliminated Ca^{2+} binding to the

putative site but did not destroy the rest of the activation pathway down-stream from Ca^{2+}

binding, which was subsequently altered by mD369G mutation to affect channel activation.

To examine if the flexibility of the channel protein matters to gating and if mD369G alters the flexibility of the channel protein, we studied the WT and mutant channels in intracellular solutions with increased viscosity. The dynamics of a protein in solution are intimately coupled to the dynamics of the solvent; the fluctuation amplitudes and relaxation rates, i.e. flexibility, of proteins can be reduced by increases in solution viscosity [31-33]. Previous studies showed that the increases in solution viscosity may affect the moving parts of voltage dependent Na^+ channels during gating to reduce activation rates [34, 35]. In our experiments, increasing the viscosity of intracellular solution by addition of sucrose (measured viscosity = 0.906 ± 0.003 mPa•s and 23.1 ± 0.1 mPa•s, mean $\pm$ s.e.m., n = 12 at 0 and 2 M sucrose, respectively) slows down the time course of activation and deactivation (Figures 4A and 4B) and enhances Ca^{2+} dependent activation (Figures 4C and 4D) of both the WT and mD369G channels. In 200 μM $[Ca^{2+}]_i$, the reduction of the deactivation rate is smaller as compared to the enhancement of activation rate (Figure 2.4B), and since BK channel activation can be approximated by a two-state voltage dependent activation mechanism in saturating $[Ca^{2+}]_i$'s [25], the changes in time courses of the current are consistent with the changes in G-V relations. Adding 9 M glycerol in the intracellular solution (measured viscosity = 20.2 ± 0.1 mPa•s, mean $\pm$ s.e.m., n = 12), which resulted in a similar increase of viscosity as 2 M sucrose, also caused similar changes in BK channel activation (Figures 4E and 4F). On the other

hand, addition of 2 M urea to intracellular solution, which alters viscosity little (measured

viscosity $= 0.906 \pm 0.003$ mPa•s and 0.987 ± 0.005 mPa•s, mean $\pm$ s.e.m., n $= 12$ at 0 and

2 M urea, respectively), had no effect on channel activation (Figures 4E and 4F),

excluding the possibility that the changes in BK channel activation with sucrose were due

to changes in osmolarity or other unknown effects associated with high concentrations of

solutes. These results suggest that gating of BK channels is affected by the flexibility of

the channel protein.
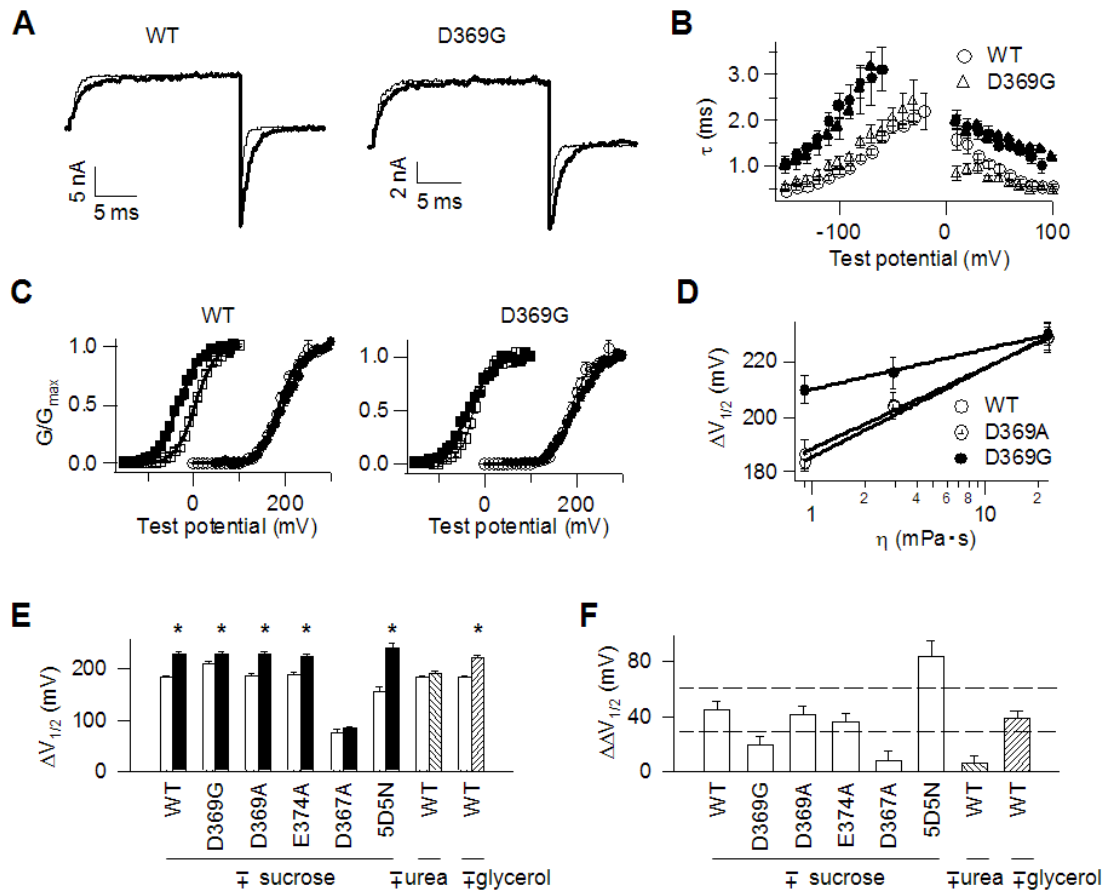
Figure 2.4. mD369G mutation alters response of BK channels to solution viscosity. (**A**) Macroscopic current traces recorded in the absence (thinner traces) or presence (thicker traces) of 2M sucrose. Currents were elicited in saturating 200 μM $[Ca^{2+}]_i$ by 70 mV. Holding and repolarizing voltages were -80 and -120 mV, respectively. Current traces with sucrose were re-scaled to have the same peak amplitude as without sucrose. (**B**) Activation (> 0 mV) and deactivation (< 0 mV) time constant in the absence (hollow symbols) or presence (solid symbols) of 2 M sucrose. $[Ca^{2+}]_i$ = 200 μM. Channels were activated by 70 mV then deactivated by various voltages to obtain deactivation time constant. (**C**) G-V curves for WT and mD369G in the absence (hollow symbols) or presence (solid symbols) of 2 M sucrose. $[Ca^{2+}]_i$ = 0 (circles) or 200 μM (squares). Solid lines are fits with the Boltzmann function. (**D**) $\Delta V_{1/2}$ versus viscosity. $\Delta V_{1/2}$ = $V_{1/2}$ at 0 $[Ca^{2+}]_i$ - $V_{1/2}$ at 200 μM $[Ca^{2+}]_i$. The solutions contained 0, 1 and 2 M sucrose, respectively. Solid lines are fits with equation $\Delta V_{1/2}$ = $\ln(\eta/\eta_0)^{\gamma}$, where η_0 is the viscosity of zero $\Delta V_{1/2}$ and γ is the slope in the semi-log plot; γ = 13.7 ± 0.9 and 6.2 ± 0.5 (value ± standard deviation) for WT and mD369G, respectively. (**E**) $\Delta V_{1/2}$ in the absence (hollow bars) or presence (solid bars) of 2 M sucrose. Hatched bar indicates $\Delta V_{1/2}$ in the presence of 2 M urea or 9 M glycerol. Asterisks indicate a significant difference ($p < 0.05$ in student's *t* test) of $\Delta V_{1/2}$ resulted from 2 M sucrose or 9 M glycerol. (**F**) $\Delta\Delta V_{1/2}$ caused by sucrose. $\Delta\Delta V_{1/2} = \Delta V_{1/2}^{2\ M\ sucrose} - \Delta V_{1/2}^{0\ sucrose}$. Hatched bar indicates $\Delta\Delta V_{1/2}$ caused by 2 M urea or 9 M glycerol. The dashed lines give the 99% confidence interval for $\Delta\Delta V_{1/2}$ of WT.

The results show that mutation mD369G alters the responses of activation and deactivation kinetics to the increased viscosity (Figure 2.4B) and causes a reduced shift of the G-V relation as compared to that in WT when the $[Ca^{2+}]_i$ is increased from 0 to the

saturating 200 µM (Figures 4C and 4D). Thus, the enhancement of Ca^{2+} sensitivity due to an increase of viscosity for mD369G channels is less than that for WT. Unlike mD369G, mutation D369A, which does not alter Ca^{2+} sensitivity (Figure 2.3F), has no effect on the response of BK channels to sucrose (Figure 2.4D). These results support that mD369G alters the flexibility of the BK channel protein to potentiate Ca^{2+} sensitivity.

Results in Figure 2.3 have shown that mD369G specifically alters the Ca^{2+} dependent activation pathway associated with D367 (Figure 2.3C), but not the pathway associated with the Ca^{2+} bowl (Figure 2.3E). Our unpublished results also indicate that mD369G does not affect Mg^{2+} dependent activation [36]. To examine if a change of solution viscosity affects any specific metal dependent activation pathways, we measured channel activation with each of the mutations E374A, D367A and 5D5N, which abolished metal binding to the Mg^{2+} binding site [16], the Ca^{2+} binding site at D367 [15, 16] and the Ca^{2+} binding site at the Ca^{2+} bowl [14], respectively. D367A, but not E374A or 5D5N, abolished the response of BK channels to sucrose (Figures 4E and 4F), suggesting that only the Ca^{2+} dependent activation pathway associated with D367 specifically depends on the dynamics of the channel protein for the coupling between Ca^{2+} binding and channel opening, which is consistent with the result that mD369G specifically affects the same activation pathway (Figure 2.3).

It is important to note that both the increase of viscosity, which reduces the overall protein dynamics, and the mD369G mutation, which enhances the local peptide

69

flexibility, potentiates Ca^{2+} sensing. This result suggests that the local peptide flexibility enhanced by mD369G may reduce the dynamics in other parts of the protein allosterically, consistent with the results in Figures 1E and 3C. Taken together, these results suggest that mD369G alters the flexibility and conformation of the channel protein to potentiate the allosteric coupling between Ca^{2+} binding at the D367 site and channel opening.

Allosteric interactions in the D367 pathway

To demonstrate more directly that mD369G affects the allosteric coupling between Ca^{2+} binding and channel opening, we find structural perturbations that affected the coupling in the D367-specific activation pathway and then test if such perturbations also alter the effect of mD369G. In search of such perturbations, we performed a mutation-scan in the AC region, which is a crucial gateway for the allosteric coupling between Ca^{2+} binding and channel opening because it physically connects the activation gate to the rest of the cytosolic domain (Figure 2.1A), and is important in determining Ca^{2+} sensitivity [11]. Furthermore, both the putative Ca^{2+} binding site D367 and the mutation mD369G are situated within the AC region so that the mutation may alter its structure to affect Ca^{2+} sensitivity. In this experiment, most residues were mutated individually to Ala and some to other amino acids (Figure 2.5A). The loss of Ca^{2+} sensitivity of the channel due to each mutation is quantified by the change in the G-V shift ($\Delta V_{1/2}$) when $[Ca^{2+}]_i$ changes from nominal 0 to the near saturating 99.3 - 111.5 μM (i.e. $\Delta\Delta V_{1/2(\Delta Ca^{2+})} = \Delta V_{1/2}^{WT}$ -

$\Delta V_{1/2}^{\text{Mutant}}$). We classify a $\Delta\Delta V_{1/2(\Delta Ca^{2+})}$ of more than $\pm\,20$ mV as significant since the G-

V relation of BK channels often exhibits variations within a voltage range of ≤ 20 mV.

Ten mutations are found to reduce Ca^{2+} sensitivity significantly (indicated by asterisks in

Figure 2.5A and Supplemental Figure S1), including D362A and D367A that have been

previously reported [15, 16]. These mutations are located in different secondary

structures within the AC region, including αA, αB, βC, and the inter loop between αA

and βB that contains Asp-Arg-Asp-Asp at positions 367-370 and is called the DRDD

loop (Figure 2.5A). Consistent with D367 being part of a Ca^{2+} binding site, mutations in

the DRDD loop resulted in large reductions in Ca^{2+} sensitivity; and D367A reduced the

G-V shift by 105 ± 4 mV (mean of difference $\pm$ standard error of difference, n = 6 for

WT and 5 for D367A) as compared to the 182 ± 3 mV (n = 6) total shift in WT mSlo1 in

response to an increase of $[Ca^{2+}]_i$ from 0 to 111.5 μM, equivalent to a ~60% reduction of

Ca^{2+} sensitivity. The functionally important mutations in other secondary structures are

separated by large distances from the DRDD loop in the structural model of the RCK1

domain (see Figures 7 and 8). These residues are important in the D367-specific pathway

(see below), but cannot be part of the Ca^{2+} binding site because of their long distances

from D367 and because they are mostly hydrophobic (Figure 2.5). The long distances

from D367 also suggest that it is unlikely for all these residues to make direct interactions

with the putative Ca^{2+} binding site. Therefore, at least some of these mutations reduced

Ca^{2+} sensitivity by perturbing the allosteric coupling between Ca^{2+} binding and channel

opening.
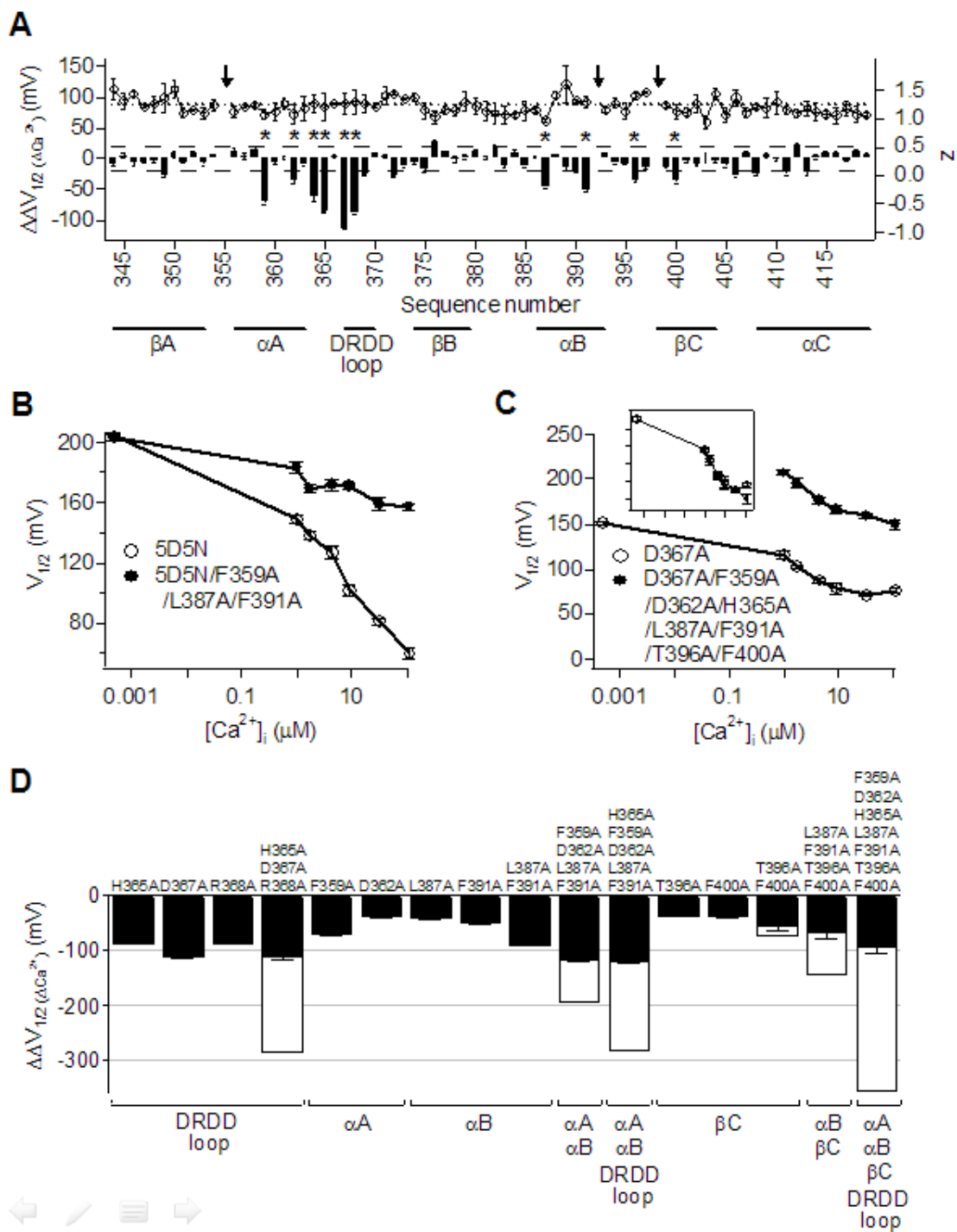
Figure 2.5. Mutations in the AC region perturb the D367-associated Ca^{2+} activation

pathway. (**A**) Effect of the AC region mutations on Ca^{2+} activation. The mutation scan includes H344 – A419 of mSlo1 (GenBank accession number, GI: 347143). The residues were individually mutated to Ala except that A389, A412 and A419 were mutated to Gly, Q397 to Cys, and E399 to Asn. $V_{1/2(\ Ca^{2+})} = V_{1/2}^{WT} - V_{1/2}^{Mutant}$, where $V_{1/2}$ = $V_{1/2}$ at 99.3 to 111.5 μM $[Ca^{2+}]_i$ - $V_{1/2}$ at 0 $[Ca^{2+}]_i$. Mutations with $V_{1/2(\ Ca^{2+})}$ falling beyond the ± 20 mV (dashed lines) interval significantly affect Ca^{2+} activation, which are (denoted by asterisks) F359A, D362A, L364A, H365A, D367A, R368A, L387A, F391A, T396A, and F400A. Open circles depict z values. The dotted line indicates the z value of WT. Structural motifs are indicated by horizontal thick lines. Arrows indicate mutations from which we were unable to obtain data because either the G-V curves at 0 $[Ca^{2+}]_i$ shifted to extremely positive potentials beyond the range of measurement (S355A and K392A) or the mutant failed to express macroscopic currents (V398A). (**B**) $V_{1/2}$ versus $[Ca^{2+}]_i$ for the combined mutation in αA and αB on the background of Ca^{2+} bowl mutation 5D5N. (**C**) $V_{1/2}$ versus $[Ca^{2+}]_i$ for the combined mutation in αA, αB, and βC on the background of D367A mutation. The G-V curve at 0 $[Ca^{2+}]_i$ for the combined mutation shifted to extremely positive potentials and hence the $V_{1/2}$ is unavailable. The two curves are shifted vertically to align at 1.0 μM $[Ca^{2+}]_i$ in the inset. (**D**) Effect of individual and combined mutations on Ca^{2+} activation (filled bars). Open bars depict the summed effects of individual mutations except for those under F359A/D362A/L387A/F391A and L387A/F391A/T396A/F400A, which show the summed effects of F359A, D362A, and L387A/F391A, and of L387A/F391A and T396A/F400A, respectively. Thick lines indicate the structural motifs where the mutations are located.

Since mD369G may enhance Ca^{2+} sensitivity by potentiating the allosteric coupling between Ca^{2+} binding and channel opening, do these perturbations also alter the effect of mD369G? Before answering this question, we examined if these mutations, like mD369G, are able to affect the activation pathway associated with D367 specifically. Figure 2.5B shows that the combined mutations in αA and αB with 5D5N (F359A/L387A/F391A/5D5N) reduced Ca^{2+} sensitivity more than 5D5N alone. Since 5D5N completely abolishes the Ca^{2+} sensitivity derived from the Ca^{2+} bowl [14, 15], the additional reduction in Ca^{2+} sensitivity suggests that the mutations in αA and αB may perturb the activation pathway associated with D367. Consistent with these results, the combined mutations in αA, αB, and βC with D367A (F359A/D362A/H365A/L387A/F391A/T396A/F400A/D367A) did not reduce Ca^{2+} sensitivity more than D367A alone (Figure 2.5C), indicating that these mutations all specifically affect the activation pathway associated with D367; once the upstream pathway is disabled by mutation D367A, additional mutations perturbing the coupling between Ca^{2+} binding and channel opening were no longer able to affect Ca^{2+} sensitivity. With more combinations of mutations, we further studied how these mutations in each individual secondary structure perturb Ca^{2+} dependent activation (Figure 2.5D and Supplemental Figure S2). The Ca^{2+} sensitivity is measured as the total G-V shift induced by a change in [Ca^{2+}]$_i$ from 0 to saturation (Figure 2.5A), which represents the free energy change during Ca^{2+} dependent channel opening ($\Delta G_{Ca^{2+}} = \Delta z e V_{1/2}$) [37], where e is the elementary charge and z is similar at various [Ca^{2+}]$_i$ (Figures 1C and 1D) and largely unchanged by mutations (Figure 2.5A). Therefore, we assumed that for any

combination of mutations, if the mutations do not affect the same molecular process, the sum of the effects on Ca^{2+} sensitivity by the individual mutations should be the same as that of the combined mutations [38]. Mutations in the DRDD loop (H365A/D367A/R368A) reduced Ca^{2+} sensitivity that is indistinguishable from that of the single mutations D367A, indicating that these mutations all affect the same molecular process. Contrarily, the reduction in Ca^{2+} sensitivity was nearly additive by mutations in αB or βC (L387A/F391A or T396A/F400A) (Figure 2.5D), suggesting that in αB or βC, each mutated amino acid may independently contribute to local interactions that are important for channel gating. However, the combined mutations in αB and βC (L387A/F391A/T396A/F400A) reduced no more or even less Ca^{2+} sensitivity than the mutations in αB alone (L387A/F391A), indicating that αB and βC also cooperate as part of a common molecular process in Ca^{2+} dependent activation. When the mutations in αA and αB were combined (F359A/D362A/L387A/F391A) they had a larger effect than mutations in individual secondary structures (F359A, D362A, or L387A/F391A); nonetheless, the effect was less than the summed effects of all individual mutations. Therefore, while αA, αB and βC may be involved in localized interactions, they also cooperate as part of a common molecular process contributing to Ca^{2+} dependent activation. Taken together, these results suggest that all perturbations in the AC region that reduce Ca^{2+} sensitivity (Figure 2.5A) affect the activation pathway associated with D367, and they all are allosterically connected such that one perturbation can affect the outcome of other perturbations.

mD369G alters allosteric interactions

We then examined how the above mutations alter the effect of mD369G by combining mD369G with mutations in αA (F359A), αB (L387A/F391A) or βC (T396A/F400A) that are likely to be located long distances away from D369 (Figure 2.6). Interestingly, while the mutations in αA, αB or βC reduce total Ca^{2+} sensitivity, they either enhanced or did not significantly alter the effect of mD369G (Figures 6A-D). Compared to the WT mSlo1, the mD369G mutation shifted the G-V relation maximally around 1.8 µM $[Ca^{2+}]_i$; however, the mutation in αA altered the profile of mD369G effects and increased G-V shift, with the largest shift at 111.5 µM $[Ca^{2+}]_i$ (Figures 6A and 6D). The mutations in αB or βC did not alter the profile of mD369G effects, nor the maximal G-V shifts (Figures 6B-D). Thus, the effect of mD369G is determined by the mutations in αA, αB and βC within the AC region. Since these mutations are all allosterically connected in perturbing the D367-specific Ca^{2+} dependent activation pathway (Figure 2.5), any of these mutations would alter most allosteric interactions within the AC region to provide a unique network of allosteric connections that determines the effects of mD369G on Ca^{2+} sensitivity. Reciprocally, mD369G also affects most allosteric interactions in the AC region to enhance Ca^{2+} sensitivity. Figure 2.6E shows that in the presence of F359A, mD369G reduced the response of channel activation to the increase of viscosity, suggesting that F359A does not alter the mechanism for the function of mD369G such that mD369G may still reduce the flexibility of the AC region even though the allosteric pathway is altered by F359A. Based on all the results presented in this paper, we conclude that mD369G

alters the conformation and dynamics of the channel protein allosterically to potentiate

Ca^{2+} sensing via the pathway associated with D367, and the AC region is an important

structural component of this pathway.
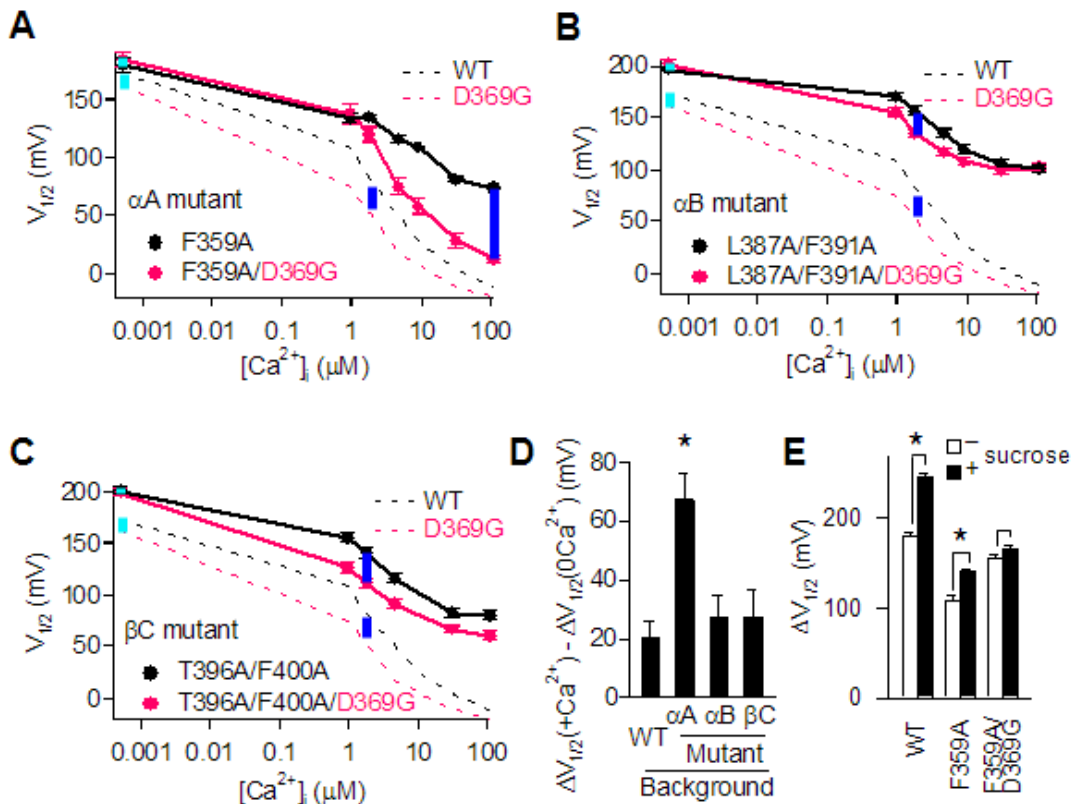
Figure 2.6. Mutations in the AC region allosterically alter the effect of mD369G mutation. (**A-C**) $V_{1/2}$ versus $[Ca^{2+}]_i$ for the background mutations in αA (A), αB (B), and βC (C) with (red circles) and without (black circles) mD369G, and on the background of WT with (red dashed line) and without (black dashed line) mD369G. (**D**) The maximum mD369G-induced increase in Ca^{2+} dependent activation on the background of WT and mutations. $\Delta V_{1/2}(+Ca^{2+})$ is the maximum $V_{1/2}$ shift caused by mD369G, and

measured by the length of the blue lines in (A-C) on respective backgrounds. Note that $\Delta V_{1/2}(+Ca^{2+})$ was measured at 1.8 μM $[Ca^{2+}]_i$ on all backgrounds except for on the background of mutation in αA, where $\Delta V_{1/2}(+Ca^{2+})$ was measured at 111.5 μM $[Ca^{2+}]_i$. $\Delta V_{1/2}(0Ca^{2+})$ is the $V_{1/2}$ shift caused by mD369G at 0 $[Ca^{2+}]_i$, measured by the length of the cyan lines in (A-C). The asterisk indicates that the data is significantly different from that on the WT background ($p < 0.0005$ in unpaired Student's t-test). (**E**) $\Delta V_{1/2}$ in the absence (hollow bars) or presence (solid bars) of 2 M sucrose. $\Delta V_{1/2}$ = $V_{1/2}$ at 0 $[Ca^{2+}]_i$ - $V_{1/2}$ at 200 μM $[Ca^{2+}]_i$. The asterisk indicates that $\Delta V_{1/2}$ in the presence of sucrose is significantly differently from that in the absence of sucrose ($p < 0.05$ in student's t test).

Discussion

This study demonstrates that mD369G enhances BK channel activity by altering the allosteric coupling between Ca^{2+} binding and gate opening. The experimental results that lead to this conclusion have also brought insights into the mechanism of such a coupling. Previous studies suggested that Ca^{2+} binds to two putative sites, the D367 site [15] and the Ca^{2+} bowl [14], in BK channels to activate the channel through two separate intra-molecular pathways, i.e., two separate subsets of conformational changes are responsible for coupling the activation gate to the two Ca^{2+} binding sites. However, aside from the putative Ca^{2+} binding sites, the structural basis of the two activation pathways was not clear. In this study, we show that the mD369G mutation and the mutations in the AC region primarily alter the Ca^{2+} dependence derived from the D367 associated activation

pathway (Figures 3, 4, 6). These results further demonstrate that Ca^{2+} activates the channel through separate intra-molecular pathways, and the allosteric interactions within the AC region are part of the D367 specific pathway.

Our results suggest that the AC region is an important structural component in coupling Ca^{2+} binding to channel opening. Consistent with this role, homology modeling of the AC region in BK channels and its superimposition on the full gating ring of the MthK channel reveal that the Ca^{2+} sensitive mutations are distributed in a distinctive fashion from the periphery of the cytosolic domain to the center of the channel (Figures 7A and 7B). The DRDD loop, where the putative Ca^{2+} binding site and the mD369G mutation are located, is positioned at the outer edge of the channel molecule, and αA, αB and βC lie just beneath the central pore, making it possible for the allosteric connection within the AC region to couple Ca^{2+} binding to the activation gate. Sequence alignments show that the residues important for Ca^{2+} sensitivity in the AC region are conserved among Slo1 channels from fruit fly to human (Figure 2.7C), suggesting that all BK channels may share the same Ca^{2+} activation mechanism. Interestingly, while the DRDD loop is highly conserved among the Ca^{2+} activated Slo1 channels, other Slo families that are activated by intracellular H^+ [39], Na^+ [40] and/or Cl^- [41] ions show variations in this region (Figure 2.7C). In addition, this loop is not present in the prokaryotic MthK or the *E. coli* K^+ channels [7, 42]. Therefore, the residues in the Slo1 DRDD loop appear to be specifically important for Ca^{2+} sensing. In contrast, the sequences of αA, αB and βC are highly conserved among all Slo families. The residues corresponding to F359, L387,

F391, T396 and F400 in mSlo1 are hydrophobic in these channels, and the residues

corresponding to D362 are either negatively charged or polar. These comparisons suggest

a common role for αA, αB and βC in the gating mechanism of eukaryotic channels that

are sensitive to intracellular ions. It is possible that in all these channels αA, αB and βC

modulate gate opening, but the modulation is allosterically controlled by various

intracellular ions that specifically bind to their respective binding sites. A change in this

allosteric mechanism such as the hD434G mutation can alter the function of these

channels and result in human diseases.
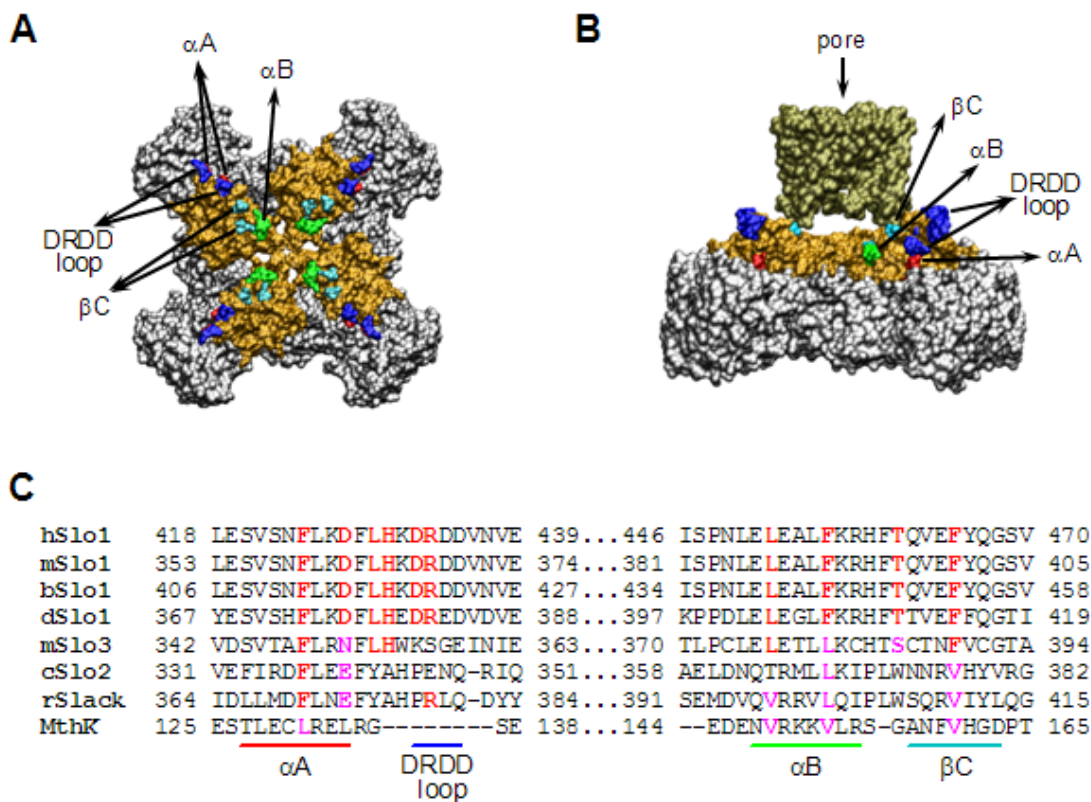
Figure 2.7. Spatial distribution and conservation of the residues important for Ca^{2+} dependent activation. (**A** and **B**) The structure of the MthK gating ring (grey) superimposed with the homology model of the BK channel AC region (orange) either without (A, top view) or with (B, side view) the pore domain of the BK channel (olive). The pore domain of the BK channel is modelled by using Kv1.2 crystal structure as the template. The residues identified in Figure 2.5A as being important for Ca^{2+} dependent activation are marked with blue, red, green and cyan colors in the structure. (**C**) Sequence alignment for the structural motifs in the AC region of Slo and MthK channels. The residues identical to those identified in Figure 2.5A as being important for Ca^{2+} dependent activation are in red, and the conserved residues are in purple. The structural motifs are indicated by horizontal lines. BK channels from different species are shown: hSlo1, human (GenBank accession number, GI: 26638649); mSlo1, mouse (347143); bSlo1, bovine (46396286); dSlo1, *Drosophila* (7301192). Also shown are mSlo3, the pH sensitive mouse Slo3 channel (6680542); cSlo2, the Cl⁻ sensitive *C. elegans* Slo2 channel (5764632); rSlack, the Na⁺ sensitive rat Slack channel (3978471); and MthK (2622639).

An increase of viscosity in intracellular solutions enhances Ca^{2+} sensitivity of BK channels, suggesting that the dynamics of the channel protein is important in the allosteric pathway associated with D367. Two lines of evidence indicate that mD369G alters the dynamics of the channel protein to potentiate Ca^{2+} sensing, namely mD369G, but not other mutations of D369, enhances Ca^{2+} sensitivity (Figure 2.3F) and alters the responses of the channel to changes in solution viscosity (Figure 2.4D). To explore the possible mechanisms of how mD369G changes channel function, we performed molecular dynamics (MD) simulations for the AC region. Previous studies have

suggested that the AC region may form an independent structural and functional unit in BK channels. First, it was demonstrated that a cleavage at 12 amino acids after the AC region does not prevent the resulting two divided peptides from forming functional channels, suggesting that the cytosolic domain in the N-terminal part of the divided Slo1 may be able to fold independently [43]. Therefore, as the core of this cytosolic domain, the AC region may be treated as a structural unit in MD simulations. Second, we previously found that the entire AC region, but not any part of it, was responsible for the Ca^{2+} sensitivity difference between two Slo1 homologs, suggesting that the AC region also acted as a functional unit to modulate Ca^{2+} sensitivity [11]. This idea is also supported by the results that mutations within the AC region are allosterically connected in perturbing Ca^{2+} sensitivity (Figure 2.5).
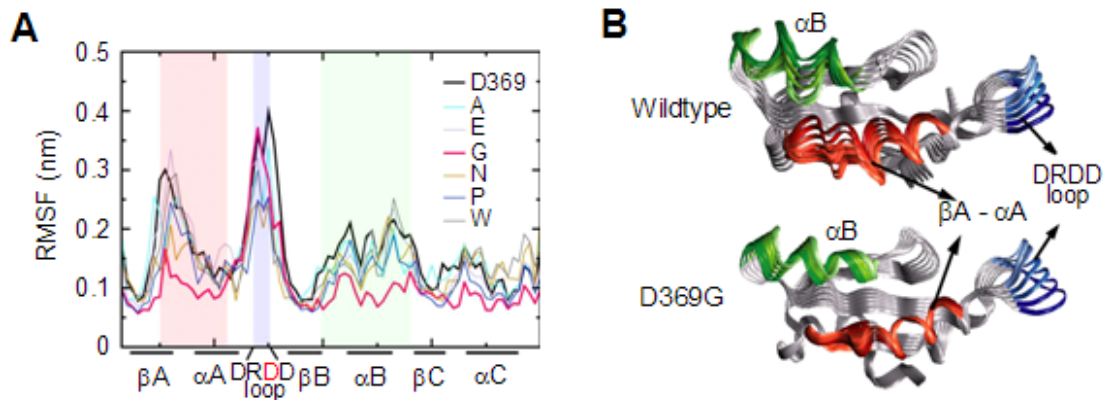
Figure 2.8. mD369G mutation reduces the flexibility of the AC region in molecular dynamics simulations. (**A**) RMS fluctuation of C_α's in the AC region obtained from molecular dynamics simulations of WT and D369A, E, G, N, P and W. Color shades

indicate the structural motifs in the AC region, the dynamics of which are significantly affected by mD369G. (**B**) Motion of the WT (**top**) and mD369G (**bottom**) AC regions along the principal eigenvector from minima to maxima. Color codes are the same as in (A).

Figure 2.8A plots root mean square fluctuation (RMSF) of the main chain C_α's for the AC regions of the WT and mD369G mSlo1, as well as the AC regions of mutations D369E, A, N, W, and P that have little effect on Ca^{2+} sensitivity (Figure 2.3F). RMSF is the standard deviation of the movement of a residue around its mean position, i.e. residues with a higher RMSF are in a more flexible region of the protein. Consistent with the experimental data (Figures 1E, 3C, 3F, 4 and 6A-D), mutation mD369G not only alters the local flexibility but also changes the overall dynamics of the AC region. The changes are most prominent in three areas of the AC region; the peak RMSF shifts in the DRDD loop and the maximum differences occur in the βA-αA linker and αB-βC (red, blue, and green shades, Figure 2.8A), corresponding to the same areas where the mutations reduce Ca^{2+} sensitivity with allosteric connections (Figure 2.5). Also correlating with the experimental results of channel activation (Figures 3F, 4E and 4F), the dynamics of the D369E, A, N, W, and P mutant AC regions do not show similar changes as that of mD369G. For a better visualization, the changes in dynamics caused by mD369G are also illustrated by decomposing the complex motion into simpler periodic orthogonal modes using principal component analysis and plotting the movements of the most significant mode (Figure 2.8B). The overall effect of mD369G is

to reduce the flexibility in the βA-αA linker and αB-βC, causing the entire AC region to move as a more rigid entity that simply follows the motion of the DRDD loop (Figure 2.8B and Supplemental Movie S1), consistent with the result that both mD369G and an increase of solution viscosity enhances Ca^{2+} sensing (Figures 1 and 4). It is remarkable that the results of MD simulation and experiments correlate well in almost every aspect although the structure of the AC region is based on a homology model derived from the structure of MthK. This result is consistent with a number of previous studies that demonstrated the structural homology between the RCK1 domain in BK channels and the RCK domain of MthK [9, 19]. Thus, the MD simulation shows a plausible mechanism for mD369G to change the dynamics of the channel protein, which affects the allosteric coupling in the D367 activation pathway by altering the traverse of a dynamic substates ensemble or entropy in the free energy of channel gating [44, 45].

This dynamic based allosteric mechanism can be an important target for BK channel modulation. For instance, reported values of intracellular viscosity range from 1 mPa•s (the viscosity of pure water) to above a hundred mPa•s [46, 47]. Such a variation may be due to different samples and techniques of measurements as well as physiological states of the cell [47]. Within this range of viscosity, Ca^{2+} sensitivity of WT BK channels increases with viscosity and can be equivalent or even larger than that of mD369G channels (Figure 2.4D). These results reveal a possibility that at certain physiological state, a high intracellular viscosity could be associated with epilepsy by altering the protein dynamics and potentiating Ca^{2+} sensitivity of BK channels. On the other hand, a

reduction of intracellular viscosity reduces Ca^{2+} sensitivity of the mD369G mutant

channels (Figure 2.4D), which may prevent the role of this mutation in epilepsy. These

possibilities need to be explored by future investigations.

Experimental Procedures

Mutagenesis and expression. The mutations were made using overlap-extension PCR

(polymerase chain reaction) from the *mbr5* splice variant of mSlo1(GenBank accession

number, GI: 347143) [23]. The PCR-amplified regions of all the mutations were verified

by sequencing. RNA was transcribed *in vitro* with T3 polymerase (Ambion, Austin, TX)

and injected into *Xenopus laevis* oocytes (stage IV-V) with an amount of 0.05–50 ng each,

followed by 2-5 days of incubation at 18 ºC.

Electrophysiology. Inside-out patches were formed from oocyte membrane by

borosilicate pipettes of 0.8–1.5 MΩ resistance. Macroscopic currents were recorded with

an Axopatch 200-B patch clamp amplifier (Axon Instruments, Foster City, CA) and

PULSE acquisition software (HEKA Electronik, Lambrecht, Germany). The current

signals were low-pass-filtered at 10 kHz with the amplifier's four-pole Bessel filter and

digitized at 20-µs intervals. The pipette solution contains (in mM): 140 potassium

methanesulphonic acid, 20 HEPES, 2 KCl, 2 $MgCl_2$, pH 7.2. The nominal 0 µM $[Ca^{2+}]_i$

solution contains (in mM): 140 potassium methanesulphonic acid, 20 HEPES, 2 KCl, 5

EGTA, 22 mg/L (+)-18-crown-6-tetracarboxylic acid (18C6TA), pH 7.2. The free $[Ca^{2+}]$

in the nominal 0 $[Ca^{2+}]_i$ solution is about 0.5 nM. $CaCl_2$ was added to a solution

containing (in mM): 140 potassium methanesulphonic acid, 20 HEPES, 2 KCl, 1 EGTA,

22 mg/L 18C6TA, pH 7.2 to obtain the desired free $[Ca^{2+}]$, which was measured by a

Ca^{2+} sensitive electrode (Thermo Electron, Beverly, MA). In experiments that changed

viscosity, sucrose, glycerol, or urea was added to either the nominal 0 μM $[Ca^{2+}]_i$ solution

or the solution containing 200 μM free $[Ca^{2+}]$ (in mM): 140 potassium methanesulphonic

acid, 20 HEPES, 2 KCl, 0.2 $CaCl_2$, pH 7.2. 200 μM free $[Ca^{2+}]$ was used to ensure a

saturating binding of Ca^{2+} to the channels. Viscosity was measured using a Brookfield

DV-III ULTRA Programmable Rheometer (Brookfield Engineering Laboratories,

Middleboro, MA) with a model 40 spindle. Viscosity was measured under two spindle

rotation rates, 30 and 60 RPM, except for solutions with 2 M sucrose or 9 M glycerol, of

which the viscosity was measured under 6 and 12 RPM. All the solutions are Newtonian

fluids so that the viscosity does not change with spindle rotation rate. All the experiments

were performed at room temperature (22–24 ºC).

Analysis. The tail current amplitudes at -50 mV were measured to determine the relative

conductance. The conductance–voltage (G–V) curves were fitted with the Boltzmann

function: $\dfrac{G}{G_{max}} = \dfrac{1}{1 + \exp(-\dfrac{ze(V - V_{1/2})}{kT})}$, where G/G_{max} is the ratio of conductance to

maximal conductance, z is the number of equivalent charges, e is the elementary charge,

V is membrane potential, $V_{1/2}$ is the voltage where G/G_{max} reaches 0.5, k is Boltzmann's

constant, and T is absolute temperature. Error bars in this paper represent standard error of means (S.E.M.).

Monod-Wyman-Changeux (MWC) model. MWC model fits use the following equation:

$$P_{open} = \cfrac{1}{1 + L(0) \cdot e^{\frac{-zeV}{kT}} \cdot \left[\cfrac{1 + \cfrac{[Ca^{2+}]}{K_C}}{1 + \cfrac{[Ca^{2+}]}{K_O}} \right]^4}$$

Where P_{open} is channel's open probability; $L(0)$ is the equilibrium-state ratio of closed to open channels ([C]/[O]) in the absence of bound Ca^{2+} at 0 mV; z, e, V, k, and T are the same as above in Boltzmann function; K_c and K_o are the dissociation constants of Ca^{2+} in the closed and open states, respectively.

Ca^{2+} sensitivity by limiting slope measurement. The limiting slope measurement is applied to determine the open probability at extremely negative voltages [27]. The open probability determined by limiting slope measurement is combined with the corresponding G-V relation to construct a P_o-V curve, which is fitted to the following HCA model [27]:

$$P_o = \cfrac{1}{1 + \cfrac{\exp(-\cfrac{z_L FV}{RT})}{L_o}\left[\cfrac{1 + \exp(\cfrac{z_J F(V - V_{hc})}{RT})}{1 + \exp(\cfrac{z_J F(V - V_{ho})}{RT})}\right]^4}$$

Where z_L is the charge associated with gate opening when all the voltage sensors are at their resting state. z_J is the charge associated with voltage sensor movements. L_0 is the intrinsic open probability at $V = 0$ while all the voltage sensors are at their resting state. V_{hc} and V_{ho} are the voltages for half of the voltage sensors to be at their activation state at the closed and the open conformations, respectively. All the fittings have fixed $z_L = 0.1$, $z_J = 0.57$, and $V_{hc} = 172$ mV; L_0 and V_{ho} are optimized for the best fitting to reflect the Ca^{2+} dependence [48].

In Figure 2.2B and C the P_o at -140 mV is obtained from the HCA model fittings, which is more accurate than that from direct measurements because the model fittings take into account all the P_o-V data at a certain $[Ca^{2+}]_i$ to eliminate experimental variations.

Homology modelling. Sequence alignment of mSlo1 (GenBank accession number, GI: 347143) with MthK channel (1LNQ, GI: 2622639) and Kv1.2 channel (2A79, GI: 1235594) was performed using ClustalW [49]. The gaps in the sequence were predicted using the Protein Loop Optimization Algorithm (PLOP) [50]. Homology models of the mSlo1 AC region (Gly341-Asp420) were generated using Modeller [51].

Molecular dynamics simulations. The package GROMACS [52] was used for all MD simulations. The simulations were performed at 300K using an NpT ensemble, OPLS/AA force field and explicit SPC solvent. In all cases 2 fs time steps were used along with periodic boundary conditions, hydrogen bond constraints and Particle Mesh Ewald for the calculation of long-range electrostatics. The protocol for the simulation involved energy minimization, followed by heating to 300 K at intervals of 50 K, equilibration for 40 ps, and finally the 80 ns production run. The coordinates were saved every 50 ps for subsequent analysis. The 80 ns simulation is limited by computation capacities and is shorter than the time scale of BK channel gating that is at ~0.1 ms. Nevertheless, motions of the backbone on the ps–ns timescale have been shown experimentally as an important carrier of allosteric energy [44, 45].

Root mean square fluctuations: The root mean squared fluctuation of every atom was found using the formula $$\mathrm{RMSF} = \sqrt{\frac{1}{N}\sum\left(x_i - \langle x_i\rangle\right)^2}$$, where x_i is the position of atom i in each simulation frame and $\langle x_i\rangle$ is the average of x over all frames.

Principal Component Analysis: The trajectory obtained from our MD simulations was decomposed into orthogonal modes and the motion of the protein along the first few modes was studied. Cij, the correlation between the movement of an atom i and atom j was found for all N Cα atoms of the protein to form an N*N covariance matrix.

$$C_{ij} = \left\langle M_{ii}^{1/2}\left(x_i - \langle x_i\rangle\right)M_{jj}^{1/2}\left(x_j - \langle x_j\rangle\right)\right\rangle$$, where M is a diagonal matrix containing the masses

of the atoms. The covariance matrix was diagonalized to get N eigenvectors and corresponding eigenvalues. The MD trajectory was projected on the eigenvector having the largest eigenvalue to get the principal mode that captures the largest amplitude motion of the protein.

Author Contributions G.K. and J.C. initiated the study. G.K., J.Y., G.Z. and J.C. made key experimental observations. A.S. and D.S. performed molecular modeling and MD simulations, which provided motivation for experiments in Figure 2.5. G.K., J.Y. and J.S. performed experiments in Figures 1, 3 and 5. J.Y. and J.S. performed experiments in Figures 2, 4 and 6. G.Z., H.Y. and K.D. also performed experiments in Figures 1 and 5. J.Y., G.K., A.S. and J.C. wrote the manuscript, with revisions from H.Y. and D.S..

References

1.   Ashcroft, F.M., *Ion Channels and Disease: Channelopathies*. 2000, San Diego, California, USA: Academic Press.

2.   Yellen, G., *Premonitions of ion channel gating.* Nat. Struct. Biol., 1998. **5**(6): p. 421.

3.   Bezanilla, F., *How membrane proteins sense voltage.* Nat. Rev. Mol. Cell Biol., 2008. **9**(4): p. 323-32.

4.   Swartz, K.J., *Sensing voltage across lipid membranes.* Nature, 2008. **456**(7224): p. 891-7.

5.   Unwin, N., Structure and action of the nicotinic acetylcholine receptor explored by electron microscopy. FEBS Lett., 2003. **555**(1): p. 91-5.

6.   Xia, X.M., et al., Mechanism of calcium gating in small-conductance calcium-activated potassium channels. Nature, 1998. **395**(6701): p. 503-7.

7.   Jiang, Y., et al., Crystal structure and mechanism of a calcium-gated potassium channel. Nature, 2002. **417**(6888): p. 515-522.

8.   Zagotta, W.N., et al., Structural basis for modulation and agonist specificity of HCN pacemaker channels. Nature, 2003. **425**(6954): p. 200-5.

9.   Cui, J., H. Yang, and U. Lee, *Molecular mechanisms of BK channel activation.* Cell. Mol. Life Sci., 2008. **66**(5): p. 852-875.

10.   Du, W., et al., Calcium-sensitive potassium channelopathy in human epilepsy and paroxysmal movement disorder. Nat. Genet., 2005. **37**(7): p. 733-738.

11.   Krishnamoorthy, G., et al., The NH_2 terminus of RCK1 domain regulates Ca^{2+}-dependent BK_{Ca} channel gating. J. Gen. Physiol., 2005. **126**(3): p. 227-241.

12.   Atkinson, N.S., G.A. Robertson, and B. Ganetzky, *A component of calcium-activated potassium channels encoded by the Drosophila slo locus.* Science, 1991. **253**(5019): p. 551-555.

13.   Shen, K.Z., et al., Tetraethylammonium block of Slowpoke calcium-activated potassium channels expressed in Xenopus oocytes: Evidence for tetrameric channel formation. Pflügers Arch., 1994. **426**(5): p. 440-445.

14.   Schreiber, M. and L. Salkoff, *A novel calcium-sensing domain in the BK channel.* Biophys. J., 1997. **73**(3): p. 1355-1363.

15.   Xia, X.-M., X. Zeng, and C.J. Lingle, Multiple regulatory sites in large-conductance calcium-activated potassium channels. Nature, 2002. **418**(6900): p. 880-884.

16.   Shi, J., et al., Mechanism of magnesium activation of calcium-activated potassium channels. Nature, 2002. **418**(6900): p. 876-880.

17.   Yang, H., et al., Activation of Slo1 BK channels by Mg^{2+} coordinated between the voltage sensor and RCK1 domains. Nat. Struct. Mol. Biol., 2008. **15**(11): p. 1152-1159.

18.   Long, S.B., E.B. Campbell, and R. MacKinnon, *Crystal structure of a mammalian voltage-dependent shaker family K^+ channel.* Science, 2005. **309**(5736): p. 897-903.

19.   Wang, L. and F.J. Sigworth, Structure of the BK potassium channel in a lipid membrane from electron cryomicroscopy. Nature, 2009. **461**(7261): p. 292-295.

20.   Magleby, K.L., *Gating mechanism of BK (Slo1) channels: so near, yet so far.* J. Gen. Physiol., 2003. **121**(2): p. 81-96.

21.   Niu, X., X. Qian, and K.L. Magleby, Linker-gating ring complex as passive spring and Ca^{2+}-dependent machine for a voltage- and Ca^{2+}-activated potassium channel. Neuron, 2004. **42**(5): p. 745-756.

22.   Brenner, R., et al., BK channel [beta]4 subunit reduces dentate gyrus excitability and protects against temporal lobe seizures. Nat. Neurosci., 2005. **8**(12): p. 1752-1759.

23.   Butler, A., et al., mSlo, a complex mouse gene encoding "maxi" calcium-activated potassium channels. Science, 1993. **261**(5118): p. 221-224.

24.   Cox, D.H., J. Cui, and R.W. Aldrich, *Allosteric gating of a large conductance Ca-activated K$^+$ channel.* J. Gen. Physiol., 1997. **110**(3): p. 257-281.

25.   Cui, J., D.H. Cox, and R.W. Aldrich, Intrinsic voltage dependence and Ca^{2+} regulation of mslo large conductance Ca-activated K$^+$ channels. J. Gen. Physiol., 1997. **109**(5): p. 647-73.

26.   Schreiber, M., A. Yuan, and L. Salkoff, *Transplantable sites confer calcium sensitivity to BK channels.* Nat. Neurosci., 1999. **2**(5): p. 416-21.

27.   Horrigan, F.T., J. Cui, and R.W. Aldrich, Allosteric voltage gating of potassium channels I. Mslo ionic currents in the absence of Ca^{2+}. J. Gen. Physiol., 1999. **114**(2): p. 277-304.

28.   Sweet, T.-B. and D.H. Cox, Measurements of the BK$_{Ca}$ channel's high-affinity Ca^{2+} binding constants: Effects of membrane voltage. J. Gen. Physiol., 2008. **132**(5): p. 491-505.

29.   Qian, X., X. Niu, and K.L. Magleby, *Intra- and intersubunit cooperativity in activation of BK channels by Ca^{2+}.* J. Gen. Physiol., 2006. **128**(4): p. 389-404.

30.   Wang, B., B.S. Rothberg, and R. Brenner, Mechanism of Increased BK Channel Activation from a Channel Mutation that Causes Epilepsy. J. Gen. Physiol., 2009. **133**(3): p. 283-294.

31.   Beece, D., et al., *Solvent viscosity and protein dynamics.* Biochemistry, 1980. **19**(23): p. 5147-57.

32.   Ansari, A., et al., The role of solvent viscosity in the dynamics of protein conformational changes. Science, 1992. **256**(5065): p. 1796-8.

33.   Frauenfelder, H., et al., *A unified model of protein dynamics.* Proc. Natl. Acad. Sci. U S A, 2009. **106**(13): p. 5129-34.

34.   Kukita, F., Solvent-dependent rate-limiting steps in the conformational change of sodium channel gating in squid giant axon. J. Physiol., 1997. **498**(Pt 1): p. 109-133.

35.   Fumio, K., Solvent effects on squid sodium channels are attributable to movements of a flexible protein structure in gating currents and to hydration in a pore. J. Physiol., 2000. **522**(3): p. 357-373.

36.   Diez-Sampedro, A., et al., *Mechanism of increased open probability by a mutation of the BK channel.* J. Neurophysiol., 2006. **96**(3): p. 1507-16.

37.   Cui, J. and R.W. Aldrich, Allosteric linkage between voltage and Ca^{2+}-dependent activation of BK-type mslo1 K^+ channels. Biochemistry, 2000. **39**(50): p. 15612-15619.

38.   Horovitz, A. and A.R. Fersht, Strategy for analysing the co-operativity of intramolecular interactions in peptides and proteins. J. Mol. Biol., 1990. **214**(3): p. 613-7.

39.   Schreiber, M., et al., *Slo3, a novel pH-sensitive K^+ channel from mammalian spermatocytes.* J. Biol. Chem., 1998. **273**(6): p. 3509-16.

40.   Yuan, A., et al., The sodium-activated potassium channel is encoded by a member of the slo gene family. Neuron, 2003. **37**(5): p. 765-773.

41.   Yuan, A., et al., *SLO-2, a K^+ channel with an unusual Cl^- dependence.* Nat. Neurosci., 2000. **3**(8): p. 771-779.

42.   Jiang, Y., et al., Structure of the RCK domain from the E. coli K^+ channel and demonstration of its presence in the human BK channel. Neuron, 2001. **29**(3): p. 593-601.

43.   Pico, A.R., *RCK domain model of calcium activation in BK channels.* PhD Thesis, The Rockefeller University, 2003.

44.   Kern, D. and E.R. Zuiderweg, *The role of dynamics in allosteric regulation.* Curr. Opin. Struct. Biol., 2003. **13**(6): p. 748-57.

45.   Popovych, N., et al., *Dynamically driven protein allostery.* Nat. Struct. Mol. Biol., 2006. **13**(9): p. 831-8.

46.   Wandelt, B., et al., Single cell measurement of micro-viscosity by ratio imaging of fluorescence of styrylpyridinium probe. Biosens. Bioelectron., 2005. **20**(9): p. 1728-36.

47.   Kuimova, M.K., et al., Imaging intracellular viscosity of a single cell during photoinduced cell death. Nat. Chem., 2009. **1**(1): p. 69-73.

48.   Horrigan, F.T. and R.W. Aldrich, Coupling between voltage sensor activation, Ca^{2+} binding and channel opening in large conductance (BK) potassium channels. J. Gen. Physiol., 2002. **120**(3): p. 267-305.

49.   Thompson, J.D., D.G. Higgins, and T.J. Gibson, CLUSTAL W: improving the sensitivity of progressive multiple sequence alignment through sequence weighting, position-specific gap penalties and weight matrix choice. Nucleic Acids Res., 1994. **22**(22): p. 4673-80.

50.   Jacobson, M.P., et al., *A hierarchical approach to all-atom protein loop prediction.* Proteins, 2004. **55**(2): p. 351-67.

51.   Sali, A. and T.L. Blundell, *Comparative protein modelling by satisfaction of spatial restraints.* J. Mol. Biol., 1993. **234**(3): p. 779-815.

52.   Lindahl, E., B. Hess, and D. van der Spoel, *GROMACS 3.0: a package for molecular simulation and trajectory analysis.* J. Mol. Model., 2001. **7**: p. 306-17.

Chapter 3: Coupling by Movements between Structural Domains

Abstract: Crosstalk between structural domains is critical to protein functions. In ion channels, gating in the pore domain is regulated by voltage- and ligand-sensing domains. While structural studies have suggested possible conformational changes that are correlated with gating, the causality of conformational changes to gating needs to be established. Here we show that gating of the voltage- and Ca^{2+}-activated K^+ (BK) channel is correlated with a change in the distance between the cytosolic and membrane-spanning domains, and these two processes are energetically coupled. A disulfide bond, which is formed between the two domains, can be formed only when the channel is closed, suggesting a distance change between the two domains during channel gating. An engineered electrostatic interaction between the two domains alters this distance and results in changed open probability of the gate. These results suggest that voltage and Ca^{2+} binding cause a relative movement between the cytosolic and membrane-spanning domains to open the BK channel.

Introduction

Most proteins contain distinguishable structural domains. Crosstalk between domains

integrates distinct functions and contributes to the diversity of protein activities. Ion

channels are important proteins for many physiological activities, including neural signal

transduction and muscle contraction [1]. Ion channels conduct ionic current across the

cell membrane through their pore domain, which is unique for various ion channels

because of its selectivity to ion species [1, 2]. The opening and closing (gating) of the

pore is often regulated by attached but distinguishable domains that sense physiological

stimuli, such as voltage [3, 4] and ligand-binding [5-10].

Recent studies on crystallographic structures have provided important information of the

conformational change that may regulate gating. For example, the crystallographic

structures of the Ca^{2+}-activated MthK channel reveal that its Ca^{2+}-sensing domain may

undergo large conformational changes upon Ca^{2+}-binding [10, 11]. MthK channel senses

Ca^{2+} binding on its ring-like intracellular domain, called the gating ring. The Ca^{2+}-bound

structure of the gating ring expands its diameter by 8 Å compared to the Ca^{2+}-free

structure [11]. The expanding motion of the gating ring is suggested to pull the pore to

open, functioning as the intermediate conformational change that couples Ca^{2+} binding to

gating, that occur in distinct domains [10, 11]. More interestingly, the regulative

conformational change may include relative movement between distinct domains. For

example, by comparing structures of Kir channels at different conduction states, Gulbis et

al. suggest that the cytosolic domain of the Kir channel undergoes twisting and latching movements accompanied with the pore switching between the conductive and nonconductive states [12].

However, although crystallographic structures may correlate conformational changes in ligand-sensing domains with gating, it is probably insufficient to establish causality relationship since the processes could be coincidently correlated and energetically irrelevant to each other. Therefore, functional studies are necessary to examine whether gating is regulated by conformational changes of regulative domains and to establish the causality relationship between these two processes.

The large conductance voltage- and Ca^{2+}- activated K^+ (BK) channel is widely expressed in a variety of tissues and plays important roles in physiological functions [13-17]. Each BK channel is composed of four identical subunits, each subunit contains one membrane-spanning domain and one large cytosolic domain [18, 19]. The membrane-spanning domain includes the pore-gate domain and a voltage sensing domain (Figure 3.1a). The large cytosolic domain is the Ca^{2+}-sensing domain which contains two Ca^{2+} binding sites and is linked to the inner helix of the pore [20-23].

Recent functional studies suggest that the regulative domains of the BK channel undergo conformational changes during gating. The BK channel is activated by intracellular Mg^{2+} in the millimolar range [24-26]. Mg^{2+} binds at the interface between the cytosolic and membrane-spanning domains [21, 27-30]. Bound Mg^{2+} activates the channel by

interacting with gating charge R213 in the membrane-spanning domain through electrostatic interaction [28, 29, 31]. The Mg^{2+}-R213 interaction is state-dependent such that its strength increases when the channel is at the open state [28]. Because the Mg^{2+}-R213 interaction occurs between the cytosolic and membrane-spanning domains, the varying strength suggests that the distance between R213 and the Mg^{2+} binding site may change with gating. Additionally, Q397, a residue on the cytosolic domain, is located beside the Mg^{2+} binding site and its positively charged mutation, Q397R, mimics bound Mg^{2+} by interacting with R213 [28]. This inter-domain R213-R397 interaction is state-dependent as the Mg^{2+}-R213 interaction [28]. This further correlates gating with conformational changes of the regulative domains. However, it is unclear whether the inter-domain distance regulates gating in a causative fashion.

In this work, we further established the correlation between gating and the inter-domain distance by demonstrating the state-dependence of the formation of a disulfide bond formed between the cytosolic and membrane-spanning domains. To examine if the inter-domain distance energetically and causatively regulates gating, we manipulated the distance by introducing an electrostatic interaction between the cytosolic and membrane-spanning domains. We found that altered inter-domain distance results in altered gating. These results established the causality relationship between gating and the conformational changes of the regulative domains represented by the change in the inter-domain distance. Our experiments further show that this change in inter-domain distance can be transformed into an overall conformational change that involves the pore domain,

suggesting that changes in inter-domain distance is one component of the overall conformational change that couples Ca^{2+}-sensing to gating.

Results

State-dependent formation of an inter-domain disulfide bond

Previous study shows that in Mg^{2+} activation of the BK channel, the intracellular Mg^{2+} binds at the interface between the cytosolic and membrane-spanning domains. The bound Mg^{2+} interacts with R213, a positively charged residue in the membrane-spanning domain, to enhance channel activation. The strength of the Mg^{2+}-R213 interaction depends on gating such that it is stronger when the pore is at its conductive state. This suggests that the distance between the bound Mg^{2+} and R213 is shorter when the pore is conductive, and thereby correlates gating with inter-domain distance around the Mg^{2+} binding site.

Previous study also shows that a disulfide bond can be formed between the cytosolic and membrane-spanning domains. D99 and Q397 are from the membrane-spanning and cytosolic domains, respectively. They form an inter-domain disulfide bond when both are mutated to Cysteine [28] (Figure 3.1a). This disulfide bond can be broken by DTT. Upon breaking of this disulfide bond, the cysteine at C397 is freed and can be modified by MTSET reagent. MTSET modification adds a positively charged group at C397 and introduces electrostatic interaction with R213 in the membrane-spanning domain. The

breaking of the disulfide bond and the addition of the MTSET group can both be detected

with shifted conductance-voltage (G-V) relation [28].
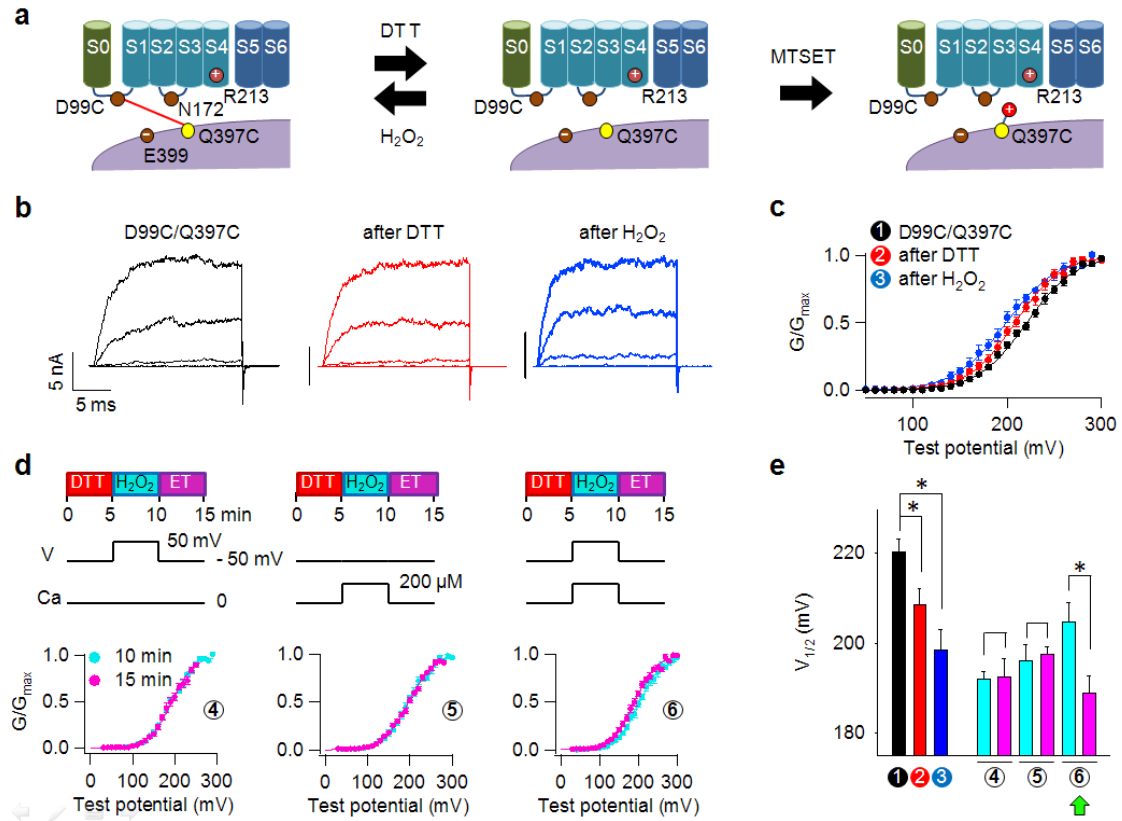
Figure 3.1 Inter-domain disulfide bond is re-formed at non-conductive state. **a**) Cartoon scheme showing the breaking and re-formation of the inter-domain disulfide bond formed between C99 and C397. The membrane-spanning domain contains seven transmembrane segments (S0-S6), which form the voltage sensor (S1-S4) and the pore domain (S5-S6). Across the interface between the membrane-spanning domain and the cytosolic domain (purple), C99 and C397 form disulfide bond (left panel), which can be broken by DTT (middle panel) and free C397 for MTSET

modification (right panel). MTSET modification adds to C397 a positively charged group, which interacts with R213 in S4 through electrostatic interaction and enhances channel activation. After DTT breaking the disulfide bond, H_2O_2 may re-form the disulfide bond. **b**) Macroscopic current traces from inside-out patches expressing D99C/Q397C before (left panel) and after DTT (middle panel) or H_2O_2 (right panel) treatment. Currents were elicited in nominal 0 $[Ca^{2+}]_i$ by voltages ranging from 50 mV to 250 mV, with 50 mV interval. The voltage before and after the pulse were − 50 mV and − 80 mV, respectively. Vertical scale bar represents 5 nA for corresponding current traces. **c**) G-V relation of D99C/Q397C before and after DTT or H_2O_2 treatment. $[Ca^{2+}]_i$ is nominal 0. Solid lines are fits with the Boltzmann equation. Circled numbers 1-3 are used to indicate corresponding experimental conditions in e). **d**) G-V relation of D99C/Q397C after sequential DTT and H_2O_2 treatments (cyan circles) or after the third treatment with MTSET (purple circles). Each treatment took 5 min. The voltage and intracellular $[Ca^{2+}]$ is indicated. The voltage and $[Ca^{2+}]$ levels during the second step of H_2O_2 treatment vary so that the pore is at its non-conductive state (left and middle panels) or conductive state (right panel). Solid lines are fits with the Boltzmann equation. Circle numbers 4-6 are used to indicate corresponding experimental conditions in e). **e**) $V_{1/2}$ of G-V relations under corresponding experimental conditions indicated by the circled numbers in c) and d). Cyan bars are $V_{1/2}$ for G-V relations after sequential DTT and H_2O_2 treatments in d). Purple bars are $V_{1/2}$ for G-V relations after the third treatment with MTSET in d). Asterisks indicate a significant difference between the indicated values (p < 0.05 in Student's t test). Green arrow indicates that this experimental condition during H_2O_2 treatment holds the pore at its conductive state. C430A is included for D99C/E399C to eliminate nonspecific MTS effects.

It is possible that after DTT breaks the disulfide bond, the disulfide bond can be re-formed under oxidative conditions, such as in the presence of hydrogen peroxide (H_2O_2). As a result, if the disulfide bond is re-formed, modification by MTSET would be prevented because C397 is protected by the disulfide bond. However, since the formation of disulfide bond requires proper distance between the two cysteines (the C_β-C_β distance for the two cysteines should be between 2.9 Å and 4.6 Å [32]), if the cytosolic and membrane-spanning domains change their distance, the disulfide bond may not be re-formed even under oxidative conditions (Figure 3.1a).

To test the re-formation of this disulfide bond, we obtained the G-V relation of the double cysteine mutation, D99C/Q397C/C430A (Figure 3.1) – C430 is mutated to Alanine in order to eliminate unspecific effect by MTSET modification [33]. After DTT treatment, the G-V relation shifts to the lower voltage range (Figure 3.1b middle, 3.1c and 3.1e), indicating that the disulfide bond is broken. On the other hand, although H_2O_2 does not break the disulfide bond, it shifts the G-V relation to the left, which is consistent with reported oxidation effect on BK channels of unidentified residues [34, 35] (Figure 3.1b right, 3.1c and 3.1e).

To examine if the disulfide bond can be re-formed by H_2O_2, we treated the mutant channel with DTT, H_2O_2 and MTSET sequentially, each taking 5 minutes (Figure 3.1d). We found that when the treatment of H_2O_2 is at the conditions where BK channels are closed, the G-V relation is unchangeable by subsequent MTSET treatment (Figure 3.1d

104

left and middle, 3.1e), suggesting that C397 is protected from MTSET modification after the preceding DTT and H_2O_2 treatments. Since DTT treatment breaks the disulfide bond and frees C397, this indicates that H_2O_2 treatment can re-form the disulfide bond between C99 and C397.

However, re-formation by H_2O_2 is conditional. As shown in Figure 3.1d, we varied voltage between – 50 mV and + 50 mV and $[Ca^{2+}]$ between 0 and 200 μM during the H_2O_2 treatment. The disulfide bond is re-formed by H_2O_2 as long as $[Ca^{2+}]$ is 0 (Figure 3.1d left, ④ in Figure 3.1e) or voltage is held at – 50 mV (Figure 3.1d middle, ⑤ in Figure 3.1e) because MTSET modification is prevented. On the other hand, the disulfide bond is not fully re-formed by H_2O_2 when voltage is held at + 50 mV while in the presence of 200 μM $[Ca^{2+}]$ because the following MTSET treatment alters the G-V relation (Figure 3.1d right and ⑥ in Figure 3.1e).

Re-formation of the disulfide bond is determined by the voltage and $[Ca^{2+}]$ level during the H_2O_2 treatment. Both high levels of voltage and $[Ca^{2+}]$ are needed to prevent full re-formation, indicating that re-formation of disulfide bond is state-dependent such that the bond is re-formed when the channel is at its nonconductive state and it is not fully re-formed when at conductive state. Consistently, the re-formation is not solely determined by voltage or $[Ca^{2+}]$ alone because high level of voltage or $[Ca^{2+}]$ without opening the channel is not sufficient to disrupt the re-formation of disulfide bond (Figure 3.1d left and middle, ④ and ⑤ in Figure 3.1e). Because the formation of disulfide bond between two

cysteines is highly determined by their distance and orientation, its dependence on gating

state indicates that the relative position between C99 and C397 changes with gating,

providing another line of evidence which correlates gating with conformational changes

of the regulative domains, in addition to the Mg^{2+}-R213 interaction.

The conformational change of the regulative domains in BK channel can be very

complicated and involve multiple motion components. One motion that is known based

on the above two lines of evidence is the change in inter-domain distance around the

Mg^{2+} binding site since both the formation of the C99-C397 disulfide bond and the

strength of the Mg^{2+}-R213 interaction are determined by the distance between these two

domains. To examine the causative relationship between gating and the conformational

change of the regulative domains, we manipulated the conformational change by simply

altering this known component: the inter-domain distance around the Mg^{2+} binding site.

Inter-domain electrostatic interaction alters channel activation

A limitation of the relative movement between the cytosolic and membrane-spanning

domains by a disulfide bond that connects the two domains reduces channel activation

(Figure 3.1). This result suggests that such a movement takes part of and contributes

energetically to the gating process of the BK channel. To further examine this mechanism,

we engineered electrostatic interactions between the two domains to alter the inter-

domain distance and to measure if channel activation is changed consequently.

N172 and E399 are located on the membrane-spanning and cytosolic domains,

respectively. These two residues are part of the Mg^{2+} binding site [29, 30] so that they are

located close to each other. We mutated both N172 and E399 to cysteine and applied

MTS reagents in the intracellular solution patch clamp recordings. The charged MTS

reagents, MTSET(+) and MTSES(-), shifted G-V relation of the channel to more positive

voltages (Figure 3.2a). The neutral MTSACE did not affect the G-V relation, and a

subsequent MTSET treatment failed to shift the G-V relation (Figure 3.2b), indicating

that both C172 and C399 were covalently modified by MTSACE but the modification did

not affect channel gating. These results suggest that charges at 172 and 399 affect

channel activation by electrostatic interactions. Consistent with this mechanism, an

increase of the ionic strength of the intracellular solution attenuated the effects of the

MTS reagents (Figure 3.2c-f). Figure 3.2c and d show that the increase of ionic strength

itself has no effect on channel activation.
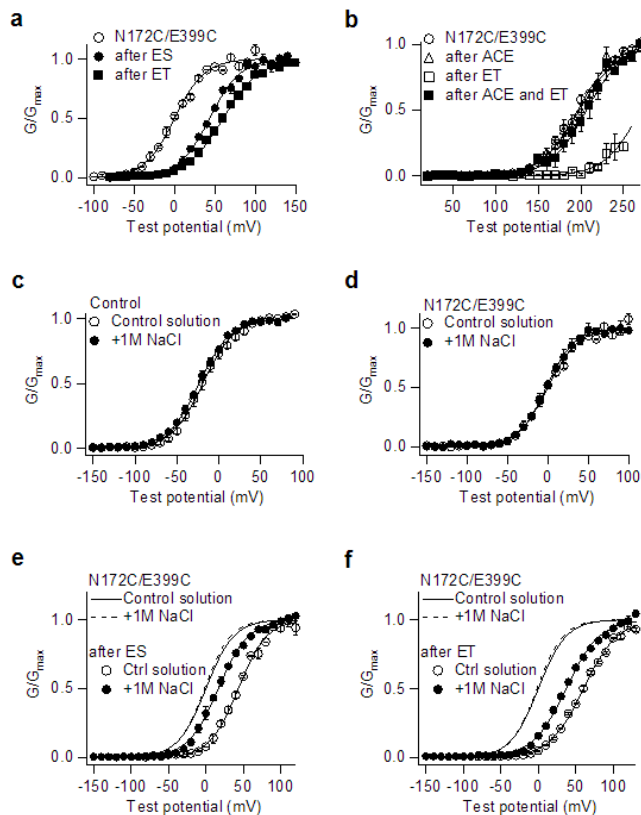
Figure 3.2 MTS modification introduces electrostatic interaction to N172C/E399C. **a**) G-V relation of N172C/E399C is shifted to higher voltage range after treatment of MTSES or MTSET reagent. MTSES adds negatively charged residue to cysteines while MTSET adds positively charged residue. $[Ca^{2+}]_i$ is 200 μM. Solid lines are fittings to the Boltzmann equation. **b**) G-V relations of N172C/E399C after MTSACE and/or MTSET modification. MTSACE adds neutral residue to cysteine. $[Ca^{2+}]_i$ is nominal 0 (~ 0.5 nM). Solid lines are fittings to the Boltzmann equation. **c**)-**f**) G-V relations in the absence (open circles) or presence (closed circles) of 1 M NaCl for control (c), N172C/E399C (d), and N172C/E399C after MTSES (e) or MTSET (f) modification. Solid lines are the fittings to the Boltzmann equation. $[Ca^{2+}]_i$ is 200 μM. C430A is

included for all the above mutations to eliminate nonspecific MTS effects.

Since both the negatively and positively charged MTS reagents alter the G-V relation similarly (Figure 3.2a), the effect on G-V relation is likely due to the electrostatic interactions between the two charges at 172 and 399 such that the same charges repulse each other. To further examine this mechanism, we altered charges at 172 and 399, respectively, either by MTS modification of a cysteine residue or by mutations to charged or neutral amino acid residues and measured the effects of these residues on channel activation (Figure 3.3a, b). As of the charge type at individual residues, the charge at 172, but not the one at 399, may affect channel activation. As shown in the left panel of Figure 3.3a, when we neutralize the charge at 399 by mutation E399C, the G-V relation is shifted to lower voltage range by a positive charge at 172 (E399C/N172R) and to higher voltage range by a negative charge at 172 (E399C/N172D). However, as shown in the right panel, if the residue at 172 is neutral, the G-V relation is not shifted by altering the charge type at 399. By correlating the $V_{1/2}$ value with the charge types at 172 and 399 for 28 mutations and/or modifications, analysis of variance (ANOVA) also shows that channel activation is correlated with the charge type at 172 (p = 0.020) but not with the charge type at 399 (p = 0.22) (Figure 3.3b). Plot of $V_{1/2}$ also shows dependence on charge type for residue 172 but not for residue 399 (Figure 3.3c). Moreover, ANOVA further shows that the interaction between 172 and 399 affects channel activation with even

greater effectiveness because the p value is 0.0005 (Figure 3.3b). Based on both the

charge types at 172 and 399, the interaction between 172 and 399 can be repulsion,

attraction, or 0. The correlation explicitly suggests that repulsion shifts the G-V relation

to a higher voltage range and attraction shifts it to a lower voltage range (Figure 3.3b, c).

Therefore, channel activation is regulated by the electrostatic interaction between 172-

399. Different types of interaction can be introduced in order to cause different effect on

channel activation. To avoid the complication of the charge type at 172, we changed the

interaction type by changing the charge type at 399 while keeping the residue at 172 for

the following each set of experiment.

a

- ● E399C/N172D
- ○ E399C/N172R
- ∗ E399C

- ■ N172Q
- # N172Q/E399N
- □ N172Q/E399R

b

No.	Charge at 172	Charge at 399	Inter.	$V_{1/2}$ (mV)
1	0 (Cys)	0 (Cys)	0	197±5
2	− (Cys/ES)	− (Cys/ES)	Rep	250±9
3	+ (Cys/ET)	+ (Cys/ET)	Rep	271±9
4	0 (Cys)	− (Glu)	0	193±2
5	− (Cys/ES)	− (Glu)	Rep	236±3
6	+ (Cys/ET)	− (Glu)	Attr	174±4
7	0 (Asn)	0 (Cys)	0	167±4
8	0 (Asn)	− (Cys/ES)	0	190±2
9	0 (Asn)	+ (Cys/ET)	0	201±2
10	− (Asp)	0 (Cys)	0	203±2
11	− (Asp)	− (Cys/ES)	Rep	237±3
12	− (Asp)	+ (Cys/ET)	Attr	177±4
13	+ (Arg)	0 (Cys)	0	148±3
14	+ (Arg)	− (Cys/ES)	Attr	165±7
15	+ (Arg)	+ (Cys/ET)	Rep	203±2
16	0 (Asn)	− (Glu)	0	198±2
17	+ (Arg)	− (Glu)	Attr	139±1
18	+ (Arg)	0 (Cys)	0	138±3
19	+ (Arg)	+ (Arg)	Rep	172±4
20	− (Asp)	− (Glu)	Rep	211±3
21	− (Asp)	0 (Asn)	0	200±4
22	− (Asp)	+ (Arg)	Attr	153±3
23	0 (Asn)	− (Glu)	0	164±2
24	0 (Asn)	0 (Asn)	0	170±4
25	0 (Asn)	+ (Arg)	0	172±3
26	0 (Gln)	− (Glu)	0	181±2
27	0 (Gln)	0 (Asn)	0	186±3
28	0 (Gln)	+ (Arg)	0	184±3
p	0.020*	0.22	0.0005*	

c

Figure 3.3 MTS modification introduces electrostatic interaction between residues 172 and 399. **a**) G-V relation is shifted by charge at 172, but not charge at 399. $[Ca^{2+}]_i$ is nominal 0 (~ 0.5 nM). Solid lines are fittings to the Boltzmann equation. **b**) Table summarizing $V_{1/2}$ of G-V relation for a variety of mutations at residues 172 and 399. MTS modification is employed to add charged groups to cysteines for some of the mutations. The charge type and corresponding residue at 172 and 399 is listed for each mutation using symbols + (positive), - (negative), and 0 (neutral). The charge type may be altered by MTSET or ES modification to the cysteine at 172 and/or 399 (indicated using "/ET" or "/ES"). As a result, the electrostatic interaction between 172 and 399 can be Repulsion (between like charges), Attraction (between opposite charges), or 0 (if not both are charged). *p* values are calculated using ANOVA test. *p* value less than 0.05 indicates significance. C430A is included for mutations No. 1-19. **c**) $V_{1/2}$ vs. charge type at 172 (top) or 399 (middle), or the interaction between residues 172 and 399 (bottom). Solid lines are fittings to linear regression. The slope of linear regression is -16.1 ± 7.5 for the charge type at 172 and -2.6 ± 7.4 for the charge type at 399. It is 33.3 ± 6.8 for the interaction type.

The electrostatic interaction between 172-399 alters inter-domain distance

Since residues 172 and 399 are located in the membrane-spanning and cytosolic domains, respectively, the electrostatic interactions between the two residues may alter the relative movements and the distance between the two domains to affect channel activation. To

further examine this mechanism, we employed two methods to detect changes in the inter-domain distance as a result of the 172-399 electrostatic interactions.

Disulfide bond formation

First, we examined if the 172-399 electrostatic interactions disrupt the disulfide bond between C99 and C397. This disulfide bond connects the membrane-spanning and cytosolic domains (Figure 3.1) and can form only when C99 and C397 are located within a certain distance (2.9 - 4.6 Å [32]). Therefore, the disruption of this disulfide bond can indicate a change in the distance between the two domains. The C99-C397 disulfide bond forms spontaneously in the absence of electrostatic interactions between 172 and 399 [29] (Figure 3.1). It can be detected by measuring changes in the G-V relation in response to DTT and MTS treatments as shown in above (Figure 3.1). If the disulfide bond is not formed, MTSET or MTSES can modify C397 and the charge added to C397 causes a shift of G-V. Consistently, DTT treatment has no effect. On the other hand, the C99-C397 disulfide bond protects C397 from MTS modification. Therefore, MTSET or MTSES treatment would not alter channel activation. Consistently, because DTT breaks disulfide bond, DTT treatment would alter channel activation.

To manipulate the 172-399 interaction, negative E399 is mutated to neutral N or positive R on the background of N172R/C430A. Thus the 172-399 interaction changes from attraction to none or repulsion (Figure 3.4). Meanwhile, both D99 and Q397 are mutated to Cysteine so that they can form a disulfide bond if the distance is appropriate. All three

mutations were treated with ES, ET, or DTT (Figure 3.4). As shown in Figure 3.4a-b

(left), ET, but not ES or DTT, changes the G-V relation of D99C/Q397C/N172R/C430A,

which has attractive 172-399 interaction. DTT has no effect because the C99-C397

disulfide bond is not formed. Therefore, C397 is subject to MTSET modification because

it is not protected by the disulfide bond. Similarly, the disulfide bond is also not formed

in D99C/Q397C/N172R/E399R/C430A, which has repulsive 172-399 interaction (Figure

3.4a-b (right)). For this mutation, ES, but not DTT, changes the G-V relation. Therefore,

both attractive and repulsive 172-399 interactions disrupt the spontaneous formation of

the inter-domain disulfide bond, suggesting that the distance between the two Cysteines

is determined by the inter-domain interaction.
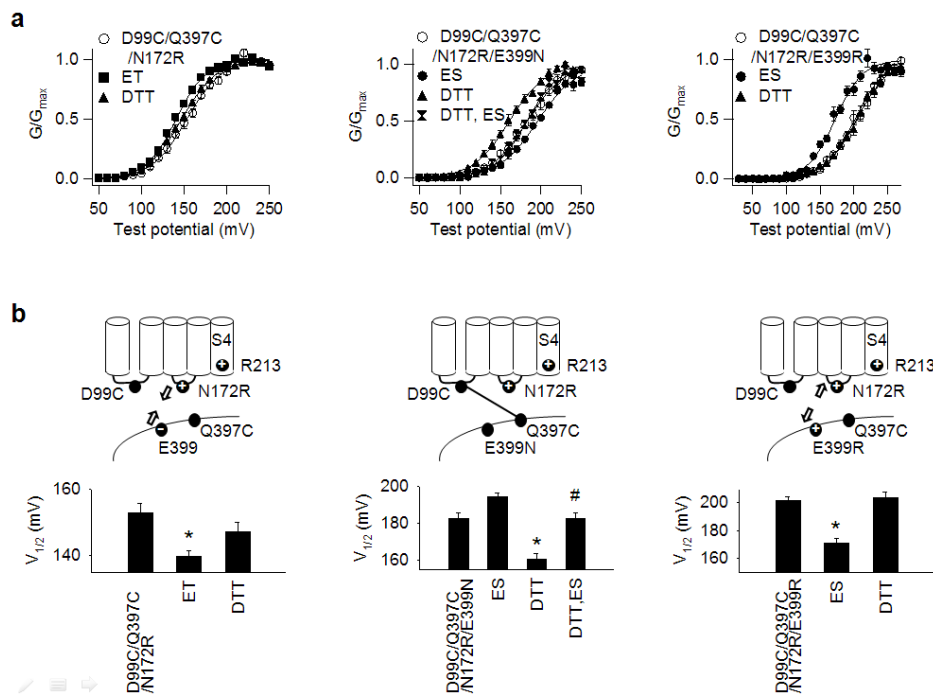
Figure 3.4 The 172-399 interaction regulates the formation of inter-domain disulfide bond. **a**) G-V relations before (open circles) and after (closed symbols) treatment of MTSES, MTSET or DTT when E399 is mutated to Asn (middle panel) or Arg (right panel) on the background of D99C/Q397C/N172R (left panel). "DTT, ES" in the middle panel represents the treatment of DTT followed by MTSES. $[Ca^{2+}]_i$ is nominal 0. Solid lines are fits with the Boltzmann equation. **b**) Top panels are cartoon schemes of the disulfide bond formation and its dependence on the 172-399 interaction for the corresponding mutations in a). The C99-C397 disulfide bond is formed when there is no 172-399 interaction (**middle**). This disulfide bond is not formed when there is attractive (**left**) or repulsive (**right**) 172-399 interaction. Bottom panels are $V_{1/2}$ of the G-V relations in a). Stars indicate the corresponding treatment significantly changes $V_{1/2}$ ($p < 0.005$). Pound indicates that $V_{1/2}$ after the treatment of MTSES following DTT is significantly different from the $V_{1/2}$ after the treatment of DTT alone ($p < 0.005$). C430A is included for all the above mutations to eliminate nonspecific MTS effects.

On the other hand, for D99C/Q397C/N172R/E399N/C430A, which has no 172-399 interaction, DTT treatment changes channel activation, indicating that the 99-397 disulfide bond is spontaneously formed (Figure 3.4a-b (middle)). Consistently, the MTSES treatment changes channel activation only after DTT treatment breaking the disulfide bond, suggesting that C99 and C397 are freed by DTT treatment.

115

Therefore, the three mutations tested in Figure 3.4 indicate that the formation of disulfide bond is determined by the inter-domain 172-399 interaction, suggesting that the 172-399 interaction determines the distance between C99 and C397. Moreover, the inter-domain disulfide bond is spontaneously formed in both D99C/Q397C/N172R/E399N/C430A (Figure 3.4a-b (middle)) and D99C/Q397C/C430A (Figure 3.1), indicating that the charge type at residue 172 or 399 does not affect its formation. Therefore, its formation is only disrupted due to the 172-399 interaction.

Gating charge movement

To further investigate if the 172-399 interaction alters the inter-domain distance, we examined its influence on gating charge movement. The movement of gating charge, particularly R213, generates transient current, called the gating current [28]. The amplitude of gating current is determined by the speed of R213 movement, which can be affected by its electrostatic interaction with the positively charged residue at 397 [28]. More specifically, the positively charged residue at 397 (introduced by mutation Q397R) repels R213 so as to slow its return from active state to resting state, resulting in smaller gating current. If the distance between R213 and R397 is shortened by the 172-399 interaction, then the repulsion would be stronger so as to further slow down R213 from returning to its resting state and decrease gating current more. Moreover, the R213-R397 repulsion occurs mainly when the channel is at its conductive state; at its nonconductive state, the returning of R213 is not slowed by R397. Therefore, by comparing the gating

currents at the channel's conductive state and nonconductive state, we may quantitate the strength of the R213-R397 interaction from the reduction of gating current.

In Figure 3.5a, the gating charge of two mutant channels is activated from – 80 mV to 300 mV for varying time duration then deactivated to – 80 mV. The movement of gating charge between its active and resting states generates spike-like transient gating current. The upward spike, I_{on}, is generated by the outward movement of the gating charge, from its resting state to active state; the downward spike, I_{off}, is generated by the opposite inward movement of the gating charge, from its active state to resting state. Because of the repulsive interaction between the gating charge, R213, and R397, I_{off} decreases with prolonged activation duration but reaches plateau at 5 ms activation duration (Figure 3.5a). The reduction of I_{off} (ΔI_{off}) is determined by the strength of the R213-R397 interaction. As shown in Figure 3.5a, ΔI_{off} for N172D/Q397R is smaller than N172D/E399R/Q397R, indicating that the R213-R397 interaction is weaker in N172D/Q397R. This suggests that distance between R213 and R397 is increased by the repulsive 172-399 interaction in N172D/Q397R, but is shortened by the attractive 172-399 interaction in N172D/E399R/Q397R. Therefore, the distance between R213 and R397 is dependent on the inter-domain 172-399 interaction.

A detailed study on the strength of the R213-R397 interaction using five mutations shows that I_{off} reduction ($\Delta I_{off}/I_{off}$) is determined by the 172-399 interaction (Figure 3.5b). All these five mutations include Q397R so that the R213-R397 interaction persists. N172D

exists in three mutations while E399 is mutated to N or R in order to change the 172-399

interaction from repulsion (N172D/Q397R) to none (N172D/E399N/Q397R) or attraction

(N172D/E399R/Q397R). As shown in Figure 3.5b, for these three mutations, with high

activation voltage (e.g. 250 mV or 300 mV), $\Delta I_{off}/I_{off}$ increases when the 172-399

interaction changes from repulsion to none and attraction, indicating that the 172-399

interaction determines the strength of the repulsion between R213 and R397, probably by

altering the distance between them. Since these two residues are located on the

membrane-spanning and cytosolic domains, respectively, this also suggests that the inter-

domain distance is determined by the 172-399 interaction.
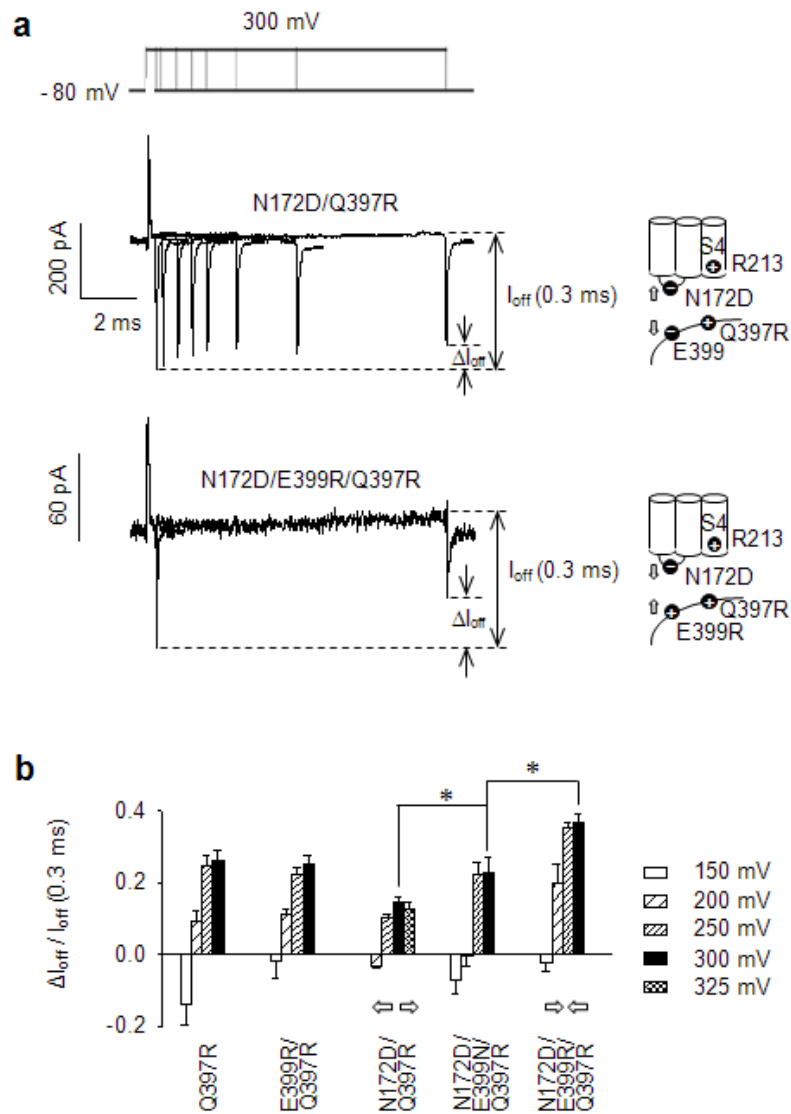
Figure 3.5 The 172-399 interaction regulates the strength of inter-domain electrostatic interaction. **a**) Gating current traces activated for varying duration for N172D/Q397R and N172D/E399R/Q397R. I_{off} is the peak off-gating current. ΔI_{off} is defined as the difference between I_{off} at 0.3 ms and 10 ms, which is used to measure the strength of the R397-R213 interaction. Right panels are cartoon schemes of the

R397-R213 interaction and its dependence on the 172-399 interaction for the corresponding mutations. **b**) $\Delta I_{off}/I_{off}$ (0.3 ms) for five mutations. The gating currents were elicited by voltages ranging from 150 mV to 300 mV, or from 200 mV to 325 mV. Arrows indicate the repulsive or attractive type of the 172-399 interaction. Asterisks indicate a significant difference.

In the other two mutations in Figure 3.5b, N172 is intact while E399 is mutated to R (Q397R and E399R/Q397R). Therefore, charge type at residue 399 is altered while no 172-399 interaction is introduced. $\Delta I_{off}/I_{off}$ for these two mutations are on the same level, indicating that charge type at residue 399 does not cause varying R213-R397 interaction. Moreover, $\Delta I_{off}/I_{off}$ of these two mutations are on the same level as the forth mutation, N172D/E399N/Q397R, which has charged residue at residue 172 but no charge at residue 399 and thereby has no 172-399 interaction. Therefore, all these three mutations (Q397R, E399R/Q397R and N172D/E399N/Q397R) have the same level of $\Delta I_{off}/I_{off}$, no matter that they have different charge types at residues 172 and 399, further indicating that the R213-R397 interaction is determined by the inter-domain 172-399 interaction, but not the charge types at the individual residues.

Additionally, only $\Delta I_{off}/I_{off}$ at high voltage (250 mV and 300 mV) is taken into account because only high voltage fully activates the voltage sensor by 0.3 ms [36]. At low voltage (< 250 mV), full activation of voltage sensor takes longer time, resulting in voltage dependence of $\Delta I_{off}/I_{off}$ at low voltage, as shown in Figure 3.5b. As long as

voltage is high enough to fully activate the voltage sensor by 0.3 ms, $\Delta I_{off}/I_{off}$ loses its voltage dependence.

The above two measurements show that the distance between the membrane-spanning and cytosolic domains is regulated by the 172-399 interaction because the interaction determines both the formation of C99-C397 disulfide bond and the strength of the repulsive R213-R397 interaction. Therefore, by using the 172-399 interaction, we successfully manipulated the inter-domain distance around the Mg^{2+} binding site. As we discussed above, this local inter-domain distance may represent one motion of the overall conformational change of the regulative domains. By manipulating this distance, we interfered the conformational change which has been suggested to be correlated with gating. As a result, gating is altered, which is indicated by G-V shift caused by the 172-399 interaction (Figure 3.2 and 3.3). Therefore, we provided functional evidence showing that gating is actually regulated by conformational change of the regulative domains and these two processes are not merely coincidently correlated, and thereby established the causality relationship.

To examine whether the 172-399 interaction alters the overall conformation beyond this local inter-domain distance, we measured the pore property because according to the structures of the cytosolic domain of BK channels, the pore is presumably located distally away from the Mg^{2+} site [22, 23] so that changes in pore property would indicate an overall conformational change.

The 172-399 interaction alters intrinsic gating.

Previous studies have shown that the pore of BK channel conducts K^+ current with small but finite open probability even when all the activation sensors are at their resting states [37]. Pore opening without activation of the sensors is determined by the intrinsic property of the pore and thereby can be used to detect changes to the pore domain. The open probability measured under extreme negative voltages ($< - 80$ mV) in the absence of Ca^{2+} reflects the intrinsic pore property in BK channels [37].
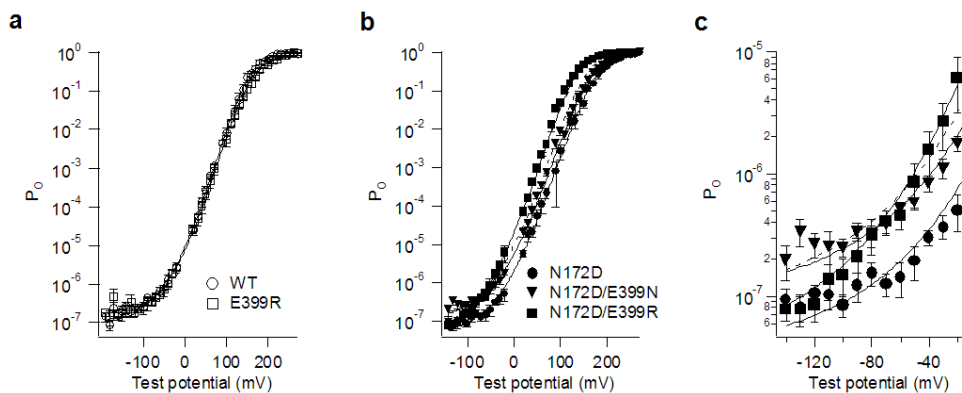
Figure 3.6 The 172-399 interaction alters the intrinsic gate opening of BK channel. **a)-b**) PO-V relation for WT and E399R (a) and N172D, N172D/E399N and N172D/E399R (b). $[Ca^{2+}]_i$ = 0 µM. Solid lines are fittings to the HCA model. Dashed line in b) is the HCA fitting for WT. **c**) Enlargement of the negative voltage range for b). All the fittings to the HCA model have fixed z_L = 0.1 and z_J = 0.57. L_0, V_{hc}, and V_{ho} are optimized for the best fitting. L_0 = 2.2×10^{-7} for WT, E399R and N172D/E399N, 0.9×10^{-7} for N172D/E399R, and 0.8×10^{-7} for N172D, respectively.

We measured the open probability for five channels. The open probability at lower voltages obtained using limiting slope measurement is combined with the G-V relation at high voltages to generate the complete curve of open probability (P_o) vs. voltage. In the five channels, N172 of the first two channels is intact while E399 is mutated to R (WT and E399R) in order to test the effect of charge type at 399 without introducing the 172-399 interaction. Figure 3.6a shows that P_o of E399R is the same as WT, indicating that the intrinsic pore property is independent on the charge type at 399. However, in the other three mutations, E399 is mutated to N and R on the background of N172D so that the 172-399 interaction changes from repulsion (N172D) to none (N172D/E399N) and attraction (N172D/E399R). As shown in Figure 3.6b, P_o is altered by the 172-399 interaction. Figure 3.6c further shows that at extreme negative voltages ($< - 80$ mV) where P_o is determined by the intrinsic pore property, both repulsive and attractive 172-399 interactions lower P_o. However, P_o is similar to WT when the 172-399 interaction is zero (N172D/E399N), indicating that the intrinsic pore property is determined by the 172-399 interaction, but not the charge type of residue 172.

Therefore, the 172-399 interaction alters the pore, which is located in the pore domain and away from residues 172 and 399. This indicates that the 172-399 interaction induces conformational changes spreading beyond the local region and reaching structures as far as the pore. The propagation of conformational change over distance suggests that neither the cytosolic nor the membrane-spanning domain is flexible enough to absorb the local change induced by the 172-399 interaction. The rigidity of both domains may transform

the change in local inter-domain distance into a global change in the relative position of the two domains which consequentially affects the pore, a structure that is connected with both domains. Furthermore, because the change in inter-domain distance induced by the 172-399 interaction is one component of the conformational change that regulates gating and change in this component causes overall conformational change, it suggests that the conformational change that regulates gating may involve overall conformational changes to the entire molecule.

The 172-399 interaction alters both voltage and Ca^{2+} activation.

By manipulating the 172-399 interaction, we further found that this inter-domain interaction regulates not only gating, but also other important functions, such as both the voltage- and Ca^{2+}-dependent activation. We examined the voltage- and Ca^{2+}-dependent activation for a number of mutations and found that both show strong correlation with the 172-399 interaction. In one group of the mutations, E399 is mutated to C and R on the background of N172R/C430A, whose 172-399 interaction thereby changes from attraction to repulsion (Figure 3.7a-c). We found that the G-V relation in the absence of Ca^{2+} ($[Ca^{2+}] = 0.0005 \ \mu M$) changes its position between the three mutations; $V_{1/2}$ value of the G-V relation changes from 139 ± 1 mV in N172R/C430A to 172 ± 4 mV in N172R/E399R/C430A, indicating that repulsive 172-399 interaction requires higher voltage for the channel to activate. $V_{1/2}$ in the absence of Ca^{2+} for more mutations is

shown in Figure 3.7d by groups; in each group, mutation at 172 remains as a background

mutation while E399 is mutated to neutral (C or N) or positive (R) residue. Therefore,

depending on the charge type at 172, the 172-399 interaction changes differently with the

residue at 399. In Figure 3.7d, the first group of three mutations are those in Figure 3.7a-c,

which shows that $V_{1/2}$ shifts to higher voltage range when the 172-399 interaction

changes from attraction to repulsion. The second group of mutations, which have N172D

as background mutation, show that $V_{1/2}$ shifts oppositely to lower voltage range when the

172-399 interaction changes in the opposite direction, from repulsion to attraction. On the

other hand, the third and forth groups, which both have neutral residue at 172 and thereby

have no 172-399 interaction, show no change in $V_{1/2}$. Therefore, $V_{1/2}$ in the absence of

Ca^{2+} is strongly correlated with the 172-399 interaction in that repulsion shifts $V_{1/2}$ to

higher voltage range and attraction shifts it to the opposite. This indicates that the

voltage-dependent activation of BK channel is regulated by the inter-domain distance.
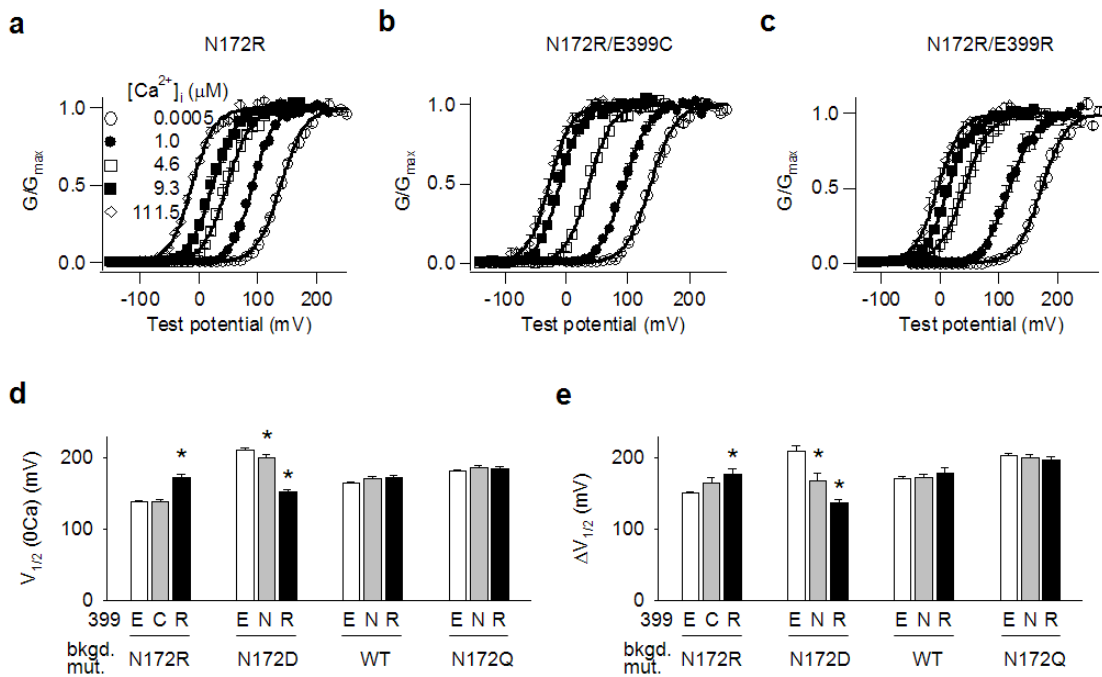
Figure 3.7 The 172-399 interaction regulates both voltage- and Ca^{2+}-activation. **a**)-**c**) G-V relation for N172R (a), N172R/E399C (b), and N172R/E399R (c) under varying $[Ca^{2+}]_i$. Solid lines are fittings to the Boltzmann equation. C430A is included for these mutations to eliminate nonspecific MTS effects. **d**) $V_{1/2}$ at nominal 0 $[Ca^{2+}]_i$. $V_{1/2}$ is the voltage value where the G-V relation equals 0.5, which indicates the position of the G-V relation. The mutations are grouped so that the negative residue E399 (hollow bars) is mutated to neutral (gray bars) or positive (black bars) residues on different mutation backgrounds. **e**) $\Delta V_{1/2} = V_{1/2}$ at 0 $[Ca^{2+}]_i - V_{1/2}$ at 111.5 µM $[Ca^{2+}]_i$, which indicates the total sensitivity to saturating $[Ca^{2+}]_i$. Mutations are the same as in d). Stars indicate significant difference from the hollow bar of the same group. C430A is included for the group of N172R mutations in **d**) and **e**) to eliminate nonspecific MTS effects.

126

We also examined the Ca^{2+}-dependent activation and found that it is regulated by the 172-399 interaction in two ways. First of all is the sensitive $[Ca^{2+}]$ range. In Figure 3.7a-c, we obtained the G-V relation under varying $[Ca^{2+}]$ ranging from nominal 0 (0.0005 μM) to near saturating (111.5 μM) for these three mutations, in which E399 is mutated to C or R on the background of N172R, causing the 172-399 interaction to change from attraction to none or repulsion. Figure 3.7a shows that the G-V relations of N172R/C430A are approximately equidistant from each other, while in Figure 3.7c, the G-V relations of N172R/E399R/C430A are concentrated between those under high $[Ca^{2+}]$, indicating that N172R/E399R/C430A is more sensitive to low $[Ca^{2+}]$ than N172R/C430A. N172R/E399C/C430A in Figure 3.7b shows intermediate Ca^{2+} sensitivity. Therefore, BK channel becomes more sensitive to Ca^{2+} when the 172-399 interaction changes from attraction to repulsion.

Second, the total shift of G-V relation caused by saturating $[Ca^{2+}]$ is regulated by the 172-399 interaction. Figure 3.7e shows the total shift of G-V relation ($\Delta V_{1/2} = V_{1/2}(0Ca) - V_{1/2}(111.5Ca)$) for a number of mutations. The mutations are grouped in the same way as in Figure 3.7d such that in each group, E399 is mutated to neutral (C or N) or positive (R) residue while the N172 mutation remains on the background. In the first group, E399 is mutated to C or R on the background of N172R/C430A, causing the 172-399 interaction to change from attraction to repulsion. As a result, $\Delta V_{1/2}$ increases, indicating that the total shift of G-V relation is regulated by the 172-399 interaction. In the second group, when E399 is mutated to N or R on the background of N172D, causing the 172-399

interaction to change in the opposite direction, from repulsion to attraction, $\Delta V_{1/2}$ also changes in the opposite direction. In the third and forth groups, which have neutral residue at 172 and thereby have no 172-399 interaction, $\Delta V_{1/2}$ no longer depends on the charge type at 399.

Therefore, the inter-domain 172-399 interaction regulates important channel functions, including the voltage- and Ca^{2+}-dependent activation. It regulates the voltage activation by affecting the activation voltage range; it regulates the Ca^{2+} activation by affecting both the sensitive $[Ca^{2+}]$ range and the total $[Ca^{2+}]$ sensitivity. The profound importance of the inter-domain distance may be the result of its influence on the pore domain. Since both voltage and Ca^{2+} activation converge at the pore domain, changes to the pore domain may affect both through allosteric mechanisms.

Discussions

By introducing the 172-399 interaction between the membrane-spanning and cytosolic domains, we manipulated the inter-domain distance around the Mg^{2+} binding site. As shown by the state-dependent re-formation of the C99-C397 disulfide bond and the studies on the Mg^{2+}-dependent activation of the BK channel, change in this local inter-domain distance is one motion component involved in the conformational change that is accompanied with gating. The 172-399 interaction alters this local inter-domain distance, and thereby alters the conformational change. As a result, we observed that gating is

altered, providing functional evidence showing that gating is energetically regulated by the conformational change.

However, although evidence indicates that this conformational change is beyond the local inter-domain distance and involves overall changes of the entire molecule (Figure 3.6), the current experiments are unable to discover more of its details. Nevertheless, the current crystal structures of the cytosolic domain may suggest that this conformational change can be very different from other channels. As shown in Figure 3.8, the AC region of the Ca^{2+}-bound crystal structure is compared with that of the Ca^{2+}-free crystal structure. We aligned these two structures by minimizing the discrepancy between the two structures in the AC region. Figure 3.8 shows that the two structures are different at the AC region, but the difference is small. This small difference may account for the conformational change that regulates gating. However, because both structures are missing the membrane-spanning domain, the relative movement of the cytosolic domain against the membrane-spanning domain cannot be detected. For example, the cytosolic domain may undergo large rotational movement, which cannot be seen by merely examining the cytosolic domain itself. It is also possible that without the membrane-spanning domain, the Ca^{2+}-bound and Ca^{2+}-free structures do not reflect actual changes in the cytosolic domain during gating.
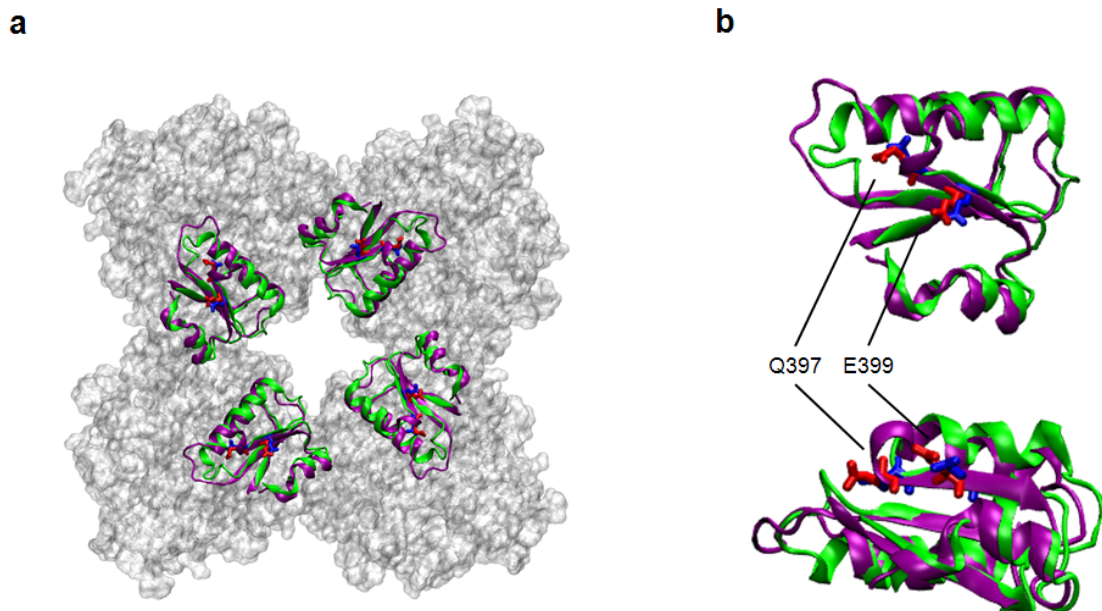
Figure 3.8 Comparison of the AC region (residues 343 to 420) between the Ca^{2+}-bound crystal structure (PDB ID code: 3MT5, green) and the Ca^{2+}-free crystal structure (PDB ID code: 3NAF, purple). **a**) Top view of the entire cytosolic domain with the structure after the AC region of the Ca^{2+}-free crystal structure in surface representation. Residues 397 and 399 are shown for the Ca^{2+}-bound structure (blue) or Ca^{2+}-free structure (red). **b**) Top view (**top**) or side view (**bottom**) of one AC region with residues 397 and 399 indicated.

Additionally, previous studies have found that the function of BK channel can be modulated by auxiliary β-subunits [38-40]. β-subunits modulate many important properties, including kinetics, voltage- and Ca^{2+}-dependent activation. Zhang et al.

130

discovered that the inactivation peptide of the β2-subunit reside in the central

antechamber between the membrane-spanning and cytosolic domains [41]. This suggests

that β-subunits may change the inter-domain distance so that they can modulate many

properties of BK channel.

Methods

Mutagenesis and expression. The mutations were made from the *mbr5* splice variant of

mSlo1(GenBank accession number, GI: 347143) using overlap-extension PCR

(polymerase chain reaction) [19]. The PCR-amplified regions were verified for all the

mutations by sequencing. RNA was transcribed *in vitro* with T3 polymerase (Ambion,

Austin, TX) and injected into *Xenopus laevis* oocytes (stage IV-V) with an amount of

0.05–50 ng each, followed by 2-5 days of incubation at 18 ºC.

Electrophysiology. Inside-out patches were formed from oocyte membrane by

borosilicate pipettes of 0.8–1.5 MΩ resistance. Macroscopic currents were recorded using

an Axopatch 200-B patch clamp amplifier (Axon Instruments, Foster City, CA) and

PULSE acquisition software (HEKA Electronik, Lambrecht, Germany). The current

signals were low-pass-filtered at 10 kHz by the amplifier's four-pole Bessel filter and

digitized with 20-μs intervals. The pipette solution comprises (in mM): 140 potassium

methanesulphonic acid, 20 HEPES, 2 KCl, 2 MgCl$_2$, pH 7.2. The nominal 0 μM $[Ca^{2+}]_i$

solution comprises (in mM): 140 potassium methanesulphonic acid, 20 HEPES, 2 KCl, 5

EGTA, 22 mg/L (+)-18-crown-6-tetracarboxylic acid (18C6TA), pH 7.2. The free $[Ca^{2+}]$

in the nominal 0 $[Ca^{2+}]_i$ solution is about 0.5 nM. $CaCl_2$ standard solution was added to a

solution containing (in mM): 140 potassium methanesulphonic acid, 20 HEPES, 2 KCl, 1

EGTA, 22 mg/L 18C6TA, pH 7.2 to obtain the desired free $[Ca^{2+}]$ ranging from 1.0 μM

to 111.5 μM, which was verified by a Ca^{2+} sensitive electrode (Thermo Electron, Beverly,

MA). The 200 μM $[Ca^{2+}]$ solution is composed of (in mM) 140 potassium

methanesulphonic acid, 20 HEPES, 2 KCl, 0.2 $CaCl_2$, pH 7.2. The treatment of DTT,

H_2O_2, or MTS reagents was performed by perfusing the intracellular side of the excised

patch for 5 min with the corresponding solution. Before each experiment, the nominal 0

μM $[Ca^{2+}]_i$ solution is used to dilute the stock DTT or MTS reagents to the final

concentration of 10 mM (DTT), 1 mM (MTSES), 0.2 mM (MTSET), or 1 mM

(MTSACE). The MTSET solution is freshly prepared before each perfusion since its

lifetime is less than 10 min. 0.1% (w/v) H_2O_2 in nominal 0 or 200 μM $[Ca^{2+}]_i$ solution is

used for H_2O_2 treatment, which is equivalent to 30 mM H_2O_2. All the experiments were

performed at room temperature (22–24 ºC).

Analysis. The tail current amplitudes at – 80 mV were measured to determine the relative

conductance. The conductance–voltage (G–V) relations were fitted with the Boltzmann

equation: $\dfrac{G}{G_{max}} = \dfrac{1}{1 + \exp(-\dfrac{ze(V - V_{1/2})}{kT})}$, where G/G_{max} is the ratio of conductance to

maximal conductance, z is the number of equivalent charges, e is the elementary charge,

V is membrane potential, $V_{1/2}$ is the voltage where G/G_{max} reaches 0.5, k is Boltzmann's

constant, and T is absolute temperature. Error bars in this paper represent standard error of means (S.E.M.). Unpaired Student's t-test and analysis of variance (ANOVA) were performed and a p-value lower than 5% is considered significant.

Gating current measurement. Gating currents were recorded using inside-out patches [36]. The pipette solution comprises (in mM): 127 tetraethylammonium hydroxide, 125 methanesulphonic acid, 20 HEPES, 2 $MgCl_2$, and 2 HCl, pH 7.1. The intracellular solution comprises (in mM): 141 N-methyl-D-glucamine, 135 methanesulphonic acid, 20 HEPES, 6 HCl, and 5 EGTA, pH 7.1. To prevent the saturation of fast capacitive transients, voltage commands were filtered at 20 kHz using an eight-pole Bessel filter (Frequency Devices, Haverhill, MA) [36]. Current signals were collected at 100 kHz with an 18-bit A/D converter (ITC-18; Instrutech, Mineola, NY) and filtered at 10 kHz with the internal filter of Axopatch. Capacitive transients and leak currents were subtracted using a P/5 protocol with holding potential of -120 mV.

Limiting slope measurement. The open probability at negative voltages was measured by single-channel recordings using patches containing hundreds of channels [37, 42]. The open probability measured at negative voltages is combined with the corresponding G-V relation to construct a P_o-V relation, which is fitted to the following HCA model [37]:

$$P_o = \cfrac{1}{1 + \cfrac{\exp(-\dfrac{z_L FV}{RT})}{L_o}\left(\cfrac{1 + \exp(\dfrac{z_J F(V - V_{hc})}{RT})}{1 + \exp(\dfrac{z_J F(V - V_{ho})}{RT})}\right)^4}$$

Where z_L is the charge associated with gate opening when all the voltage sensors are at their resting state. z_J is the charge associated with voltage sensor movements. L_0 is the intrinsic open probability at $V = 0$ while all the voltage sensors are at their resting state. V_{hc} and V_{ho} are the voltages for half of the voltage sensors to be at their activation state at the closed and the open conformations of the gate, respectively. All the fittings have fixed $z_L = 0.1$ and $z_J = 0.57$; L_0, V_{hc} and V_{ho} are optimized for the best fitting[43].

References

1.   Hille, B., Ion Channels of Excitable Membranes. 3rd ed. 2001, Sunderland, MA: Sinauer Associates, Inc.

2.   Doyle, D.A., et al., The structure of the potassium channel: molecular basis of K+ conduction and selectivity. Science, 1998. 280(5360): p. 69-77.

3.   Sigworth, F.J., Voltage gating of ion channels. Q Rev Biophys, 1994. 27(1): p. 1-40.

4.   Bezanilla, F., The voltage sensor in voltage-dependent ion channels. Physiol Rev, 2000. 80(2): p. 555-92.

5.   Finn, J.T., M.E. Grunwald, and K.W. Yau, Cyclic nucleotide-gated ion channels: an extended family with diverse functions. Annu Rev Physiol, 1996. 58: p. 395-426.

6.   Zagotta, W.N. and S.A. Siegelbaum, Structure and function of cyclic nucleotide-gated channels. Annu Rev Neurosci, 1996. 19: p. 235-63.

7.   Schreiber, M. and L. Salkoff, A novel calcium-sensing domain in the BK channel. Biophys. J., 1997. 73(3): p. 1355-1363.

8.   Xia, X.M., et al., Mechanism of calcium gating in small-conductance calcium-activated potassium channels. Nature, 1998. 395(6701): p. 503-7.

9.   Jiang, Y., et al., Structure of the RCK Domain from the E. coli K+ Channel and Demonstration of Its Presence in the Human BK Channel. Neuron, 2001. 29(3): p. 593-601.

10.   Jiang, Y., et al., Crystal structure and mechanism of a calcium-gated potassium channel. Nature, 2002. 417(6888): p. 515-522.

11.   Ye, S., et al., Crystal structures of a ligand-free MthK gating ring: insights into the ligand gating mechanism of K+ channels. Cell, 2006. 126(6): p. 1161-73.

12.   Clarke, O.B., et al., Domain reorientation and rotation of an intracellular assembly regulate conduction in Kir potassium channels. Cell, 2010. 141(6): p. 1018-29.

13.   Du, W., et al., Calcium-sensitive potassium channelopathy in human epilepsy and paroxysmal movement disorder. Nat. Genet., 2005. 37(7): p. 733-738.

14.   Fettiplace, R. and P.A. Fuchs, Mechanisms of hair cell tuning. Annu. Rev. Physiol., 1999. 61: p. 809-34.

15.   Ledoux, J., et al., Calcium-activated potassium channels and the regulation of vascular tone. Physiology (Bethesda), 2006. 21(1): p. 69-78.

16.   Salkoff, L., et al., High-conductance potassium channels of the SLO family. Nat. Rev. Neurosci., 2006. 7(12): p. 921-31.

17.   Toro, L., et al., Maxi-K(Ca), a Unique Member of the Voltage-Gated K Channel Superfamily. News Physiol. Sci., 1998. 13: p. 112-117.

18.   Adelman, J.P., et al., Calcium-activated potassium channels expressed from cloned complementary DNAs. Neuron, 1992. 9(2): p. 209-216.

19.   Butler, A., et al., mSlo, a complex mouse gene encoding "maxi" calcium-activated potassium channels. Science, 1993. 261(5118): p. 221-224.

20.   Wei, A., et al., Calcium sensitivity of BK-type KCa channels determined by a separable domain. Neuron, 1994. 13(3): p. 671-81.

21.   Xia, X.-M., X. Zeng, and C.J. Lingle, Multiple regulatory sites in large-conductance calcium-activated potassium channels. Nature, 2002. 418(6900): p. 880-884.

22.   Wu, Y., et al., Structure of the gating ring from the human large-conductance Ca(2+)-gated K(+) channel. Nature, 2010. doi: 10.1038/nature09252.

23.   Yuan, P., et al., Structure of the human BK channel Ca2+-activation apparatus at 3.0 A resolution. Science, 2010. 329(5988): p. 182-6.

24.   Golowasch, J., A. Kirkwood, and C. Miller, Allosteric effects of Mg2+ on the gating of Ca2+-activated K+ channels from mammalian skeletal muscle. J Exp Biol, 1986. 124: p. 5-13.

25.   Oberhauser, A., O. Alvarez, and R. Latorre, Activation by divalent cations of a Ca2+-activated K+ channel from skeletal muscle membrane. J Gen Physiol, 1988. 92(1): p. 67-86.

26.   Shi, J. and J. Cui, Intracellular Mg2+ enhances the function of BK-type Ca2+-activated K+ channels. J. Gen. Physiol., 2001. 118(5): p. 589-606.

27.   Hu, L., et al., Effects of multiple metal binding sites on calcium and magnesium-dependent activation of BK channels. J. Gen. Physiol., 2006. 127(1): p. 35-49.

28.   Yang, H., et al., Mg2+ mediates interaction between the voltage sensor and cytosolic domain to activate BK channels. Proc. Natl. Acad. Sci. U S A, 2007. 104(46): p. 18270-5.

29.   Yang, H., et al., Activation of Slo1 BK channels by Mg2+ coordinated between the voltage sensor and RCK1 domains. Nat. Struct. Mol. Biol., 2008. 15(11): p. 1152-1159.

30.   Shi, J., et al., Mechanism of magnesium activation of calcium-activated potassium channels. Nature, 2002. 418(6900): p. 876-880.

31.   Hu, L., et al., Participation of the S4 voltage sensor in the Mg2+-dependent activation of large conductance (BK) K+ channels. Proc. Natl. Acad. Sci. U S A, 2003. 100(18): p. 10488-93.

32.   Hazes, B. and B.W. Dijkstra, Model building of disulfide bonds in proteins with known three-dimensional structure. Protein Eng., 1988. 2(2): p. 119-125.

33.   Zhang, G. and F.T. Horrigan, Cysteine modification alters voltage- and Ca2+-dependent gating of large conductance (BK) potassium channels. J. Gen. Physiol., 2005. 125(2): p. 213-236.

34.   Tang, X.D., et al., Oxidative regulation of large conductance calcium-activated potassium channels. J Gen Physiol, 2001. 117(3): p. 253-74.

35.   Santarelli, L.C., et al., Three methionine residues located within the regulator of conductance for K+ (RCK) domains confer oxidative sensitivity to large-conductance Ca2+-activated K+ channels. J Physiol, 2006. 571(Pt 2): p. 329-48.

36.   Horrigan, F.T. and R.W. Aldrich, Allosteric voltage gating of potassium channels II. Mslo channel gating charge movement in the absence of Ca2+. J Gen Physiol, 1999. 114(2): p. 305-36.

37.   Horrigan, F.T., J. Cui, and R.W. Aldrich, Allosteric voltage gating of potassium channels I. Mslo ionic currents in the absence of Ca2+. J. Gen. Physiol., 1999. 114(2): p. 277-304.

38.   Torres, Y.P., et al., A marriage of convenience: beta-subunits and voltage-dependent K+ channels. J Biol Chem, 2007. 282(34): p. 24485-9.

39.   Patterson, A.J., J. Henrie-Olson, and R. Brenner, Vasoregulation at the molecular level: a role for the beta1 subunit of the calcium-activated potassium (BK) channel. Trends Cardiovasc Med, 2002. 12(2): p. 78-82.

40.   Orio, P., et al., New Disguises for an Old Channel: MaxiK Channel {beta}-Subunits. News Physiol Sci, 2002. 17(4): p. 156-161.

41.   Zhang, Z., et al., A limited access compartment between the pore domain and cytosolic domain of the BK channel. J Neurosci, 2006. 26(46): p. 11833-43.

42.   Cui, J. and R.W. Aldrich, Allosteric linkage between voltage and Ca^{2+}-dependent activation of BK-type mslo1 K^+ channels. Biochemistry, 2000. 39(50): p. 15612-15619.

43.   Horrigan, F.T. and R.W. Aldrich, Coupling between voltage sensor activation, Ca^{2+} binding and channel opening in large conductance (BK) potassium channels. J. Gen. Physiol., 2002. 120(3): p. 267-305.

Chapter 4: Conclusions

The large conductance voltage- and Ca^{2+}-activated K^+ (BK) channel is important for many physiological functions, such as controlling muscle contraction, mediating neuronal spike frequency adaptation, and regulating neurotransmitter release. The BK channel is activated by both membrane depolarization and intracellular ligands, including Ca^{2+} and Mg^{2+} ions. The BK channel is unique among K^+ channels because its function integrates two important cellular signals: voltage and Ca^{2+}.

Ca^{2+} sensing of the BK channel involves the large cytosolic domain. Functional studies have found two Ca^{2+} binding sites. One is in the RCK1 sub-domain and comprises D367 and E535 as the binding coordinates; the other is in the RCK2 sub-domain, comprising a series of negatively charged Asp residues (D897-D901). With the discovery of the structure of the cytosolic domain, it is evident that a mechanism coupling Ca^{2+} binding sites to the gate is required for Ca^{2+}-dependent activation because both Ca^{2+} binding sites are located away from the pore-gate domain. By such a coupling mechanism, the energy of Ca^{2+} binding travels first within the cytosolic domain and then across the interface between the cytosolic and membrane-spanning domains to reach the pore-gate domain, eventually activating the gate. Nevertheless, little is known about the coupling mechanism of the Ca^{2+}-dependent activation.

In this dissertation, I focus on the molecular mechanism of the allosteric coupling for

Ca^{2+}-dependent activation of the BK channel. I first studied the coupling mechanism

within the cytosolic domain and then the coupling across the interface between the

cytosolic and membrane-spanning domains. As of the coupling mechanism within the

cytosolic domain, we found that the AC region, which is on top of the cytosolic domain

and adjacent to the membrane, is the coupling structure for the Ca^{2+}-dependent activation

derived from the RCK1 binding site. By using a point mutation D369G, which is

associated with coexistent epilepsy and dyskinesia in human, we discovered that the

dynamics of the AC region mediates Ca^{2+}-dependent activation. Mutation D369G

increases the rigidity of the AC region to enhance Ca^{2+}-dependent activation. Our

discovery of this novel property of the AC region suggests that the BK channel can be the

target protein for treating epilepsy and dyskinesia and that manipulating protein dynamics

may represent a possible therapeutic strategy.

As of the coupling mechanism across the interface between the cytosolic and membrane-

spanning domains, we found that it is in the form of relative movements between the two

domains. We first discovered that gating process of the pore-gate domain is correlated

with a relative movement between the two domains. We further established the causality

relationship between these two processes by showing that gating can be changed if a

relative movement is introduced by an electrostatic interaction between the two domains.

The relative movement is found to regulate both the voltage- and Ca^{2+}-dependent

activation in BK channels, suggesting that the relative movement between the two domains can be the coupling mechanism for both activation pathways.

However, it is unclear what form of relative movement is responsible for the coupling. By comparing two structures of the cytosolic domain which are formed in the presence and absence of Ca^{2+}, respectively, we found that the two structures differ from each other. Since these two structures may represent the open and closed structures, respectively, the discrepancy between them may indicate the relative movement on the side of the cytosolic domain. Nevertheless, rotational movement can also happen for the cytosolic domain.

In conclusion, we have revealed novel properties of the coupling mechanism for Ca^{2+}-dependent activation in BK channels. Our findings are particularly important for understanding the structure-function relationship of the BK channel. Moreover, these findings have provided more approaches to studying coupling mechanisms of other proteins.